Escola de Camins
Escola Tècnica Superior d'Enginyeria de Camins, Canals i Ports
UPC BARCELONATECH

TREBALL FINAL DE MÀSTER

Structural optimization of horizontal links

Treball realitzat per:
Carlos Ramonell Cazador

Dirigit per:
Rolando Chacón Flores

Màster en:
Enginyeria de Camins, Canals i Ports

Barcelona, juny de 2020

Departament d'enginyeria civil i ambiental.

Resumen

El creciente desarrollo de herramientas computacionales y de modernas técnicas de fabricación permite a los ingenieros abordar el diseño de elementos estructurales usando herramientas de diseño asistidas por ordenador. Recientemente, se han desarrollado algoritmos de optimización estructural para su uso en las industrias de automoción y aeroespacial, proporcionando elementos estructurales optimizados con respecto a su rendimiento y uso de material.

La optimización estructural incluye algoritmos para la optimización topológica y optimización de forma, que están directamente relacionados con determinar la distribución del material y la forma de los límites de un espacio de diseño, dado un conjunto de condiciones de contorno, lo que conduce a nuevas geometrías con características mejoradas.

La ingeniería estructural, en particular la Ingeniería sismo-resistente, tiene como objetivo disipar energía usando elementos específicos dentro de la estructura (disipadores). Hoy en día, con estas nuevas herramientas computacionales y el horizonte del desarrollo de la impresión 3D, permiten considerar otras alternativas a los métodos de diseño actuales para disipadores estructurales.

El TFM realizado tiene como objetivo implementar estos algoritmos de optimización estructural en los disipadores horizontales de pórticos excéntricos (EBF), con el fin de obtener geometrías que proporcionen nuevas vías de diseño para estos elementos. Se ha creado un procedimiento de optimización basado en una carga lateral controlada por desplazamiento (push-over) aplicada a un EBF de una sola planta, utilizando Abaqus FEA y su módulo de optimización (ATOM).

El comportamiento de los disipadores optimizados se ha comparado con el comportamiento de los disipadores originales en cuestiones de rigidez inicial, límite elástico, carga máxima resistida y energía disipada. Los resultados de la optimización muestran geometrías poco convencionales que pueden mejorar las características de los disipadores.

Abstract

Growing development of computation and modern manufacturing techniques allow engineers to approach design of structural elements using new computer-aided design tools. In recent years, structural optimization algorithms have been developed to be used in automotive and aerospace manufacturing industries, providing structural elements with optimized performance and material utilization.

Structural optimization includes topology optimization and shape optimization algorithms, which are directly involved in determining the material distribution and the shape of the boundaries of a design space, given a set of boundary conditions, leading to new geometries with improved characteristics.

Structural engineering, particularly earthquake-resistant structural engineering aims to dissipate energy using specific elements within the structure (dissipators), Nowadays, with these new computational tools and the horizon of development of additive-manufacturing, alternative ways to current design methods for structural dissipators can be considered.

This TFM aims to implement these structural optimization algorithms to the horizontal links of Eccentrically Braced Frames (EBFs), in order to obtain new geometries that open new design paths for these types of elements. An optimization procedure based on a displacement-controlled lateral load (push-over) applied to a single-storey EBF has been created using Abaqus FEA and Abaqus Optimization Module (ATOM).

Optimized links performance has been compared with the performance of original links in terms of initial stiffness, yield strength, maximum strength and energy dissipation. Optimization results show interesting geometries that are able to improve the characteristics of the links.

Key words: Topology optimization, shape optimization, additive manufacturing, EBF horizonal links, compliance optimization, capacity curve, push-over analysis, stiffness, yield strength, energy dissipation.

Index

1. Introduction

1.1. Background

Structural optimization methods have gained popularity in recent years, mainly due to the great improvement of computation capacity of modern computers. Topology optimization, among others, is one of the most used optimization algorithms, especially in industrial product design in aircraft and automobile industry.

The topology optimization algorithms are mathematical approaches that aim at finding an optimal solid-void pattern of the material layout over a specific design domain, given specific boundary conditions, in order to reach maximums or minimums of a selected function (target function). Consequently, they provide a powerful computer-aided design tool that is often used in a conceptual design stage to set strategies to optimize the global performance of the structure, for example, rigidity and natural frequencies.

Topology optimization techniques result in non-canonical shapes and dispositions that regular product manufacturing methods are not able to produce. Nowadays, development of additive-manufacturing provides the design freedom needed to translate the outputs from a topology optimization procedure into real elements, being able to print using materials that are of special interest for the construction field, like metals and, in a more immature stage, concrete.

For those reasons recent research is expanding the scope of optimization methods to construction and architectural fields, especially in metallic structures, providing high performance designs with optimized material usage of building structural systems and specific structural elements. Despite it is still in a gestation stage, this design approach could lead to more efficient, economic, and environmentally friendly construction methods.

This study focuses in the optimization of eccentrically braced frames (EBF) which are metallic structural systems used in seismic design of buildings due to their high ductility when subjected to large displacements. Ductile behaviour of these structures is dependent on high performance elements called links, which are replaceable elements that concentrate all ductile deformations of the whole systems. Seismic design usually involves an additional construction cost caused by the over-dimensioning needed in structural members to bear seismic loads applied.

Characteristics of links in EBF allow them to be produced using additive manufacturing, so topological optimization focused on these elements could lead to performance improvement of the entire structural system and, at the same time, show new design paths for these type of dissipative elements, improving the cost of the overall structure.

1.2. Objectives

In this section, the general and specific objectives are described

1.2.1. General objective

The general objective of this TFM is to apply topology optimization on horizontal EBF links when a they are subjected to large horizontal forces, to obtain new geometrical typologies of links that provide an improvement of their characteristics.

1.2.2. Specific objectives

The specific objectives are defined as follows:

- Study the principal forms of structural optimization and their different algorithms. Explore current applications for optimization algorithms in structure and civil engineering and define which of these optimization algorithms are of interest for this TFM. Finally study how these algorithms are implemented and how commercial software use them.

- Study how EBFs work, focusing specifically in the typology using horizontal links. Study the main typologies of links that are currently in use and define their main characteristics. Finally, understand how the links behave when the structure is subjected to large deformations

- Define how to carry out a push-over analysis using commercial software and Study how horizontal links are modelled. Finally, determine which modelling method fits better with the interests of this TFM

- Evaluate the behaviour of shear and flexure links when a push-over analysis is carried out for different link sections, using a single-story frame configuration.

- Obtain new geometries carrying out topology and shape optimization on horizontal EBF links.

- Finally, assess the behaviour of the optimized links submitted to a push-over analysis and compare it to the behaviour of original links

1.3. Methodology

The methodology to fulfil the general objective and the list of specific objectives is presented below.

First, a review on available literature has been carried out regarding general structural optimization, topology and shape optimization algorithms, topology and shape optimization applications in current industrial processes and study cases of topology optimization in building engineering and its application in structural elements and systems.

Secondly, a review on available literature has been carried out regarding the behaviour of EBF structural systems, their advantages when compared with other steel frame structures, the behaviour of the horizontal links and experimental studies regarding their yield and failure modes, the comparison between shear, flexure and intermediate links and, finally, the approach of the codes with regard to EBF using horizontal links.

I-shaped horizontal links are considered for this TFM which are studied using FEA models. Then, Abaqus FEA is used to define the model elements and characteristics and the Abaqus optimization module is used to carry out the topology and shape optimization procedures on the links.

To ensure that the results obtained from the different analysis and optimization procedures are accurate, mesh dependence studies have been done on the push-over analysis results for original links and on the topology optimization geometric results.

Once the results can be considered accurate enough, push-over analysis are carried out for different I-shape sections of the links and for their corresponding optimized version. The resulting capacity are approximated using linear functions, which parameters are used to compare the behaviour between original and optimized geometries. The plastic energy dissipated is calculated for original and optimized links using Abaqus and it is also submitted to comparison.

Finally, the comparison stablished allow to evaluate the level of improvement of the optimized links behaviour with respect to the original links.

1.4. Content

This TFM is divided in 6 chapters which are briefly described below.

Chapter 1: Introduction

The TFM is introduced by presenting its background and motivations, its main objectives and the methodologies used to accomplish them and, finally, a summary of the content included.

Chapter 2: Literature review

A theoretical review regarding structural optimization is done, focusing on topology and shape optimization algorithms. Additionally, a theoretical approach of the behaviour of EBFs and horizontal I-shaped links is presented, by introducing empirical observations and current formulations used to describe and design this type of structure. Finally, relevant works regarding optimization applied for structural purposes and studies regarding the modelling and behaviour of EBF horizontal links are presented.

Chapter 3: Numerical modelling

In this chapter, the models that are used to evaluate and optimize the links are defined, that is: geometries, material assignment, application of boundary conditions and the mesh used for the analyses. Furthermore, the Abaqus Optimization Module (ATOM) is described and the optimization problem is defined, presenting the formulation used for topology and shape optimizations.

Chapter 4: Numerical studies

In this chapter, the numerical studies carried out in this TFM are defined i.e. push-over analyses and optimizations. The conditions for the push-over analysis are explained and the optimization procedure is defined in detail.

Chapter 5: Results

In this chapter, the results for the numerical studies are exposed. First, the results for the push-over analysis of the original links are exposed. Then, results for mesh dependence of the optimization outputs are presented, and the optimization results for the different link sections are described. Finally, a comparison of the results observed is carried out.

Chapter 6: Conclusions

The main conclusions for all the chapters of the TFM are presented and an evaluation of the optimization techniques used is done for further work definition.

2. Literature review

2.1. Structural opimization

A structural optimization is based on the mathematical design optimization method, where a problem is formulated as a function and constraints and the 'optimized form' of the function are also written mathematically, so multiple design steps run automatically instead of using a iterative-intuitive design approach, where every design step is analysed and comprehended to advance to the next design step (It is a standard procedure in research involving computer based methods as FEM). In a structural optimization problem, the following functions and variables need to be defined [1]:

- Objective function f(x,y): For every possible case, f returns a value that is evaluated according to the purpose of the design. It is usually selected to minimize the objective function. Some examples of objective functions to evaluate are weight, displacement in any direction, stresses, volume etc.
- Design variables x: They are functions or vectors that can be changed during the optimization process. In structural optimization x will always represent some kind o geometric feature.
- State variable y: For a given function x, y is a function or vector that represent the response of the structure

Then, the structural optimization problem is defined as the minimization or maximization of *f(x,y)* subjected to behavioural constraints on *y*, design constraints on *x* and equilibrium constraints.

Structure optimization methods are divided into three different approaches: sizing optimization, shape optimization and topology optimization which address different aspects of the structural design problem [1] [2] [3]:

- *Sizing optimization*: The feature of sizing optimization is that the domain and the variables included are known a priori and are modified throughout the optimization process. It is addressed to models with many geometric variables. Normally the design variables are related to the thickness of a membrane plate or shell, or the cross-sectional dimensions of a truss, beam or frame. Suh variables are predefined and then submitted to the optimization process, where are modified to maximize or minimize the objective function *f(x,y)* (See *Figure 2-1*)

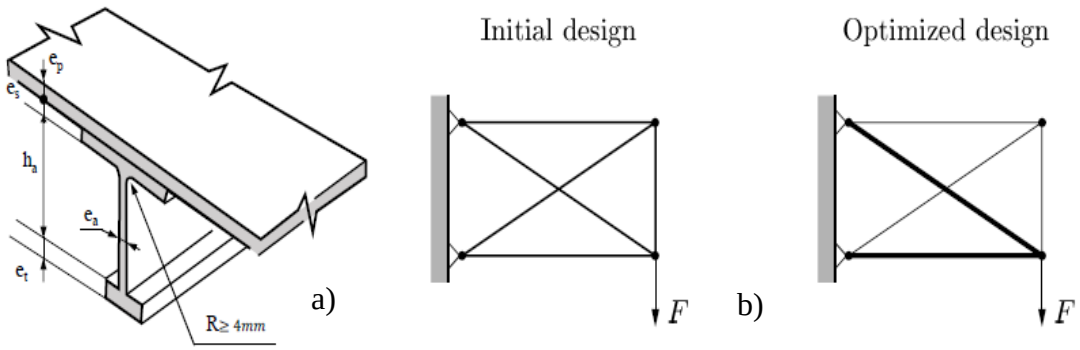

Figure 2-1 a) Example cross-section sizing optimization variables definition [2]. b) Sizing optimization of the cross-sectional areas of a truss member [1].

- *Shape optimization*: The optimization is focused in finding the optimal shape of the design domain, then, x is defined as the form or contour of some part of the boundary of the domain. In practice, it is used to lessen local performances as concentration of stresses. Shape optimization changes the geometrical definition of the model; however, it does not involve and change of the specific topology of the domain.

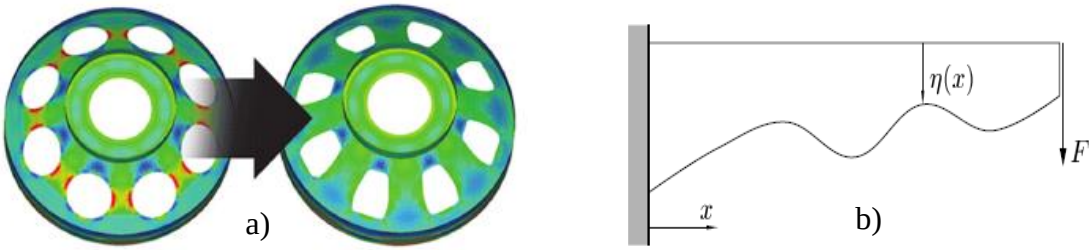

Figure 2-2 a) Shape optimization of the contours of the cut-outs of a structure. b) shape optimization of the shape function (height) for a beam-like structure which is clamped at one of its ends and submitted to a force F at the other end.[2].

- *Topology optimization:* It is the most general case of structural optimization. Its aim is to find an optimal solid void of a material layout over a specific design domain, given a set of boundary conditions. Then, variable x is defined as a density-like parameter that allow to change material concentrations in the design domain. It could be said that shape optimization is a more specific case of a topology optimization, however, they are used with conceptual approaches completely different, then, they are treated separately.

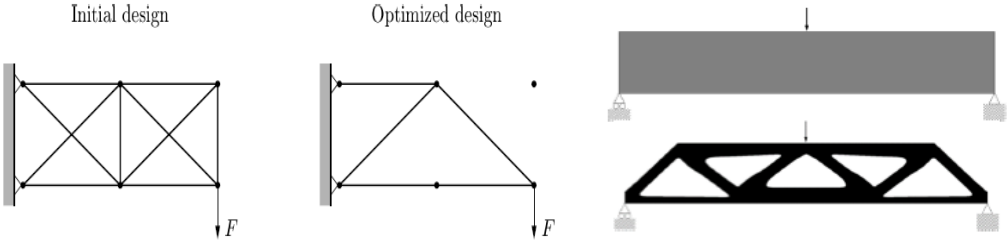

Figure 2-3 a)discrete approach of a topology optimization on a truss-like structure. b) Design optimization of a beam in a continuum sheet-like design domain [2].

Different types of structural optimization approaches address different problems in a structural design. However, literature shows that in product manufacturing processes normally various optimization techniques are used in order to obtain results for the geometry of an optimized element (normally topology and shape optimization, (see *Figure 2-4*).

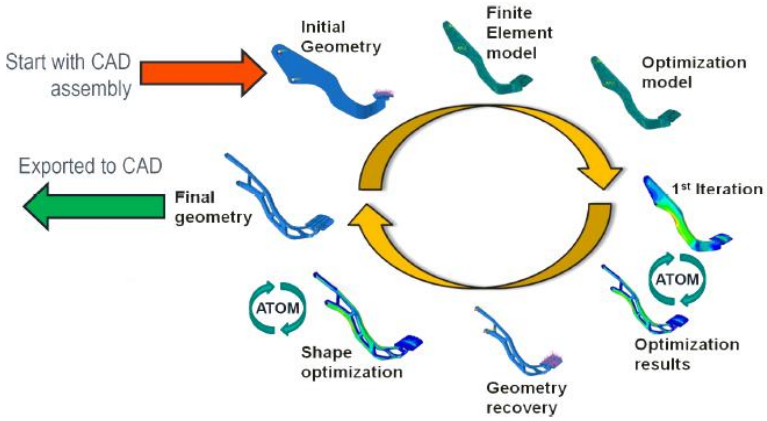

Figure 2-4 Structural optimization process according to Dassault Systèmes [4].

As mentioned previously, this thesis is focused in the conceptual optimization of the links in EBF, then, general topology optimization will be implemented using FEM software. In the following sub-chapters, theory regarding optimization process and different optimization algorithms as well as current research works regarding structural topology optimization are presented.

2.1.1. Theoretical background of topology optimization

This theoretical overview on topology optimization will follow the nomenclature and formulation described in [3].

The first problems in structural optimization, due to their large-scale computational requirements, were dedicated to the simplest type of problem in terms of objective and constraints definition: The *minimum compliance* problem definition (also known as maximum stiffness problem definition). In the following pages, the minimum compliance case will serve to illustrate most of the aspects regarding structural topology optimization

Consider a mechanical body that occupies a domain Ω^{mat} included in a reference domain Ω in $\mathcal{R}^2$ or $\mathcal{R}^3$, also labelled in the literature as 'the ground structure'. In the ground structure we define the optimization problem as to find the optimal stiffness tensor $\mathbb{E}_{ijkl}(x)$, variable over the domain. The bilinear form of energy defined in *Equation 2.1* depends on the equilibrium (or solution) displacement *u* and an arbitrary displacement *v* (also understood as test displacement). The load linear form of energy is defined in *Equation 2.2*. Using both the bilinear form of energy and the load linear form of energy allows the minimum compliance problem to be defined in *Equation 2.3* in its weak form.

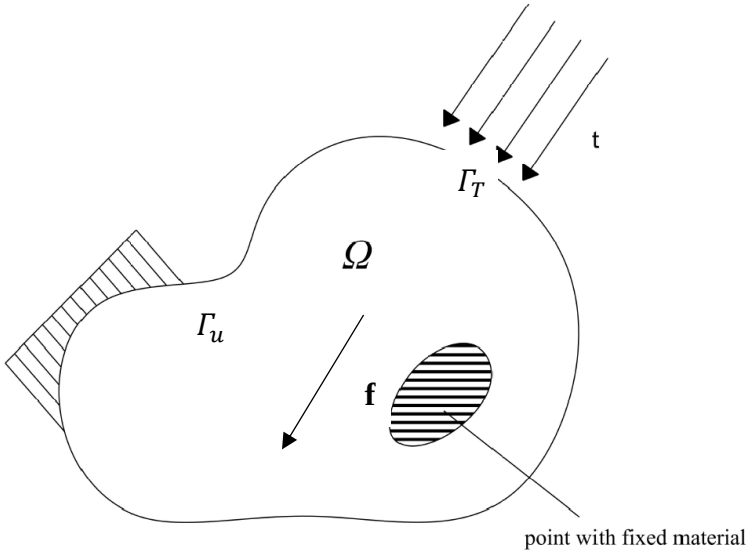

Figure 2-5 Generalized design problem

$$a(u,v) = \int \mathbb{E}_{ijkl}(x)\varepsilon_{ij}(u)\varepsilon_{kl}(v)\, d\Omega \quad \text{where} \quad \varepsilon_{ij}(u) = \frac{1}{2}\left(\frac{\partial u_i}{\partial x_j} + \frac{\partial u_j}{\partial x_i}\right) \tag{2.1}$$

$$l(u) = \int fu\, d\Omega + \int tu\, d\Gamma_T \tag{2.2}$$

Minimum compliance problem form

$$\min_{u \in U, E} l(u) \quad s.t. \quad a_E(u,v) = l(u), \quad for\ all\ v \in U\ and\ E \in E_{ad} \tag{2.3}$$

Where U is the space with kinematically accepted displacement field, f are the body loads, t are the boundary tractions on Γ_T and E_{ad} is the set of admissible tensors for the design problem.

For solving such type of problems by computational means, discretization methods such as FEM are generally required. Then the discretized form of the problem is shown in *Equation 2.4.*

Minimum compliance problem discretized form

$$\min_{u \in U, E} f^T u$$
$$s.t. \quad \boldsymbol{K}(E_e)u = f, \quad for\ E_e \in E_{ad} \tag{2.4}$$

Where *f* and *u* are the loads and displacements vector respectively, and $\boldsymbol{K}$ is the stiffness matrix dependent on the stiffness in every element E_e and can be written in the form $\boldsymbol{K} = \sum_{e=1}^{N} \boldsymbol{K_e}(E_e)$ where K_e is the stiffness matrix of every element in its global form.

For the optimization problem defined previously, the allowable set of stiffness tensor can have different admissibility approaches. Assuming that the material in the design space is entirely isotropic, then, one could set the admissibility of the stiffness tensors as a discrete value design problem (0-1) as shown in *Equation 2.5.*

$$E_{ijkl} = 1_{\Omega^{mat}} E^0_{ijkl},\ 1_{\Omega^{mat}} = \begin{cases} 1\ if\ x \in \Omega^{mat} \\ 0\ if\ x \in \Omega \backslash \Omega^{mat} \end{cases}$$
$$\int 1_{\Omega^{mat}} d\Omega = Vol(\Omega^{mat}) \leq V \tag{2.5}$$

In which boundary conditions are fixed within the volume of the ground structure V. However, the most common formulation to solve the problem is to substitute the discrete variables by a continuous one, normally interpreted as the density of the material, and introduce a penalty to evaluate whether the solution is represented as a 0 value or as 1 value. The continuous density function, denoted by $\rho(x)$, affects directly the stiffness of the material and interpolates the stiffness resulting in a map of $E_{ijkl} = 0$ when $\rho(x) = 0$, $E_{ijkl} = E^0_{ijkl}$ when $\rho(x) = 1$ and a set of intermediate values ranging from 0 to E^0_{ijkl}.

To obtain physically acceptable integer solutions, intermediate results are made unfavourable using penalization techniques [5]. There are two main reason for allowing but penalizing intermediate densities [6]: (1) post processing solution to relaxed problems and (2) to avoid integer programming techniques when solving large-scale topology optimization problems.; therefore, for computational reasons it is suggested to allow intermediate density values and use penalization to somehow approximate the results to the 0-1 approach.

The difference between topology optimization algorithms is how they manage these intermediate results, and how do they decide whether an element has material in it. There are many possible algorithms in literature. This research will only consider algorithms that are already implemented in Simulia Abaqus ATOM [4] since it is defined as a numerical tool for the development of optimization studies. Namely, these algorithms are called the SIMP-model and the RAMP-model, which are described in the following.

2.1.1.1. The SIMP model

The Solid Isotropic Material with Interpolation, also called the penalized proportional stiffness model, has proven popularity and an extreme efficiency [3]. The binary constraints (0-1) are

relaxed using the density function and intermediate values are penalized by applying a factor $p > 1$as shown in *Equation 2.6.*

$$E_{ijkl} = \rho(x)^p E^0_{ijkl},\ p > 1$$
$$\int \rho(x) d\Omega \leq V;\quad 0 \leq \rho(x) \leq 1,\ x \in \Omega \tag{2.6}$$

Choosing a p higher than one yields intermediate values unfavourable, since the stiffness-volume ratio decreases. To obtain true binary (0-1) solutions in 3D problems, a value for p higher than 3 is usually required. Indeed, the appearance of many intermediate values causes a conflict in the interpretation of the results, without being able to clearly establish what would be the barrier that separates the initial isotropic material of the design space from another that shows the characteristics of the intermediate zone. For this reason, the SIMP model is not considered as a single material model if it meets the conditions in *Equation 2.7 [3]*.

$$p \geq max\left\{\frac{2}{1-\upsilon^0},\ \frac{4}{1+\upsilon^0}\right\}\ in\ 2D\ problems$$
$$p \geq max\left\{15\frac{1-\upsilon^0}{7-5\upsilon^0}, \frac{3}{2}\frac{1-\upsilon^0}{1-2\upsilon^0}\right\}\ in\ 2D\ problems \tag{2.7}$$

Where υ^0 is the poison ratio of the bas material with stiffness tensor E^0_{ijkl} .

SIMP model is the basis for most computational results for Isotropic material interpolation, however, these kinds of interpolation present some numerical drawbacks [6] that ca be split into three categories: Checkerboards, Mesh dependence and Local minima.

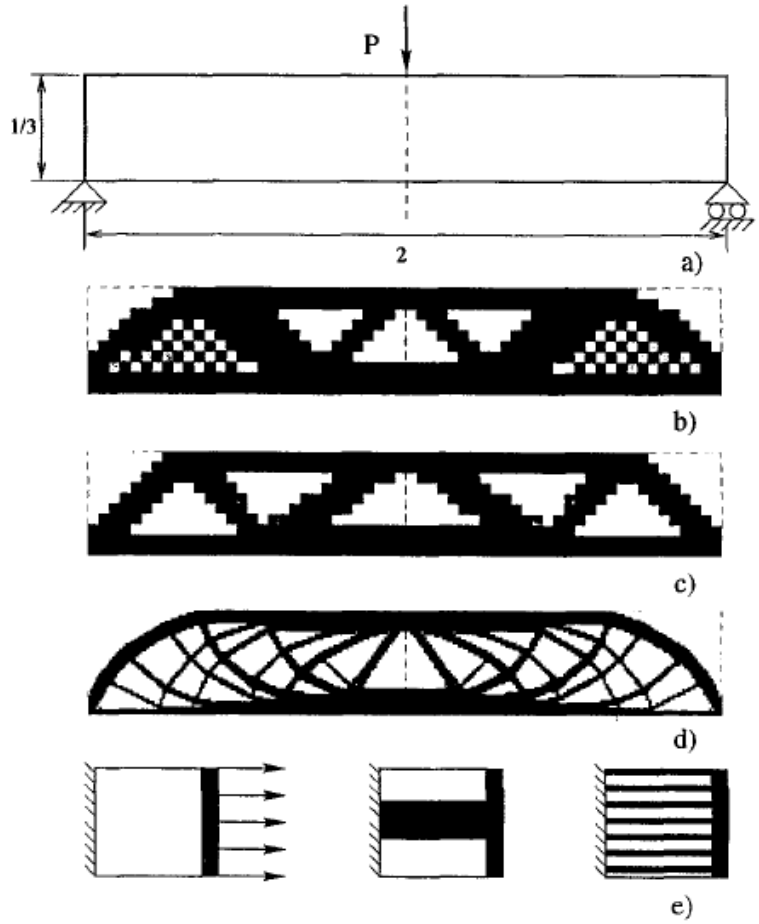

Figure 2-6 (a) Design problem (b) Checkerboards (c) solution for a large mesh size (d) solution for a small mesh size (e) no uniqueness example [7].

Checkerboards refer to a problem of formation of alternating solid and void elements in a checkerboard like fashion. The reason of the appearance of checkerboards are a bad modelling of the stiffness of the checkerboards and they are a typical example of nonconvergence of the FE. Different methods are proposed in literature to avoid this problem. Smoothing techniques, which use higher order finite elements, Patches or Filtering techniques from image processing are some of the used strategies.

Mesh dependence refers to the problem of not obtaining the same solution for different mesh sizes or mesh topologies. Such kind of problems may appear in two cases: i) when the solution is not unique and therefore more than one optimum result can be displayed, ii) when the solution is non-existent, which leads to a finer structure with every mesh refinement. Possible solutions for this type of problem are: (1) relaxation of the interpolation techniques, which, as mentioned previously, drives to a great number of intermediate density elements which result in something that is not easily manufacturable, (2) Impose restriction methods over the variation of density, (3) Perimeter control techniques, among others [6].

Local minima refer to the problem of obtaining different solutions to the same discretized problem when choosing different algorithmic parameters. Small variations in initial parameters can result in drastic changes in the optimal design. Experience has shown that continuation methods are suitable to face this type of problem, which consist of gradually increasing the penalization factor throughout the process in order to ensure the convexity of the optimization process and thus, converging to the discretized solution 0-1.

2.1.1.2. The RAMP model

The Rational Approximation of Material Properties (RAMP) model was first introduced by Stople and Svanberg [7] as an alternative interpolation scheme for minimum compliance topology optimization. They proposed a model based on SIMP, proposing a penalization based on a rational function determined by a factor q. Such proposal improved the probability of reaching the discretized solution 0-1 in cases with very low-density values in presence of design loads what solved some numerical problems regarding low density cases in SIMP models.

The Ramp model includes in each iteration an interpolation of the material characteristics in the elements where the density has been modified. Thus, the initial properties of the design are updating constantly, which makes this model useful to solve problems of time-dependent loads like pressure loads from wind, water etc.

2.1.1.3. Solution methods

For the topology optimization problem there are two common solution methods: Firstly, the explicit convex approximation method and, secondly, the Optimality Criteria Method (OC).

The explicit convex approximation methods are generally adopted to solve the complexity of writing explicitly both objective and constraints for large scale problems. Then, a sequence of explicit subproblems that approximate the real one is defined (nested problems). The most used method for explicit approximation is the Method of Moving Asymptotes (MMA), but there are others like the Sequential Linear Problem (SLP), Sequential Quadratic Problem (SQP) and Convex Linearization (CONLIN). A detailed explanation of these methods is provided in Chapter 4 of [1].

The OC method proves very efficient for compliance topology optimization problems. It uses Lagrange multipliers for the optimization task where compliance is minimized for a volume constraint. It proves very efficient when the definition of the compliance problem is simple, showing a faster convergence, however, for complex problems with, for example, multiple load cases, MMA shows a better convergence

2.1.2. Theoretical background of shape optimization

Shape optimization is a special case of structural optimization in which the shape of a component (its boundary) is modified such that certain boundaries are reached, obtaining the 'best' boundary function (see *Figure 2.7* for a beam like structure) for the imposed constraints. Shape optimization approaches are usually utilized when minor optimization is needed i.e. the general topology of the structure needs to be maintained. Typically, these approaches are focused on reducing stress concentrations in specific regions of the structure. The available methods for shape optimization can be divided in parametric and non-parametric shape optimizations [8].

Parametric shape optimization is classically linked to a CAD geometry, in which its dimensions are the parameters to be varied. To carry out the optimization the model and the mesh need to be updated at each iteration due to large modifications of the parameters and it is limited to tetrahedral elements and to the condition that the CAD geometry needs to be clean(no duplicated elements such points or lines), which is not always the case. Then the parametric approach does not work very well with complex 3D geometries but is suited well for 2D geometry where the parameters can be modified.

Non-parametric shape optimization approach builds up a design space by implicit parameters from a chosen set of surface nodes from the finite element model. The implicit parameters are the scalar optimization displacements along a local optimization vector for each design node, which is normally taken the outer local normal for each design node. Then, each design node can be modified by the optimization algorithm giving this method more versatility against parametric approaches. However, as all possible solutions along the design vectors are considered the problem need to be constrained to reach certain design conditions required, depending on the designer. To avoid jagged boundaries in stress due to geometric sensibility of stresses due to geometric changes and to handle economically the large number of design variables, node-based Optimality criteria methods are used for the shape optimization task. Further development of nonparametric shape optimization techniques are further developed in [2].

2.1.3. Research

Optimization techniques have been widely implemented in research regarding industrial and aeronautic product design, however, research focused on optimization methods for structural performance of bridges and buildings is less abundant. In this chapter, some of the studies carried out regarding optimization in structural engineering are described for different levels: full structural design, structural element design and material scale design).

Hassanzadeh and Gholiazadeh [9] performed a Collapse-performance-aid design optimization of steel concentrically braced frames. A Sizing and topology optimization of steel concentrically braced frames of three design example of 5-,10- and 15-story SCBFs was carried out. In the discrete topology optimization, the cross-section of the structural members and the placement of the braces were set as the topology design variables. Thus, a fully braced frame build was considered as the ground structure and during the process, braces would be sized, and the unnecessary ones would be removed, carrying out a performance-based topology optimization.

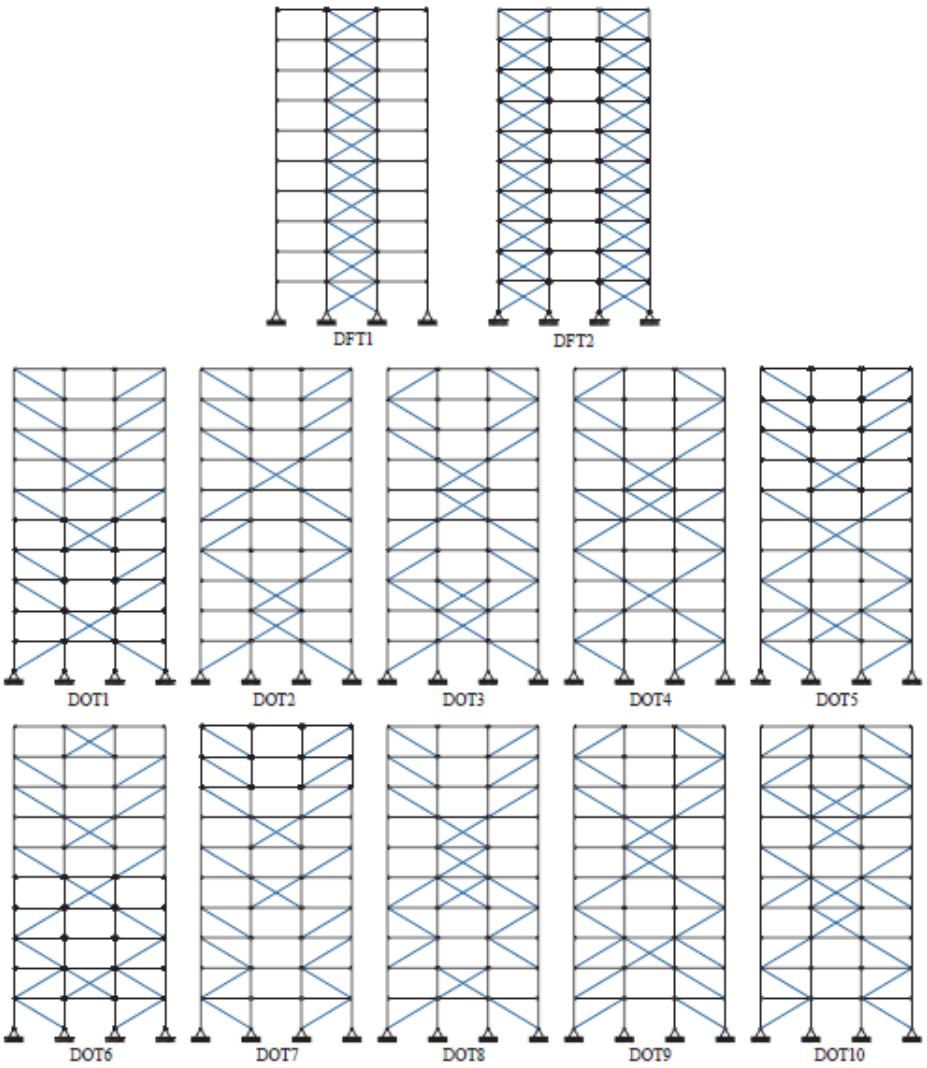

Figure 2-7 optimized design using collapse -performance-aided optimization method of a 10-story SCBF.

The optimization results showed several 'optimal' configurations of brace framing that were later subjected to an incremental dynamic analysis and finally compared in terms of structural weight and seismic collapse capacity. At the end, optimized structures showed to be around 20% lighter weight and an improved collapse performance.

Lee and Tovar [10] presented a novel design methodology for outrigger placement in tall buildings using topology optimization. The builds were loaded using a wind force calculated following codes and the objective of the optimization was set to find a binary distribution that minimized the building compliance subjected to a limited number of outriggers using a SIMP relaxation algorithm. A continuation method was implemented to avoid premature convergence in a non-optimal solution.

First the optimization solution was implemented in a low scale problem (1 and 2 outriggers) where optimum design could be numerically obtained, and the method was applied to 3 and 4r outriggers (*Figure 2-8*). The results proved the efficiency of the method reducing the compliance of the full structure

Outrigger number	Optimum location by TO	Compliance ($\times 10^6$ N m)
1	21st	2.2323
2	16th, 29th	1.8540
3	11st, 19th, 28th	1.6628
4	11st, 28th, 37th, 47th	1.5660

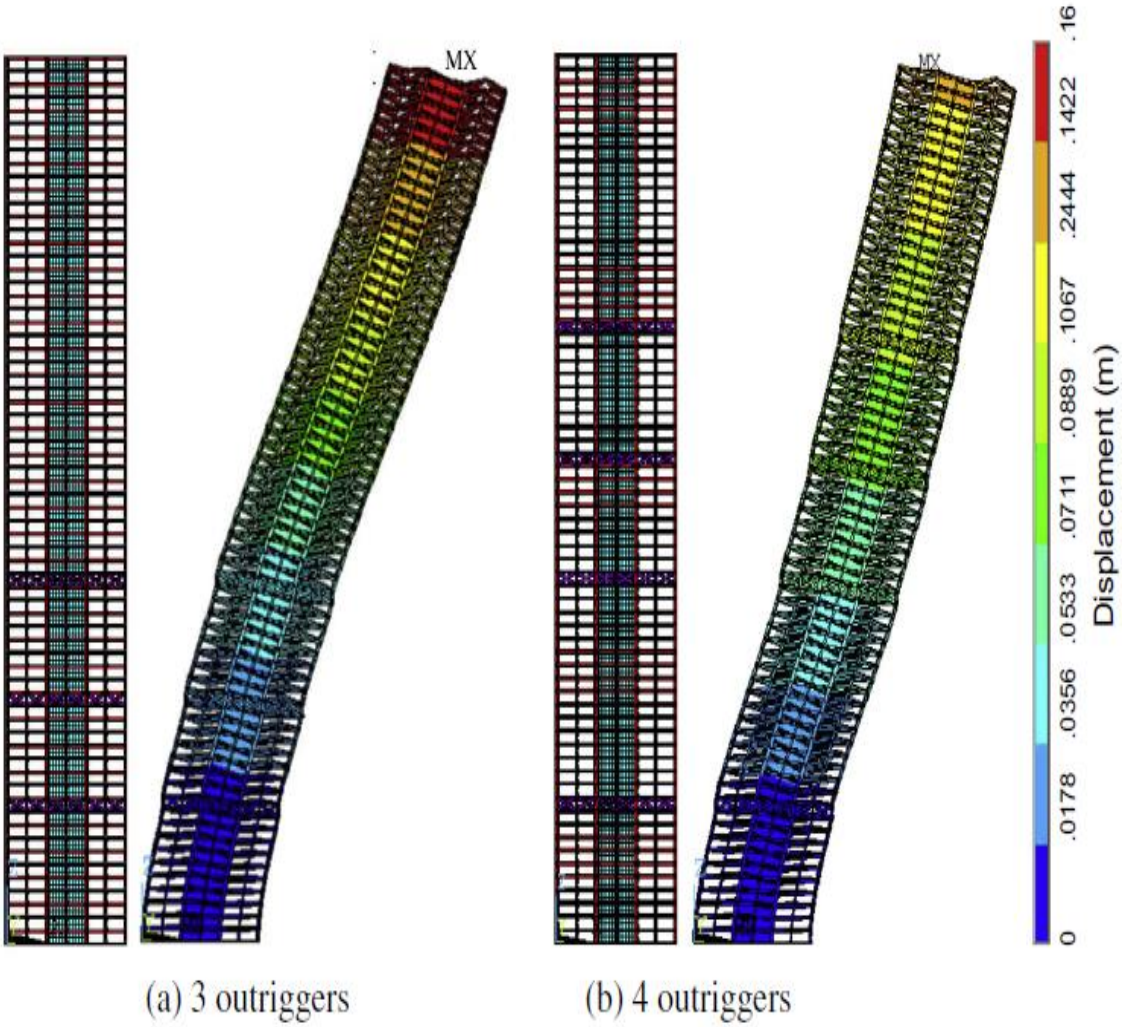

Figure 2-8 Outrigger optimized placement for (a) 3 outriggers and (b) 4 outriggers[10].

Jewett and Carstensen [11] conducted a topology-optimized design of plain concrete beams using a density-based approach and a subsequent construction and experimental evaluation. Three elastic design cases were considered to study the effect of using different topology optimization problem formulations and different safety factors on the material strengths. The study contained two optimization approaches: in the first one the compliance was minimized and in the second one under the limit of material use and stress limits were imposed with a Drucker-Prager criterion while the volume was minimized. The results of the constructed optimized samples showed that all experimental specimens appear to have an elastic behaviour under design loads, then, their work demonstrated that plain concrete structures can be designed with topology optimization.

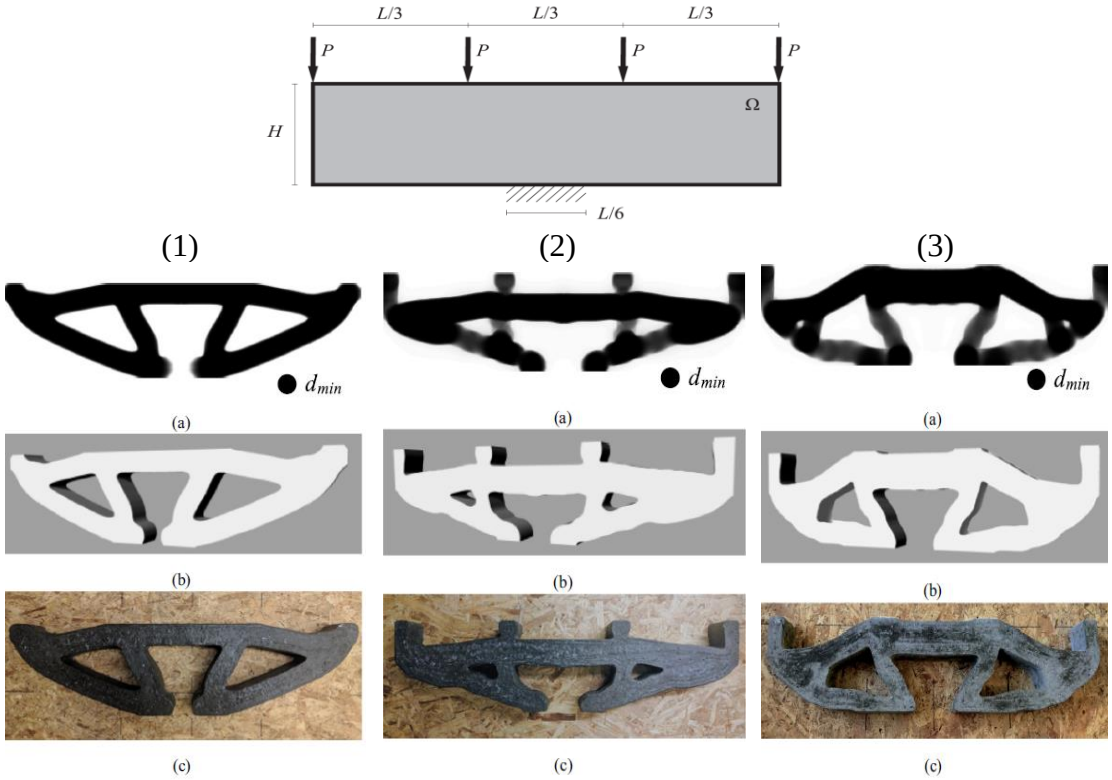

Figure 2-9 Space design of the study; (a) optimization results (b) post-processed optimized design (c) constructed sample. (1) Minimum compliance design. (2) High tension design. (3) Low tension design [11].

Performance properties that were not included in the design framework were not capable to be controlled and showed significant variation from one design approach to the other.

The minimum compliance design was able to converge to the discretized 0-1 solution, showing expected results in the experimental studies, however the stress-based design was not capable of achieving the binary 0-1 solution, then, a great amount of post-processing was needed for the design to be established. This post-processing resulted to be detrimental for the behaviour of the experimental samples, which showed that the model over-estimated the capacity of the samples.

Tsavdaridis et.al. [12] studied the application of topology optimization to optimize the behaviour in aluminium beam's cross-section and develop novel structural aluminium beam and column profiles. The study included forty standard loading combinations using the Sectional Optimization Method (SOM) for the optimization. Ten different cross-sections for beams and columns were presented and the shape of the best optimized cross-sections was simplified by providing cross-section elements with a uniform thickness and using curved elements of constant radius. Additionally, heuristic cross-sectional shapes were created according to the original optimization results.

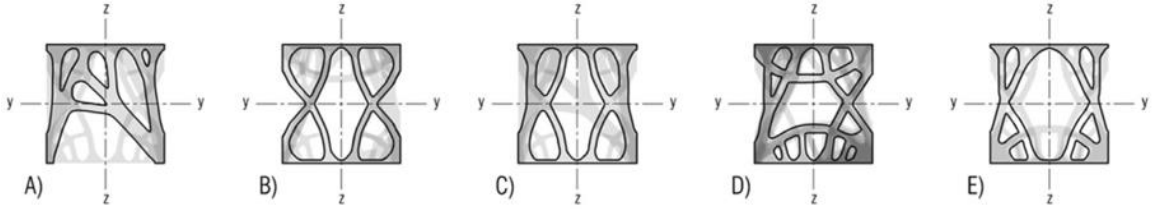

Figure 2-10 Final SOM results of beam cross-sectional designs[12].

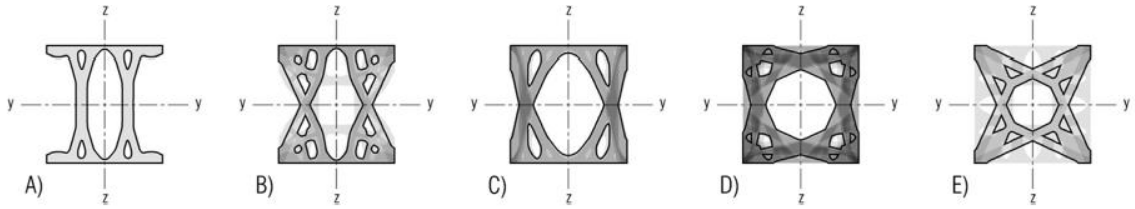

Figure 2-11 Final SOM results of column cross-sectionals designs [12].

Both approaches for beams and columns predominantly resulted in irregular hollow-based sections. Beam sections have an approximately central neutral axis despite only one plane of symmetry being applied. All column sections resulted in symmetrical shapes about both axes and with high stiffness. After simplifying the cross-sectional shapes, buckling parametric studies were carried out on beams and columns using FE-analysis. Results showed that 9 out of ten cross-sections behaved according to the predictions made using codes.

Novel studies at the same group were conducted on structural optimization on perforated I-section steel beams [13]. Solid Isotropic Material with Penalization (SIMP) was used as optimization technique. FE analysis was carried out in order to predict the load carrying capacity of the optimized beam, resulting in an increased stiffness and yield load. A parametric study was conducted to analyse solutions for a wide range of I sections, thus obtaining optimum designs for beams between 270 mm and 750 mm (*Figure 2-12*) and for beams deeper than 750 mm (*Figure 2-13*).

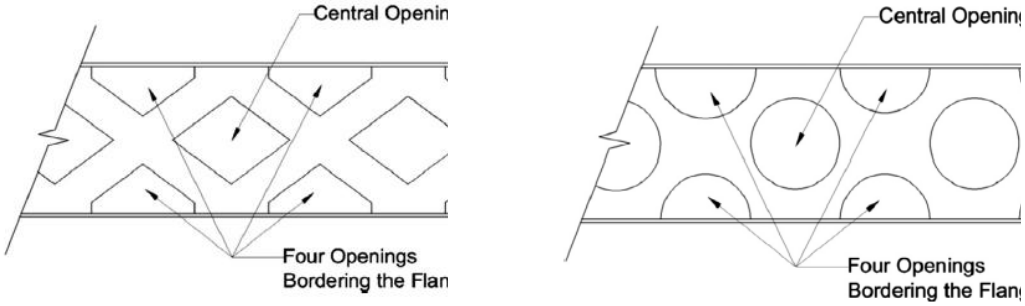

Figure 2-12 Optimum geometry for beams between 270 and 750 mm deep [13].

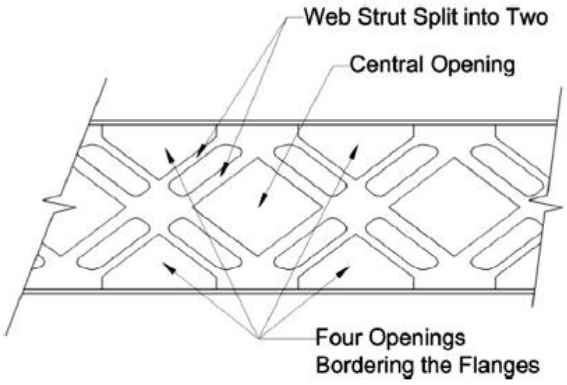

Figure 2-13 Optimum design for beams greater than 750 mm deep[13].

Additionally, it was observed that the optimized sections had a higher buckling capacity compared to a cell section of the same weight.

Regarding material scale studies, Xiao et. al. [14] Evaluated topology-optimized lattice structures manufactures via selective laser melting (SLM). Additive manufacturing and topology optimization are combined for designing Face Centre Cube (FCC) Vertex cube (VC) and edge centre cube (ECC) using ABAQUS software.

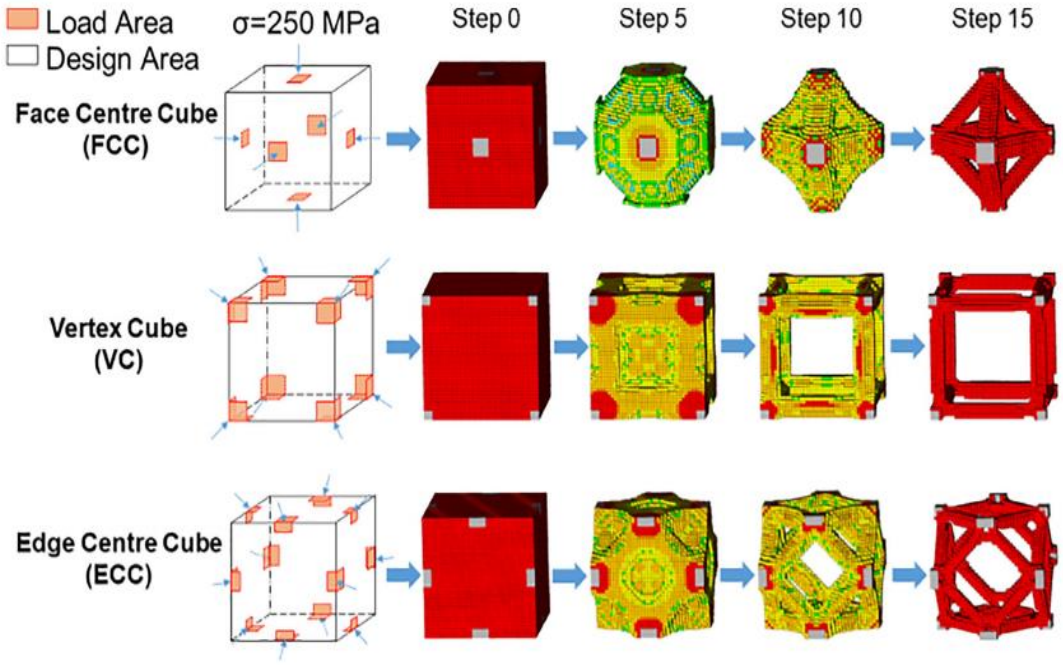

Figure 2-14 FCC, VC and ECC cell optimization process.

Mechanical properties were evaluated from experimental tests and Gibson-Ashby models were fitted to describe the relation of the Young's modulus and the relative density of the different structures evaluated. Results of the optimized weight 'lattice structures were competitive with actual SLM 316L stainless steel lattice structures.

Summarizing, research of optimization applications in all scales is developing, leading to more efficient structures.

2.2. Eccentrically Braced Frames (EBFs)

In steel construction, framed structures are very popular. Moment resisting frames (MRF) and concentrically braced frames (CBF) are the most utilized. Regarding seismic performance, MRF have a high level of ductility, making them an excellent option to dissipate energy during seismic events, however, this property lead to a lack of lateral stiffness, which can cause story drifts beyond the drift limitations. Thus, the design of MRF is guided by the drift design instead of performance strength design. In the other hand, CBF have a high level of lateral stiffness and a low level of ductility, then, for CBF to be utilized in high seismic zones a special detailing is required to ensure that frames behave in a specific manner.

Eccentrically braced frames (EBFs) were developed to combine the properties of MRF and CBF, while reducing the disadvantages. In EBFs, the axial forces in the braces are transmitted to the column through bending and shear in the beams. If properly designed, the system may possess more ductility than concentrically braced frames while retaining the advantage of reduced horizontal deformations which braced frames have over moment-resisting frames. Such system also conforms to requirements of 'failure mode control', with the inelastic behaviour being largely confined to selected portions of the beams, referred to as 'links' (e) and sudden failure modes being suppressed. However, considerable attention should be given to issues related to the repairability of the link areas.

2.2.1. EBF system

The use of EBF systems was first developed for resisting seismic actions in Japan in the 1970s during that decade several experiments demonstrated that Eccentrically braced frames were effective to resist forces caused by earthquakes. There are several configurations for EBF systems, presented in *Figure 2-15* along with their performance mechanism. In EBFs, yielding is concentrated in the links while the rest of elements are designed to remain essentially elastic. Then, during seismic actions links can be considered as structural fuses that will dissipate the earthquake input energy by means of a controlled plastic deformation.

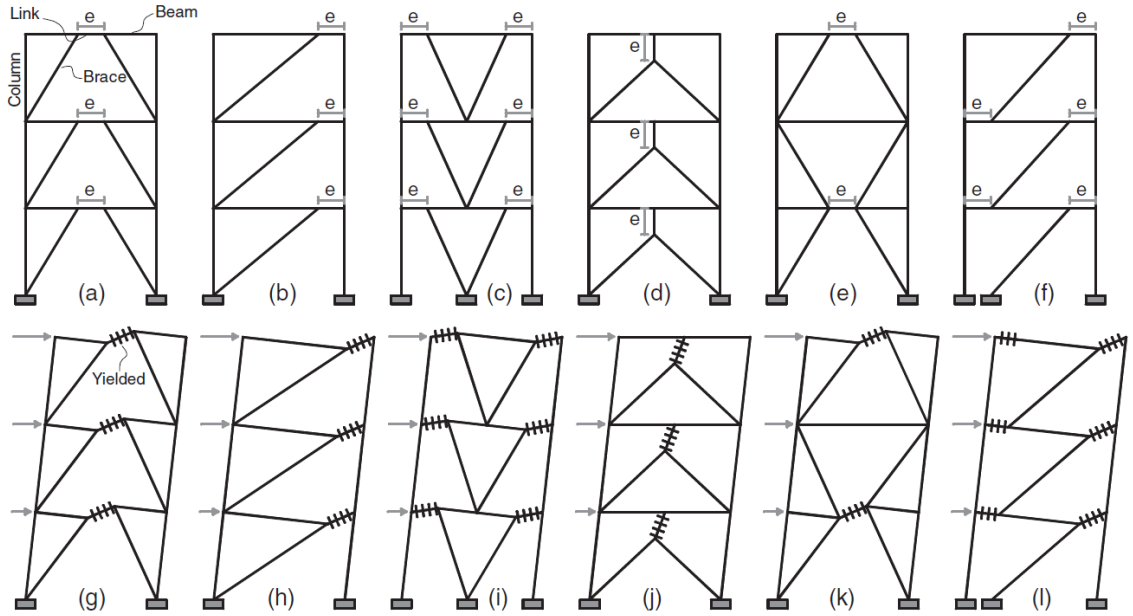

Figure 2-15 EBF configurations and their corresponding mechanisms [16]

The typical design approach for in EBF systems is the capacity design, which designs to ensure concentration plastic behaviour and yielding in the links while keeping the rest of elements in the elastic behaviour range. To do so, in the current practice, an elastic design is conducted, first sizing the links and then the rest of the members are designed to resist the loads generated by the yielded and strain hardened links.

To ensure that the links yielding is produced before the yielding of the rest of the structure, an overstrength factor Ω must be used during the design of members surrounding the links to estimate the maximum loads applied on these members by the yielded link. Overstrength factors provided differently by design codes.

During the design process, it is necessary to determine the distribution of shear and bending stresses within the link to predict a possible plastic mechanism formation. To determine bending stresses, moments at the ends of the links are determined. The moment has not necessarily to be of the same value at both ends of the link. For example, in cases (a) and (e) in *Figure 2-15*, the links are located in the centre of the span (internal links) and the moments are almost equal throughout a seismic loading, while for the rest of the cases the links is connected to a column (external links) or to the floor slab in case of vertical links (case (d)), then, the moments are not equal at both ends of the link during in the elastic range.

Additionally, in order to achieve an efficient design of a multi-storey building, it is necessary to pursue a reasonable distribution of links inelastic behaviour along the height of the building. An undesired design of the dimensions of the links would cause yielding only in the links located in lower stories, leading the building to a soft story mechanism, reducing

considerably its deformation capacity. Despite the correct plastic distribution along the EBF system height and a global deformation mechanism is achieved, the energy dissipation is non-uniform, concentrated in the first and last storey links.

2.2.2. Link characteristics

As mentioned previously, links are the main dissipative zones that determine the behaviour of EBFs. Studies and codes provide different formulations to simulate their behaviour. Their length 'e' is one of the key parameters which controls stiffness, strength, ductility, and behaviour of the overall system. Longer links provide more architectural freedom for openings and potential replacement, however whereas studies demonstrate that short links behave better under seismic actions as they provide higher stiffness, strength, and ductility.

The link yield behaviour is typically measured using its length ratio, defined in *Equation 2.8*:

$$\rho = e/\left(M_p\ /V_p\right) \tag{2.8}$$

Where e is the eccentricity of the link and M_p and V_p are the plastic moment and the plastic shear capacity of the link. Based on equilibrium, considering equal end moments and no moment-shear interaction, considering an elastic-perfectly plastic material the theoretical dividing link length ratio between shear dominated and flexure dominated behaviour is $\rho = 2.0$ [?]. In short or shear links, the predominant plastic mechanism is the yielding of the web, while in long or flexure links, a flexural yielding controls the plastic behaviour of the link. Experimental studies state that there is a gradual transition from shear-dominant yield behaviour and flexural-dominant yield behaviour between $\rho = 1.6$ and $\rho = 3.0$, where a shear-moment interaction modifies the plastic domains. Then three types of link are differentiated: short(shear) links, long (bending) links and intermediate (shear-bending) links.

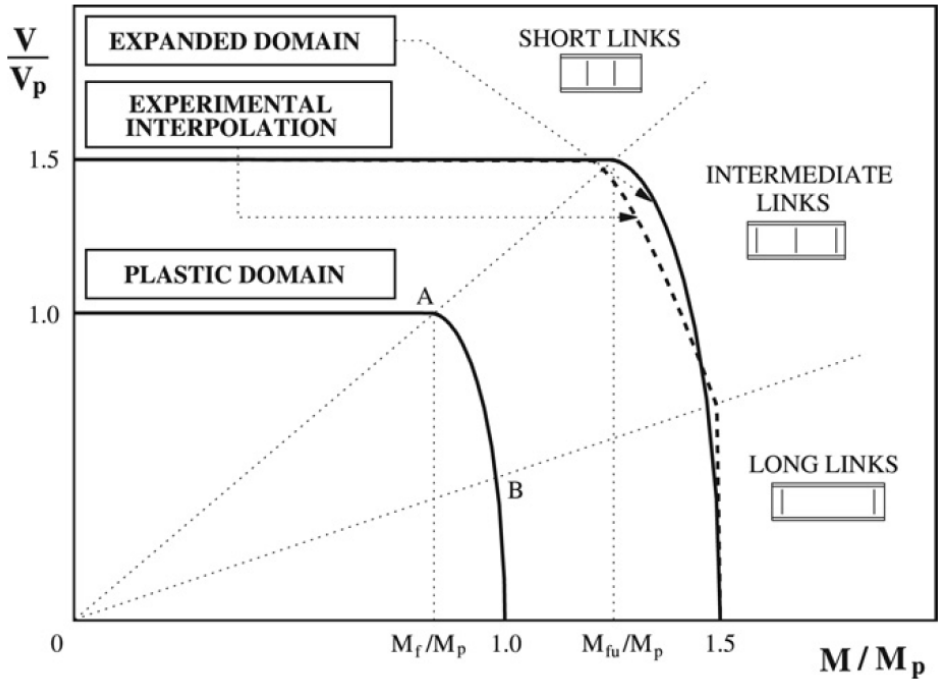

Figure 2-16 V-M interaction diagram and comparison between ultimate interaction domains[20].

In *Figure 2-16* can be seen the shear-moment interaction diagrams of the links, with a clear separation for short links, where shear stresses in the webs represent the mayor resisting force summed to the moment contribution of the flanges; long links which basically work resisting flexure stresses; and intermediate links that, according to the experimental observation the curve is corrected to descend linearly from short link behaviour to long link behaviour. In the graph, there are represented two different domains: the plastic domain, which represent the plastic-shear interaction takin as domain boundary the plastic shear strength and the plastic resisted moment; and the experimental expanded domain, which takes into account the overstrength of the link for the design of its adjacent members, multiplying the overstrength factor considered by the previous domain boundaries (in the case of the graph the overstrength has been taken as 1.5). A structural element other than the link which plastic shear force and moment are within the experimental expanded domain could suffer from an early yield, and thus do not reach the capacity design conditions.

In most cases, to achieve a stable and controlled responses against seismic actions, EBF links need from the collaboration of intermediate and end web stiffeners. Links without stiffeners may suffer from severe strength degradation due to buckling in different parts of the link. For short links, the potential buckling may occur within the link web while in long links, loss of strength is not necessarily caused instabilities in the web but mainly due to buckling in the link flanges, approximately at a distance of 1.5 times the width of the flange from the end of the link while for intermediate links, both failure may occur at the same time. Then stiffeners are essential to increase the strength and energy dissipation of links.

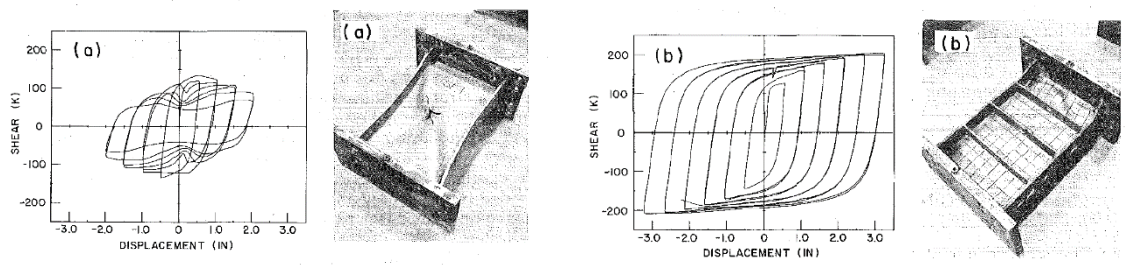

Figure 2-17 Hysteretic behaviour and collapse of a short link without stiffeners (a) and with stiffeners (b)

In *Figure 2-17* it can be observed that the hysteretic behaviour in figure (a) present a histogram which is translated in a low energy dissipation of the due to stress degradation after buckling of the web, while in figure (b), the link provided with the stiffeners increase clearly its performance, providing larger rotation capacities with no strength degradation in the cycles, which is translated to large energy dissipation.

As previously mentioned, an overstrength factor is needed to meet the objectives of capacity design approach, then it is necessary to estimate the maximum shear force that can be developed by the link (Equation 2.9) when strain hardened. The rest of the structural elements shall remain elastic when resisting this maximum shear force (V_{max}), then, its underestimation may lead to unfavourable ductile failures of the structural system.

$$V_{max} = \Omega(R_y V_n) \tag{2.9}$$

$$V_n = \min\left(V_p, \frac{2M_p}{e}\right) \tag{2.10}$$

Where R_y is the ratio of expected to nominal yield stress, determined using statistical data for each steel grade; V_n is the nominal shear capacity and Ω is the overstrength factor due to strain hardening. Generally, a value of $\Omega = 1.5$ is suggested, since it results a good upper-bound for links that are not extremely short with $\rho < 1$, which overstrength factor is clearly underestimated due to their high deformation capacity (see *Figure 2-18*).

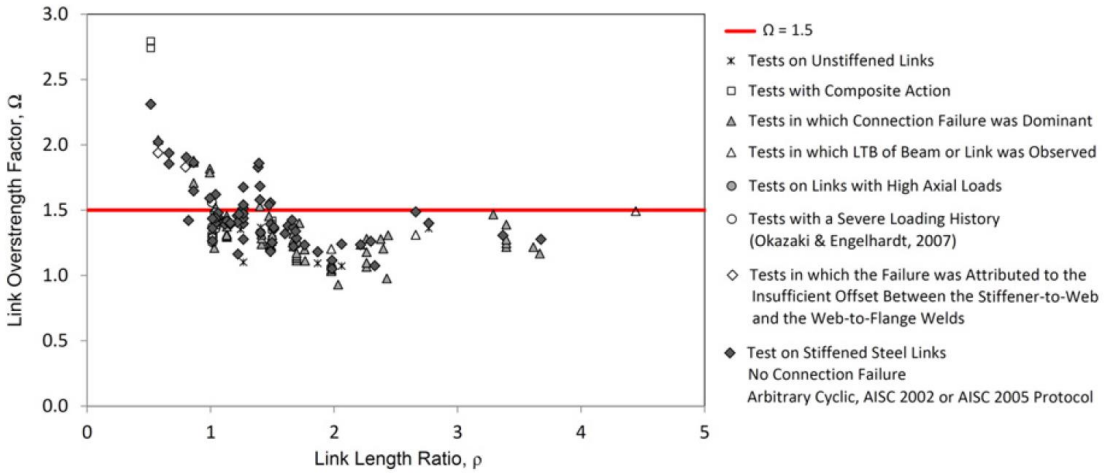

Figure 2-18 Link overstrength factor for different experimental studies.

Despite *Figure 2.18* shows overestimated overstrength factors for intermediate EBF links, it still guarantees the accomplishment of ductile behaviour prescribed by the capacity design approach.

2.2.3. Research and Modelling of EBF links

Behaviour of EBF links and adjacent members have been widely studied. Research on this structural element would necessarily require a huge amount of economic resources to get results from experimental studies, then, most of research on this topic is also companied with numerical models that can efficiently predict the behaviour of the links. Also be said that part of this research is focused only in the development and verification of this numerical models.

Typically, for localized studies on specific regions of the links, general FE models are used: G. Della Corte et.al. [17] conducted an analytical and numerical study on the overstrength in shear links carrying out a parametric study basing on the axial strength acting on the link, the ratio of the link flange and the ratio between the link depth and the cross-section depth. To do so, an FE model using shell elements in ABAQUS was used, in which steel was modelled by means of Von Mises yield and non-linear hardening was applied. Stress deterioration was considered applying the option of large deformations, which resulted to be effective, and the boundary conditions at the nodes located at the ends of the link were slaved to master nodes, one at each end. Displacements transverse to the links axes were imposed to simulate the deformation of the link (see *Figure 2-19*). The effects of residual stresses, geometric imperfections and fracture phenomena were not considered since they seem not affect results when links are subjected to large plastic deformations. The theoretical predictions and experimental test results indicate that the proposed model is able to predict the mechanical behaviour of the links in terms of stresses and displacements. The parametric study show that the larger is the area of the flanges and the shorter the link, the larger is the link shear force developed leading sometimes to an overstrength higher than 2.

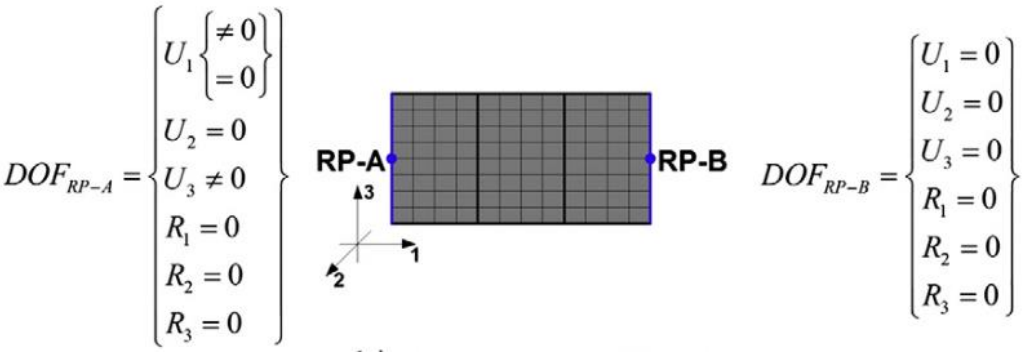

Figure 2-19 Link model using shell elements and slaved ends to reference nodes A and B [17].

Paul W. Richards & Uang [18] and Mohebkhah & Chegeni [19] developed similar models using shell elements to study the effect of flange width-thickness ratio on links and the overstrength and rotation capacity for EBF links made of European IPE sections. Their model is depicted in *Figure 2-2*0). Those models were also validated with previous experimental data matching with the experimental results. In [18] it was observed that actual improvements in steel classes allow a relaxation in the requirements for width-thickness ratio for the American code, while realizing that stiffeners that stiffeners used in links according to codes, that are usually extended from short links, are nonconservative in intermediate and long links. In [19] it is concluded that the American codes are unconservative regarding the use of short IPE sections, that should be increased in about a 10%.

These are just some examples of successful studies carried out basing on computer models of EBF links, which have proven accuracy in the results even not considering second order effects in the structure.

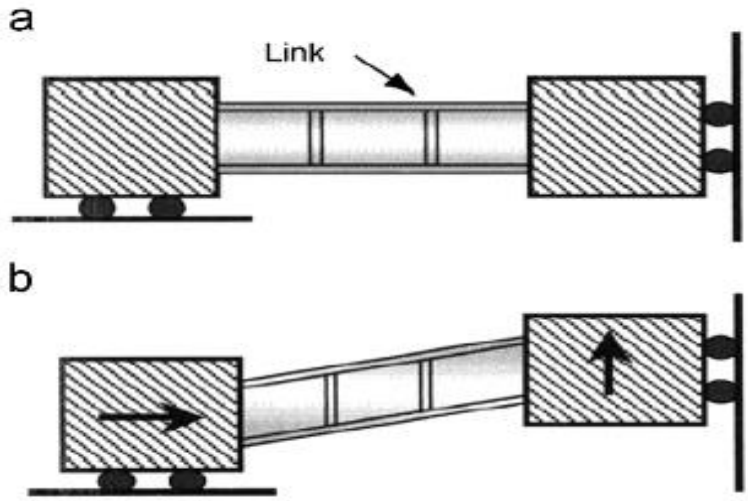

Figure 2-20 (a) model configuration and (b) model deformed configurations [18]..

However, when large scale models are required to evaluate complete structures, the complexity and numerical burden of these methods are replaced by simplified models using a combination of line elements nodal constraints, springs, or plastic hinges. Several authors have tried to develop simplified models to represent EBF mechanism and several pages could be filled comparing their efficiency, complexity, and ease of implementation. Hence, here are presented only models which are used as direct references in this thesis.

Mastrandrea and Piluso [20] presented a procedure for computing the ultimate shear forces and end moments of intermediate link dealing with the problem of shear-moment interaction within the framework of rigid-plastic analysis (see *Figure 2-21*) for different collapse

mechanisms in order to translate the effects of these interactions in a simplified equivalent moment at the link' ends. The study allows to determine the analytical formulations for evaluating the internal actions and the plastic deformations of intermediate links occurring in ultimate conditions (see *Figure 2-16*), also allowing extrapolation of results to pure flexure (long) and pure shear (short) links.

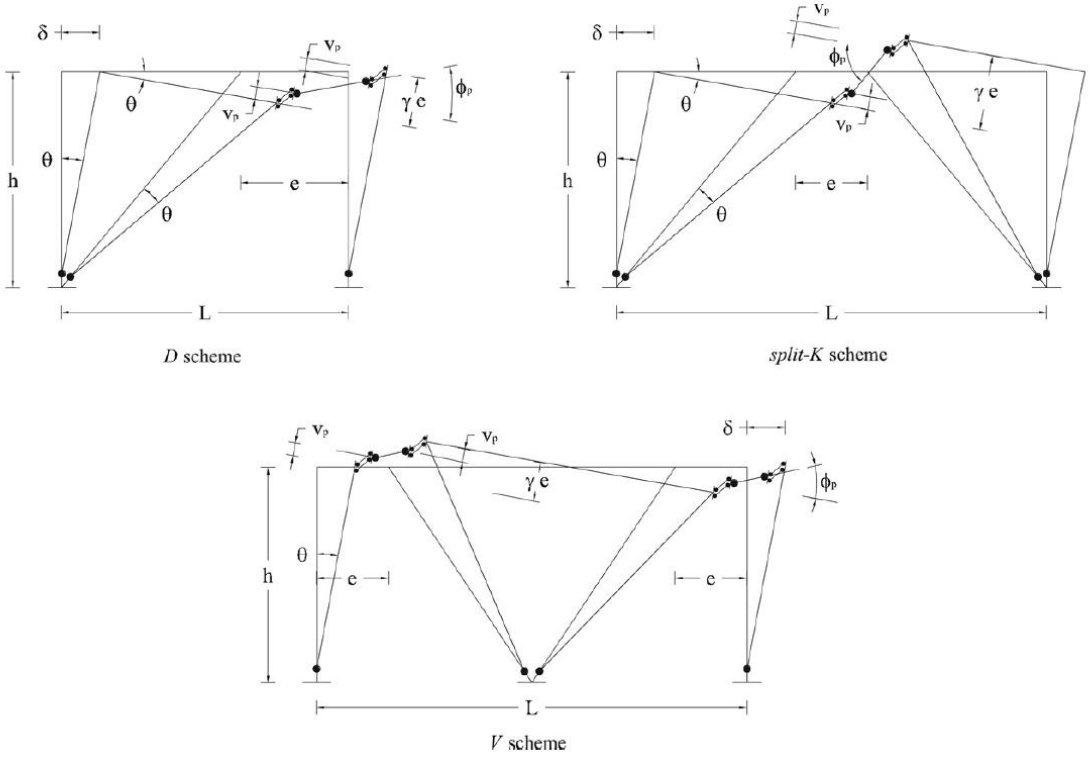

Figure 2-21 Lumped plasticity collapse mechanisms for horizontal EBF links [20].

The formulation of the equivalent moment allowed, through an internal work derivation, representing the complex link behaviour using simple bending plastic hinges, available in most commercial FE software packages in the form of concentrated plasticity (or lumped plasticity). Furthermore, from the equivalent moment definition, it is possible to define simple design criteria to avoid yielding of braces and beams adjacent to the link beam, which is in agreement with the capacity-based design philosophy.

In the same research group, a design method for multi-storey EBF's to assure global failure mechanism of the building was presented [21]: For specific vertical design loads, an 8-storey building model was subjected to push over and seismic analyses to validate the failure mechanism proposed. The analysis were applied on building models in which the links were imposed to maintain a constant link length ratio ρ along the height of the structure for short ($\rho = 1.6$), intermediate ($\rho = 2.3$) and long ($\rho = 3.0$) links. The size of the elements was calculated according to failure mode control methods. Global failure mechanisms were pinpointed for all the models. The results of the analysis showed that short links provide best results, with a high global ductility and energy dissipation and better lateral strength when compared to long and intermediate links, which is consistent with previous experimental and analytical studies.

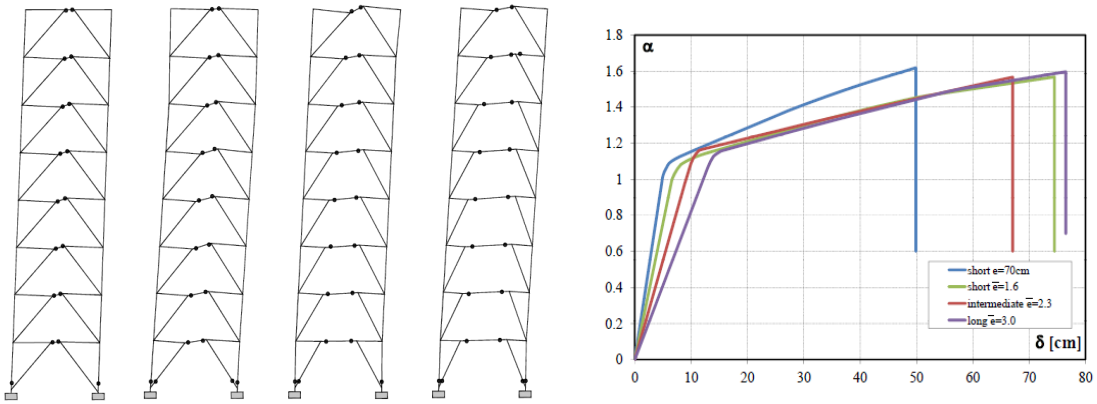

Figure 2-22 patterns of yielding under push-over analyses, showing global failure mechanisms for different link length ratios and capacity curves [21].

2.2.4. Design of EBF links according to EC8

Eurocode 8 [23] provide design and detailing rules for frames with eccentric bracing. In this section, an overview of Eurocode 8 provisions regarding links characteristics and design. EBF links are defined as I -shape beam like dissipators which are divided into 3 categories according to the type of plastic mechanism developed, as mentioned in the previous subsections:

- Short links, which dissipate energy by yielding essentially in shear
- Long links, which dissipate energy by yielding essentially in bending
- Intermediate links, which is a mix of the previous links, where bending and shear occur at the same time.

The link length ratio, $\rho = e/\ (M_p\ /V_p)$, where e is the link length and M_p and V_p are the plastic moment and the plastic shear capacity of the link is the measure used to evaluate the yielding behaviour of the links:

Plastic moment capacity (M_p) $$M_{p,link} = f_y b t_f (d - t_f) \quad (2.11)$$

Plastic shear capacity (V_p) $$V_{p,link} = \left(\frac{f_y}{\sqrt{3}}\right) t_w (d - t_f) \quad (2.12)$$

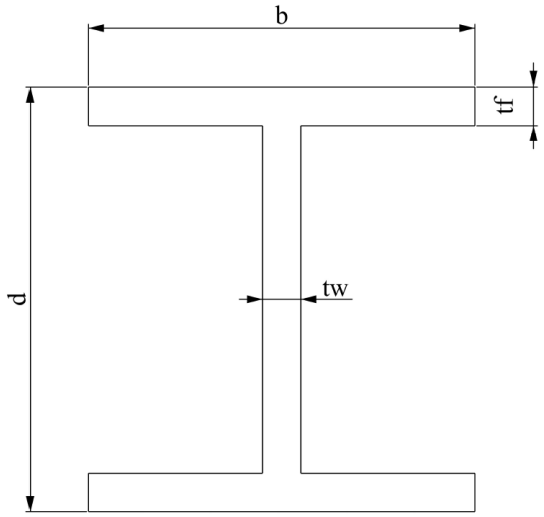

Figure 2-23 design I-beam section for EBFs

Eurocode differentiate shear links (short) and flexure links (long) by means of the link length ratio depending on how moments act in the link. See free body diagram in *Figure 2-24*:

- For designs where equal moments form simultaneously at both ends of the link (for example case *(g)* in *Figure 2-23*), links are classified according to the link length ratio as:
    - Short links when $\rho_s < 1.6$
    - Long links when $\rho_l > 3.0$
    - Intermediate links when $1.6 < \rho_i < 3.0$

- For designs where only one plastic hinge would form at one end of the links (for example in case *(j)* in *Figure 2-15*) link length ratio is modified by α as follows:
    - Short links when $\rho_s < 0.8\ (1 + \alpha)$
    - Long links when $\rho_l > 1.5\ (1 + \alpha)$
    - Intermediate links when $0.8\ (1 + \alpha) < \rho_i < 1.5\ (1 + \alpha)$

  Where α is the ratio of the smaller bending moment at one end of the link in the seismic design situation, to the greater bending moment at the end where the plastic hinge would form.

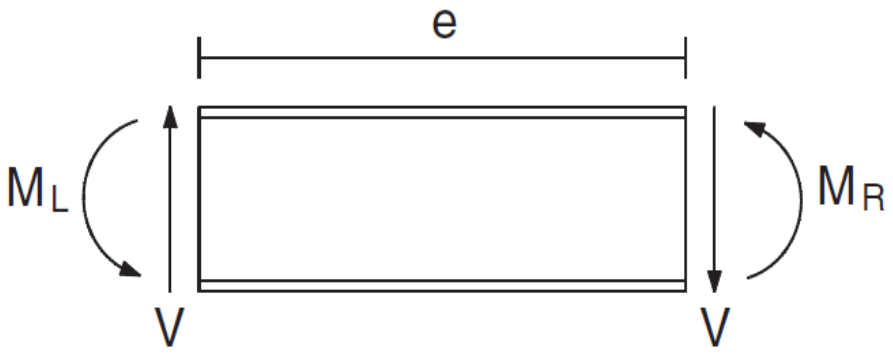

Figure 2-24 Free body diagram o f a link element

If the design value of the axial force of the link in the seismic design situation is not greater than 0.15 times the axial plastic resistance of the link i.e. $\frac{N_{Ed}}{N_{pl,Rd}} \leq 0.15$ the following relations must be satisfied at both ends of the link:

$$V_{Ed} \leq V_p \quad (2.13)$$
$$M_{Ed} \leq M_p \quad (2.14)$$

In the case that $\frac{N_{Ed}}{N_{pl,Rd}} > 0.15$ expressions 1.4 and 1.5 should be satisfied with reduced values of $V_p = V_p \left[1 - \left(\frac{N_{Ed}}{N_{pl,Rd}}\right)^2\right]^{0.5}$ and $M_p = M_p \left[1 - \frac{N_{Ed}}{N_{pl,Rd}}\right]$

The rotation angle between the link element and the outside of the link, θ,also is limited to given values depending on its plastic behaviour:

- For short links, $\theta < 0..08\ radians$
- For long links $\theta < 0.02\ radians$
- For intermediate links θ is determined by linear interpolation between the values for short and long links.

Eurocode 8 also defines the link overstrength Ωi, evaluated in each link using the following relations:

$$\Omega_i = 1.5V_{p,i}/V_{Ed,i} \quad \text{for short links} \tag{2.15}$$
$$\Omega_i = 1.5M_{p,i}/M_{Ed,i} \quad \text{for long and intermediate links} \tag{2.16}$$

and recommend that the individual values of the ratios Ω_i do not exceed the minimum value of Ω_{min} by more than 25% of this minimum value. This provision aims at avoiding partial or storey collapse mechanisms i.e. achieving a global dissipative behaviour of the structure.

2.2.5. Optimization in EBF links

Optimization techniques were developed with the initial objective of improving the efficiency of production in applications for aerospace, automobile and industrial manufacturing sectors. However, as previously mentioned, in structural applications, optimization is still looking for developmental paths. Regarding structural members which function is to serve as a fuse of the structure, as in the case of EBF links, the research applying numerical optimization techniques is scant (experimental attempts are more profuse though). Nevertheless, some authors are starting to use these optimization tools to find advantages in the design of links:

M. Oshaki and T.Nakajima [24] presented a method for optimizing energy dissipation finding the optimum thicknesses and locations of the stiffeners of the link using an heuristic approach called 'tabu'. For a given link was modelled using ABAQUS and the whole optimization process was companied with a python script which generated the new geometry after every optimization cycle and read the FE hysteretic analysis outputs to compute the energy dissipated.

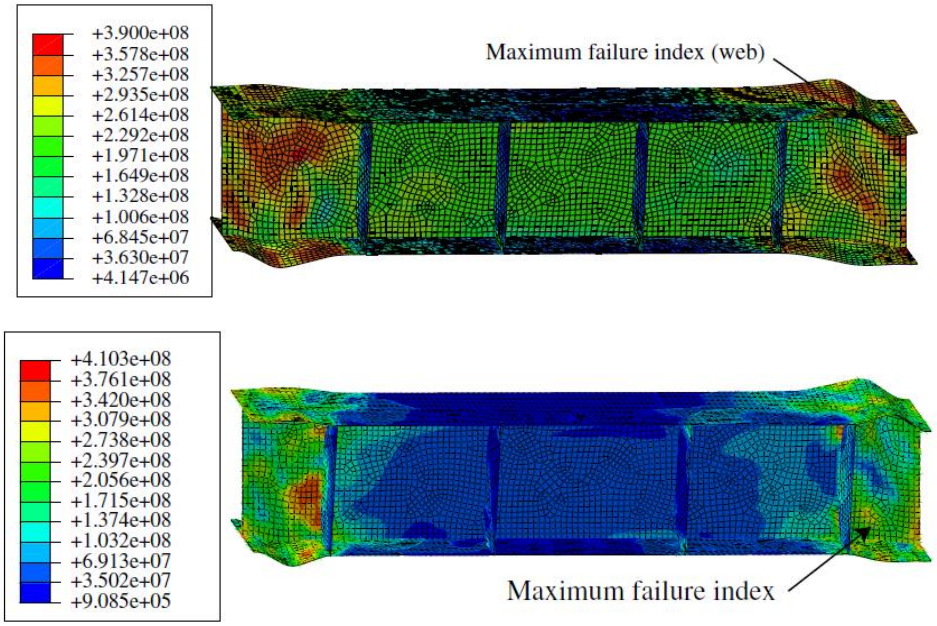

Figure 2-25 On top, stress distribution after FE analysis of a standard link configuration. The bottom figure shows the improved stress distribution in the link [24].

The results showed that the energy dissipation can be considerably increased by modifying the variables of thickness and location of stiffeners despite a large computational cost.

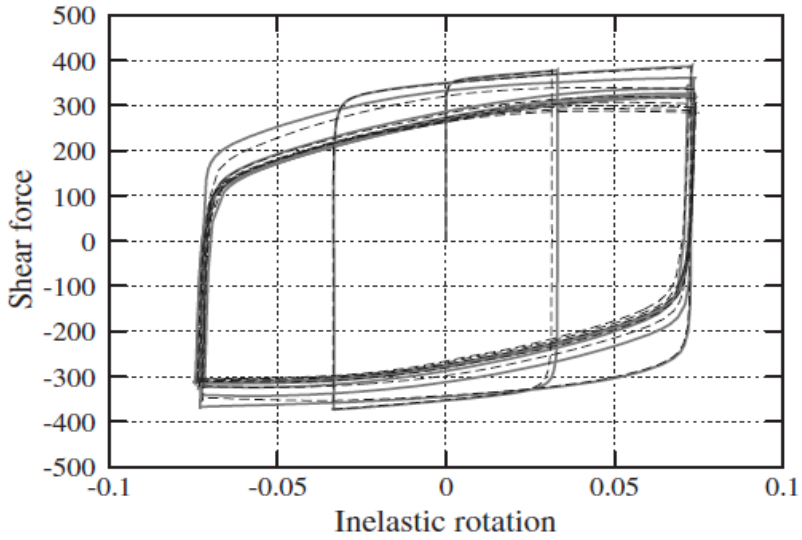

Figure 2-26 In thick grey, optimized hysteretic curve of the link. Dashed, the standard link [24].

2.2.6. Discussion

Eccentrically braced frames are considered as an effective system to provide the building a combination of lateral stiffness and ductility. EBF links have been widely studied in both numerical and experimental research and standardized by different design codes. Few are the studies aiming to optimize the geometry of the links and the use of advanced numerical tools for topology optimization have not been used yet.

Then, in the following chapters, with the aim of improving the whole topology of the links, topology optimization tools that can be found in a FE commercial software package are used in order to find new design paths that can improve links economically and mechanically. However, the application in real cases of the optimized geometries of the links is strictly linked to additive manufacturing (AM) technologies, since the expected shapes are complex and not possible to create with traditional manufacturing techniques. Then, a brief introduction is made to current AM status in the following chapter.

2.3. Additive manufacturing in construction

Additive manufacturing (AM) has gained popularity in aerospace and biomedical industries and is now being explored to be used in the construction sector. Construction sector is still using traditional design and manufacturing methods leading to a loss of knowledge upon project completion and a greater risk of accidents. AM offers numerous benefits over conventional manufacturing methods: greater structural efficiency, geometric freedom, free customization and reduced material use, among others.

Nowadays, concrete AM is more developed and utilised in construction than polymer or metallic printing. There can bee seen multiple projects using concrete AM to build office and residential builds and various pedestrian bridges [28] as the Winsun houses and offices or the Castilla la Mancha park bridge (See *Figure 2-27*). These projects had reduced labour time and no use of formwork or any other kind of auxiliar construction was used, reducing the cost and providing new geometries that could not have been provided using traditional manufacturing techniques.

Figure 2-27 To the left, a Winsun dubai office building; to the right, the Castilla la Mancha park bridge [28].

Metal additive manufacturing in construction is still at an experimental stage. The manufacturing times and the processing and post-processing of the models can still be very time-consuming. In exchange of traditional manufacturing methods as hot-rolling, cold-forming and extrusion, there exists various additive manufacturing methods to work with materials as aluminium, stainless steel or carbon steel, which are very used in construction. The most promising methods are powder bed fusion (PBF) and directed energy deposition (DED).

In powder bed fusion PBF, material within a powder bed is selectively fused together using thermal energy from a laser or electron beam. This method is useful for elements with complex geometries; however, it is limited to elements with a very reduced size (within 250 mm^3) that need to be contained in an inert environment [28].

Directed energy deposition (DED) features metallic powder or wire being fed directly into the focal point of a heat source, resulting in a molten pool that can be selectively deposited [28]. Powder based DED has similar characteristics and limitations than PBF.it is used for high complexity geometries and it is limited to reduced geometries treated within an inert environment. On the other hand, wire and arc AM techniques (WAAM) are suitable for medium to large parts, being able to build entire structures with low to medium geometric complexity. WAAM technique consists in using arc welding tools and wire to build up a component formed entirely from the deposited weld material. The combined conceptual simplicity and the effectiveness of WAAM make it the most promising AM technique for construction, to which a lot of research and investment is being dedicated.

Pinelopi Kyvelou et.al. conducted a study regarding the structural performance of WAAM material [29]. In the study, tensile tests were conducted in flat plates built using WAAM with different thickness, finishes (as-built and machined) and printing orientation (0º , 45º and 90º with respect the loading direction) in order to determine the influence of the geometrical irregularities and the anisotropy of the resulting material.

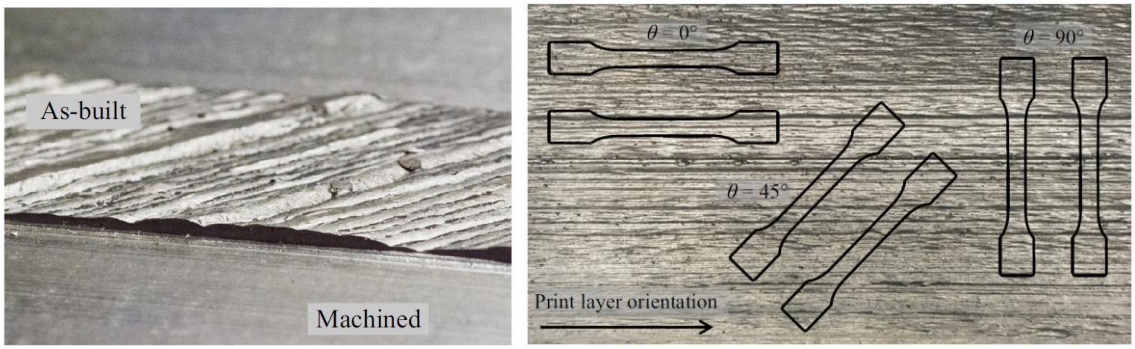

Figure 2-28 Manufacturing results and material orientations of the plates [29].

Results showed a high anisotropy, where the specimens loaded 90º with respect the direction of the printed layers exhibited the lowest properties while the specimens loaded at 45º showed the higher values of strength and young modulus. Furthermore, the young modulus presented a high degradation in specimens with non-treated finishes, due to the geometrical variations.

Pioneering projects using AM have been developed using WAAM powered by robotic arms, like the MX3D bridge, which is the first additively manufactured pedestrian metal bridge (see *Figure 2-28*). It was designed, modelled, built and tested by Arup engineers in collaboration with researchers from the Imperial College of London. The bridge has a width of 2.5m and a span of 10m. In 2019, the bridge passed the final load test, supporting more than 20 tones and a next stage is being approached in which UT Twente in collaboration with Autodesk are going to add sensors on the bridge to collect usage and material data [30].

Figure 2-298 MX3D pedestrian bridge[?].

2.3.1. Discussion

Since AM technology is developing satisfactorily, it is conceivable that in a few years this type of practice in the design of structures will begin to take center stage. In this way, to study the optimization results on elements like horizontal EBF links makes sense since the results are projectable in the short-medium term. In the following chapters, modelling and optimization methods, results and evaluation of horizontal EBF links are presented.

3. Numerical modelling

To conduct topology optimization on EBF links a series of hybrid numerical models (beam and solid elements) are developed. Stresses are applied to the links to drive them to the optimization conditions, and then topology optimization is conducted given those conditions. To do so, ABAQUS FEA software package is used in companionship with Rhinoceros for some of the post-processing

Abaqus is a Finite Element Analysis software package developed by Dassault Systems commonly used for multi-physics and various engineering disciplines [25]. The Abaqus software package has different products designed for different applications within its own suite. Abaqus/CAE is used to generate the models i.e. generate the geometries of the different 'parts' of the model, applying loads, boundary conditions, etc; to manage the different analysis 'jobs' and to visualize the results. Abaqus/Standard use to provide accurate stress solutions in static and low speed dynamics and other Abaqus products like Abaqus/Explicit and Abaqus/CFD are used for transient dynamics and impacts and fluid dynamics and heat transfer, respectively.

In this study, Abaqus/CAE altogether with Abaqus/standard and Abaqus Topology Optimization Module (ATOM) are used. The aim is to get a series of topological outputs considering shear and flexure EBF links conditions for different link sizes. To do so, the models constructed are based on the performance of a single-storey EBF of 3 meters high and 6 meters of span adapted to the different links eccentricities, as it can be seen in *Figure 3-1*. In this section is shown a step-by-step explanation of the generation of the models.

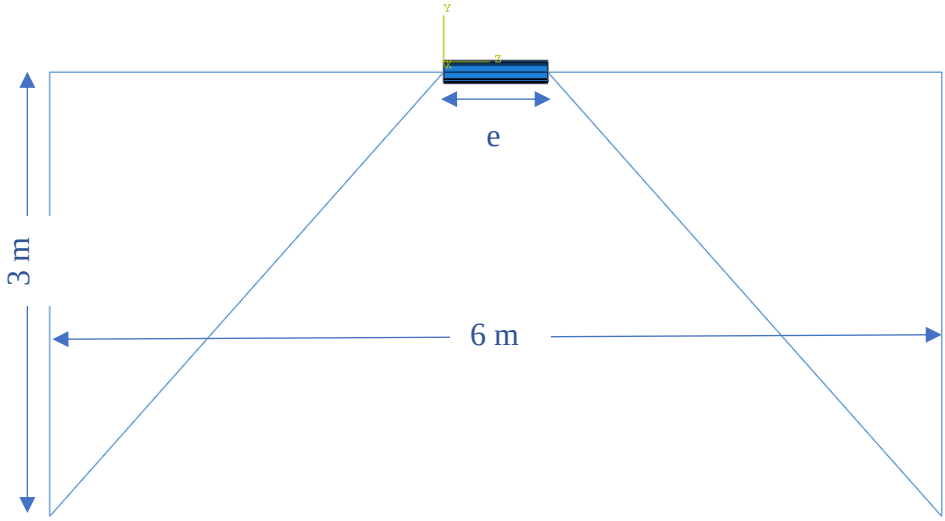

Figure 3-30. General frame to be modelled.

3.1. Geometry

The first step is to create the geometry. For the links, 3D solid deformable element type was selected to generate the whole I-shaped section. According to the literature review, those are the most common shapes to be used in EBF links. No stiffeners are modelled at this stage since the objective of the study is to search new improving paths for links, the topology optimization outputs will be compared to the behaviour of an I-shaped beam that has not been modified to conceptually see which new design approaches to improve them when carrying the task of building fuse.

The links were modelled according to the links used in a current EBF design extracted from Mastandrea and Piluso [20] were HEB sections were used. Four different sections using S275 steel, HEB140, HEB160, HEB180 and HEB220 are modelled according to the dimensions provided in EN1993-1-1:2005+AC2:2009, Sections 6.2 and 6.3. As previously mentioned, both shear (short) and flexure(long) links are generated according to the definitions appearing in EN 1998-1:2004 in which long links are defined with a link length ratio $\rho_l = 3.0$ and the short links with $\rho_s = 1.6$. For the calculations of the link lengths, equations 3.1 to 3.3 are used:

$$e = \rho \times \frac{M_p}{V_p} \tag{3.1}$$

$$M_p = f_y \times W_p \tag{3.2}$$

$$V_p = \frac{f_y}{\sqrt{3}} \times tw \times (d - t_f) \tag{3.3}$$

Where 'e' is a length that defines the link eccentricity, 'ρ' is the link length ratio, 'M_p' is the plastic moment capacity of the section and 'V_p'is the plastic shear capacity of the section; 'f_y' is the plastic limit of the steel material and 'W_p'is the plastic modulus of the section; 'tw' is the thickness of the web of the section, 'd' is the total height of the section and ' t_f' is the thickness of the flanges

Figure 3-2 shows a typical modelled beam while *Tables 3-1* and *3-2* show, respectively, the mechanical characteristics and geometric characteristic of the beam. *Table 3-3* represent the calculation done to determine the final length of the links to study.

(a) HEB160_LONG (b) HEB160_short

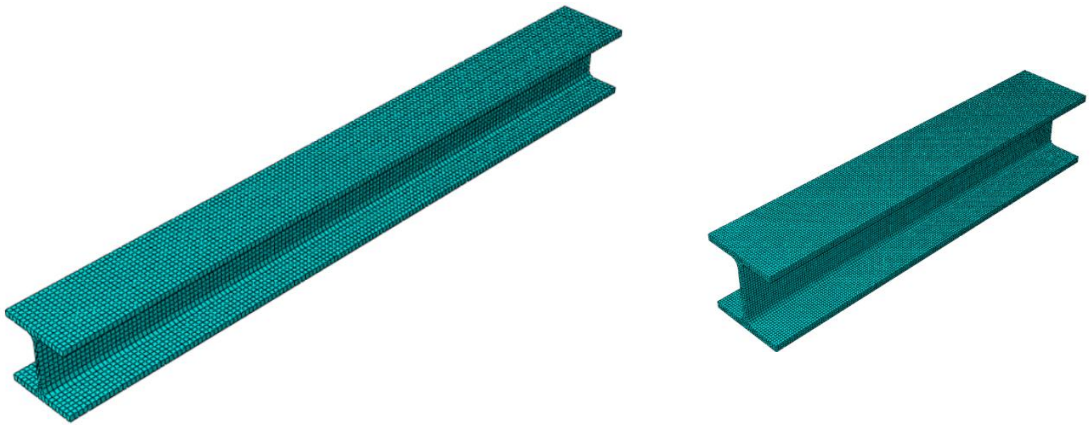

Figure 3-31. Geometry model for the beam: example for HEB160 flexure beam and shear beam.

Link Section	d (mm)	b (mm)	tw (mm)	tf (mm)	r(mm)
HEB140	140	140	7	12	12
HEB160	160	160	8	13	15
HEB180	180	180	8.5	14	15
HEB220	220	220	9.5	16	18

Table 3-1.Geometric properties of the sections in the model

Link Section	A (mm2)	Iy ($x10^6$ mm4)	Wel,y ($x10^3$ mm)	Wpl,y ($x10^3$ mm)	fy (Mpa)
HEB140	4296	140	215.6	245.4	275
HEB160	5425	160	311.5	354.0	275
HEB180	6525	180	425.7	481.4	275
HEB220	9104	220	735.5	827.0	275

Table 3-2 Mechanical properties of the sections in the model

Link Section	M_p (Nmm)	V_P (N)	ρ	e (mm)
HEB140_short	67485000	142259,1063	1.6	750
HEB140_long	67485000	142259,1063	3.0	1424
HEB160_short	97350000	186715,0771	1.6	830
HEB160_long	97350000	186715,0771	3.0	1565
HEB180_short	132275000	224026,3382	1.6	940
HEB180_long	132275000	224026,3382	3.0	1775
HEB220_short	227425000	307698,826	1.6	1180
HEB220_long	227425000	307698,826	3.0	2220

Table 3-3 Tabulation with the calculation of the eccentricities for the modelled links

For the structure adjacent to the links, linear beam elements are used according to the design that can be found in [?], which ensure that the bases of capacity design are accomplished, and the plastic dissipation is concentrated in the links. All sections assigned to such linear elements are also HEB profiles of different sizes, summarize in *Table 3-4:*

Model	Short links (ρ=1.6)				Long links (ρ=3.0)			
	Link HEB	Beam HEB	Diag. HEB	Col. HEB	Link HEB	Beam HEB	Diag. HEB	Col. HEB
1	140	140	200	180	140	140	140	120
2	160	160	200	200	160	160	180	140
3	180	180	200	200	180	180	240	140
4	220	220	200	220	220	220	260	200

Table 3-4 sizes of the elements for the EBF frames

To ensure that both types of elements work as one single structure when the calculations are done, a kinematic coupling has been established in the junctions between the frames and the links, to ensure that the movement of the frame transmits displacements and rotations to the link ends.

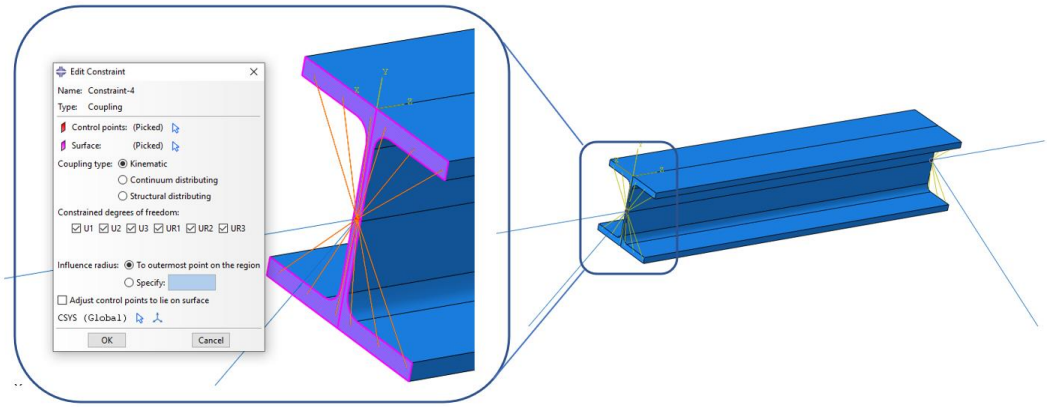

Figure 3-32. Kinematic coupling of the frames with the links.

3.2. Material

The material used for all the elements in the model carbon steel S275. Material properties are defined according EN1993-1-1, EN10025-2 Hot rolled products- Non alloy structural steels:

Material property	**Value**
Density	7850 kg/m^3
Young's modulus (E)	210000 Mpa
Shear Modulus (G)	81000
Yield strength (fy)	275 Mpa
Ultimate strength (fu)	430 Mpa
Poisson ratio	0.3

Table 3-5 sizes of the elements for the EBF frames

The non-linear behaviour of the material is represented by a bilinear curve: the elastic range is defined by the yield strength following the strains that the elastic modulus E provide. The non-linear range is represented by a straight line from the yield point to the ultimate strength at a maxim strain of a 20% (see Figure 2-3):

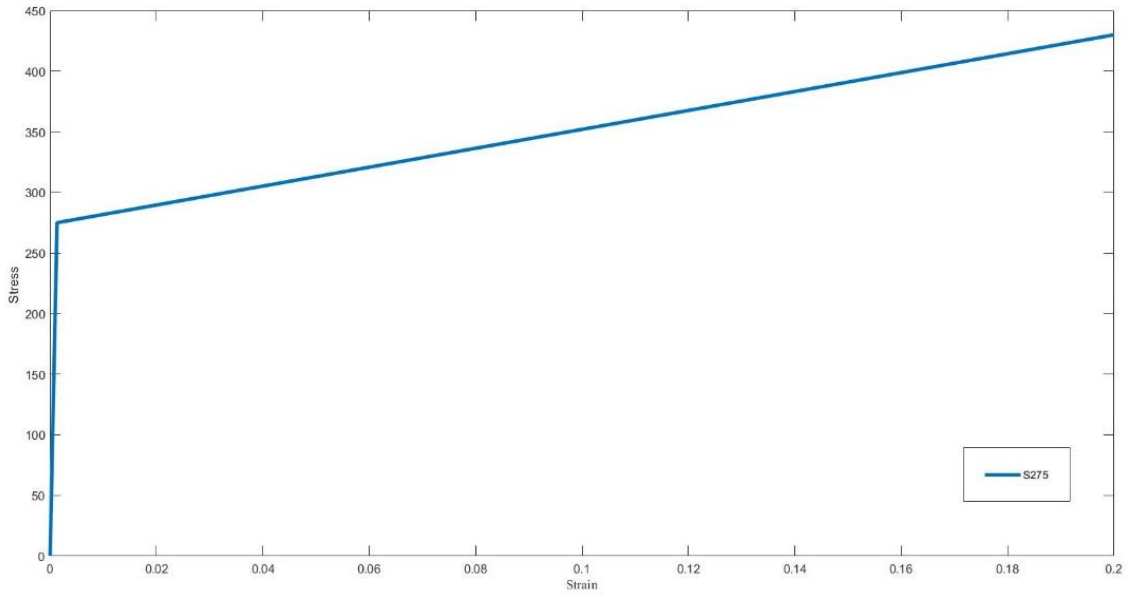

Figure 3-33. S275 bilinear curve to represent its non-linear behaviour.

3.3. Boundary conditions

The optimization process is highly sensible to the way the boundary conditions are set up. Despite the configurations described in section 2.1, the process to apply the boundary conditions did not start using a complete frame in the model but a sub-part. Consequently, it is needed to describe all steps that led to adequate simplifications of the final boundary condition configuration.

Initially, auxiliary SAP2000 push-over analysis of multi-storey building were used in order to determine, from the results, the rotations and displacements of the ends of the links and apply them directly on an isolated link model in Abaqus. The SAP2000 model was based on linear elastic elements with concentrated plastic hinges at specific locations of the building, including both link ends.

However, to ensure global plastic behaviour of the structure with the aim to get realistic rotations in the links, the plastic hinges needed to be specifically configurated consistently with the design of the building, as it done in the design case in [21]. Then it is decided to derive analytically the rotations and displacements at the ends of the links, following the formulation used in [22] corresponding to the plastic hinges design in [20]. The formulation is based on single storey EBF plastic mechanisms using plastic hinges, defined in Figure 3-5:

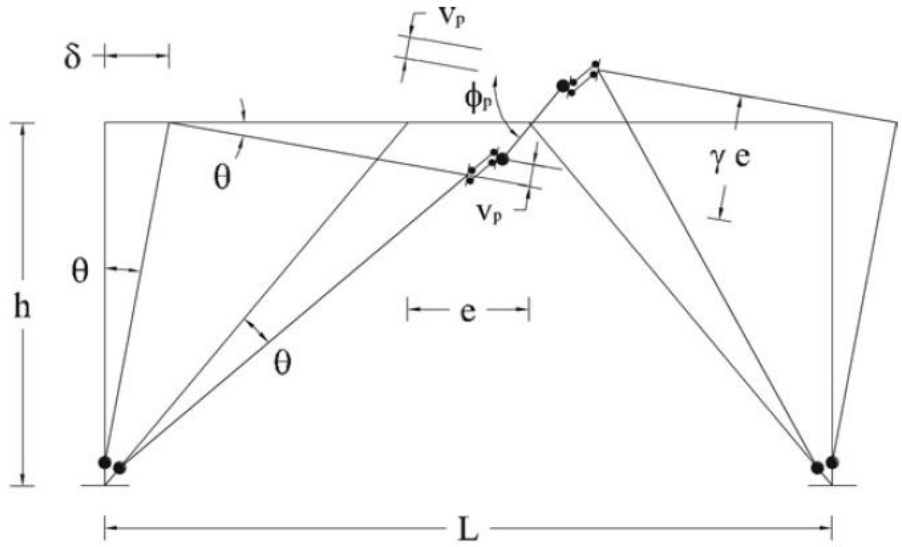

Figure 3-34. single-storey model with concentrated plastic hinges for EBF systems [20].

The variables showed in Figure 3-5 were able to track the movement of the ends of the links after an imposed lateral displacement on the frame. This procedure was implemented in the optimization process that is presented in other chapters of this document, however the final position of the end nodes of the links cannot describe their entire deformation path, and thus can not provide accurate time-dependent stress distribution within the links that can generate realistic optimized elements.

Then it is concluded that the adequate boundary conditions need to be applied through an auxiliary structure, i.e. the frames, that deform compatibly with the link and represent as accurately as possible all the stress path that the links are subjected to. The final model design is homologous to the one presented in *Figure 3-5* using fully non-linear elements, which is computationally expensive but importantly, provide more reliable results.

A displacement-controlled analysis is conducted over the frames applying a displacement δ at one of their top corners to cause incremental lateral displacement of the frame and

consequently the link undergoes plastic deformation. For simplicity, vertical loads are not applied in the frames.

The boundary conditions at the base consist of pinned nodes that allow full rotation of the columns and diagonal members. The overall rotation of the frame concentrates all the stresses in the zones surrounding the link and the link itself. This is the expected behaviour of EBF in which energy dissipation is entirely expected at the links. This approach makes the performance of the frame against a lateral imposed load totally dependent of the performance of the links, and thus, it is easier to compare how modifications in their topology affect the behaviour of the frames since the non-linear contribution of the frame bases do not blur the results of the links' resistance. Other design approaches such as dual MRF-EBF frames allow energy dissipation in beams and/or columns.

A planar analysis was performed in order to avoid out-of-plane instabilities. The frames were pinned to prevent displacement in the out-of-plane direction and provide a bold in-plane lateral displacement (see *Figure 3-6*).

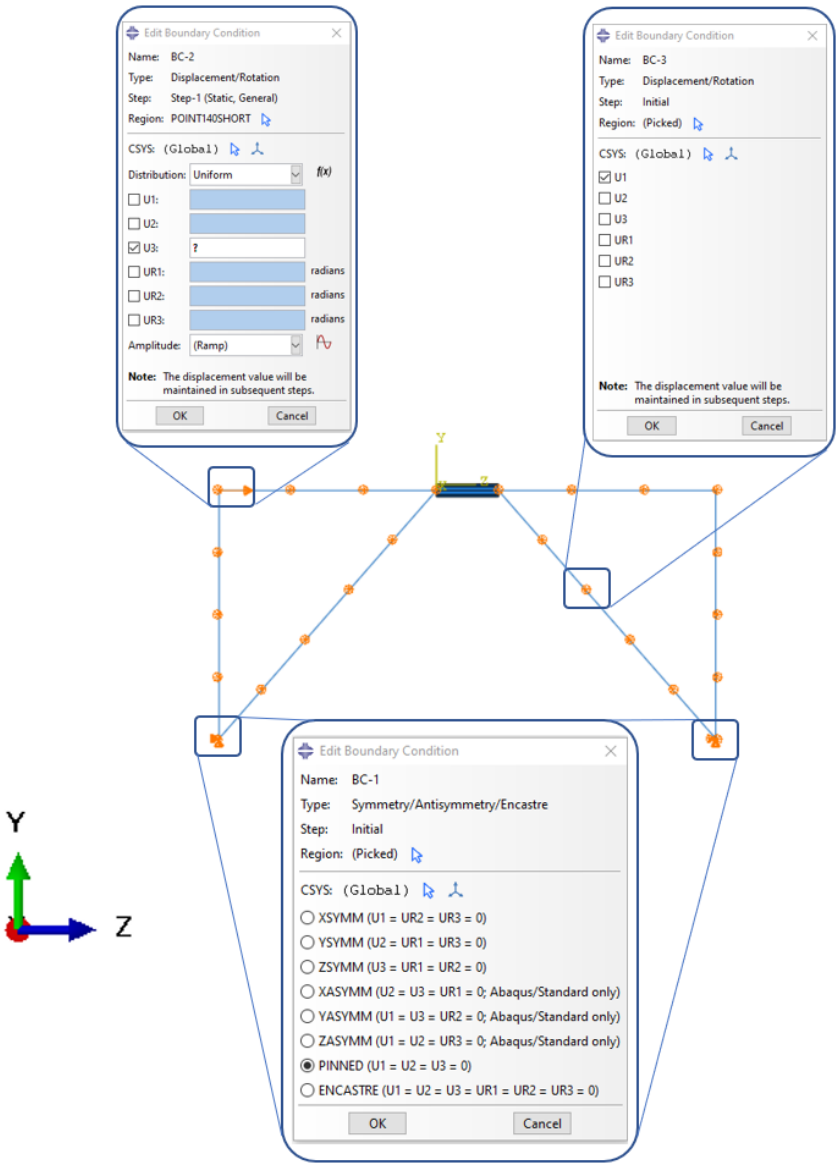

Figure 3-35. Boundary conditions applied in the model

3.4. Mesh

C3D8R element types from Abaqus libraries were chosen for the link model. This is a general-purpose linear brick element with reduced integration (one integration point). This is computationally efficient but due to its reduced integration, it is needed a reduced mesh size to ensure accurate results. For optimized elements, tetrahedral C3D10 elements are used due to their complex geometry.

A convergence study was carried out using the push-over analysis on the smallest link (HEB140). The mesh that showed convergence in the case of HEB140 is used as reference to calculate the mesh elements density, which is applied approximately to the rest of bigger elements. This also ensures accurate results since the same type of problem is being solved. After a full push-over analysis is carried out, it is determined that at a displacement of 10mm the maximum strength capacity of the link is obtained. Then the displacement applied horizontally to the frame for the preliminary study is 10 mm

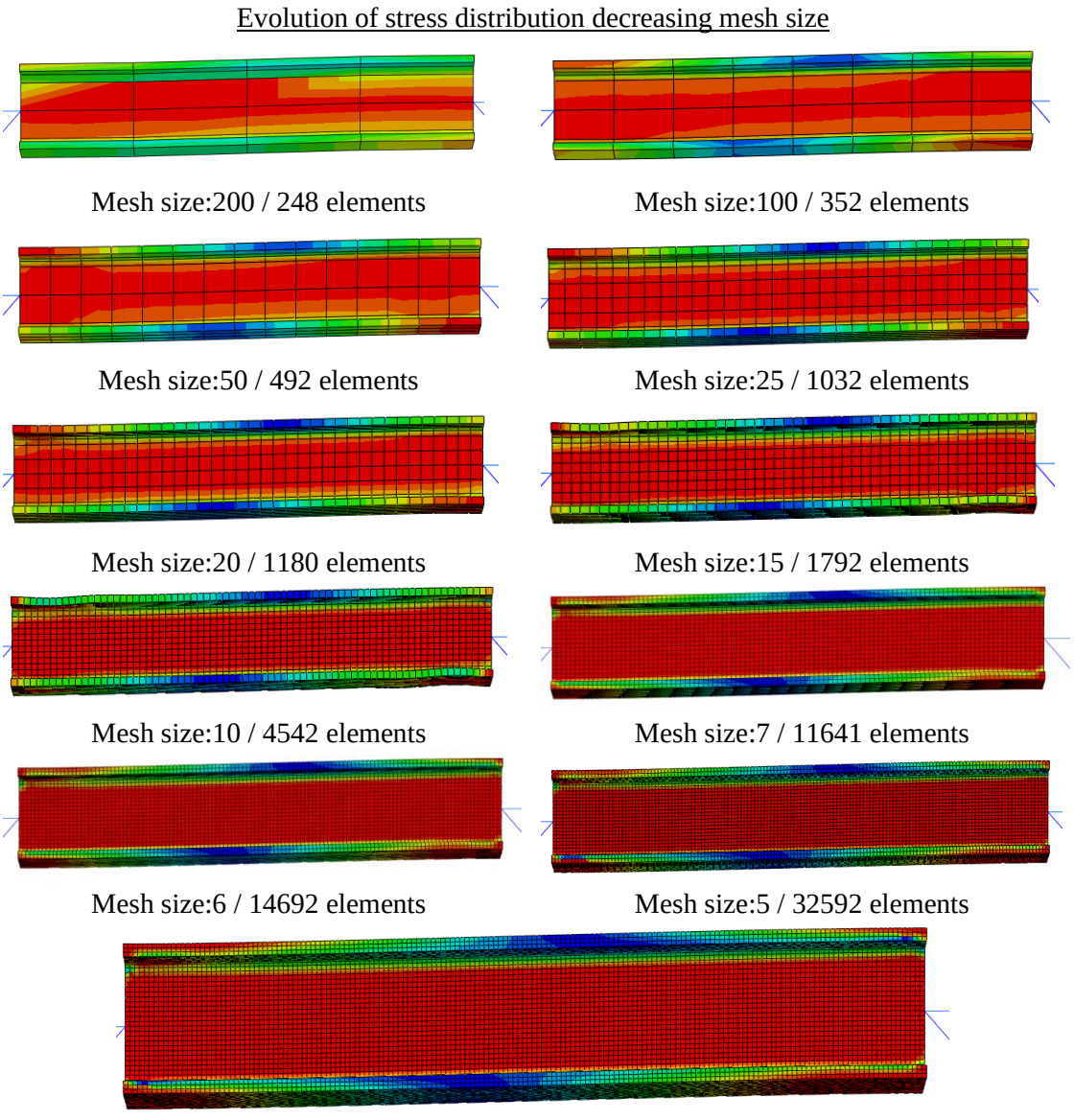

Figure 3-36. Evolution of the stress distribution increasing mesh density

The convergence is considered in terms of displacements and reaction forces of the frame. The reaction forces in the direction of the movement (RF3) have been measured in POINT1, located at the same point where the displacement is applied to the structure while displacements have been measured in POINT2, located at the right end of the link (Figure 3-8).

Figure 3-37. scheme including the points from which the results have been recorded for the convergence analysis

The results from the analyses are plotted in Figure 2-8. The results obtained are unstable for element densities below 3.6e-3 elements per cubic millimetre, corresponding in HEB140 shear link to 11641 elements. Finally, it can be considered that the results converge at a mesh density of 10.11e-3 elements per cubic millimetre, which is going to be considered as the reference density for the calculation of subsequent meshes for HEB160, HEB180 and HEB220. Results are summarized in Table 2-6.

Mesh size	**Nodes**	**Elements**	**RF3 (N)**	**Error RF**	**Disp. (mm)**	**Error Disp.**	**Element density** ($\frac{El.}{mm^3}$)
200	312	248	297389	-	11,36	-	7,6978E-05
100	480	352	294844	0,8558%	11,3539	0,0537%	0,00010926
50	736	492	291931	0,9880%	11,3758	0,1929%	0,00015271
25	1711	1032	291360	0,1956%	11,3691	0,0589%	0,00032033
20	2142	1180	289831	0,5248%	11,3768	0,0677%	0,00036626
15	3354	1792	288688	0,3944%	11,3471	0,2611%	0,00055623
10	7716	4542	288463	0,0779%	11,2942	0,4662%	0,00140981
7	18144	11641	292256	1,3149%	11,3476	0,4728%	0,0036133
6	23184	14692	292138	0,0404%	11,3455	0,0185%	0,00456031
5	**45039**	**32592**	**292597**	**0,1571%**	**11,3395**	**0,0529%**	**0,01011636**
4,5	58464	43278	292633	0,0123%	11,3386	0,0079%	0,01343323

Table 3-6 sizes of the elements for the EBF frames

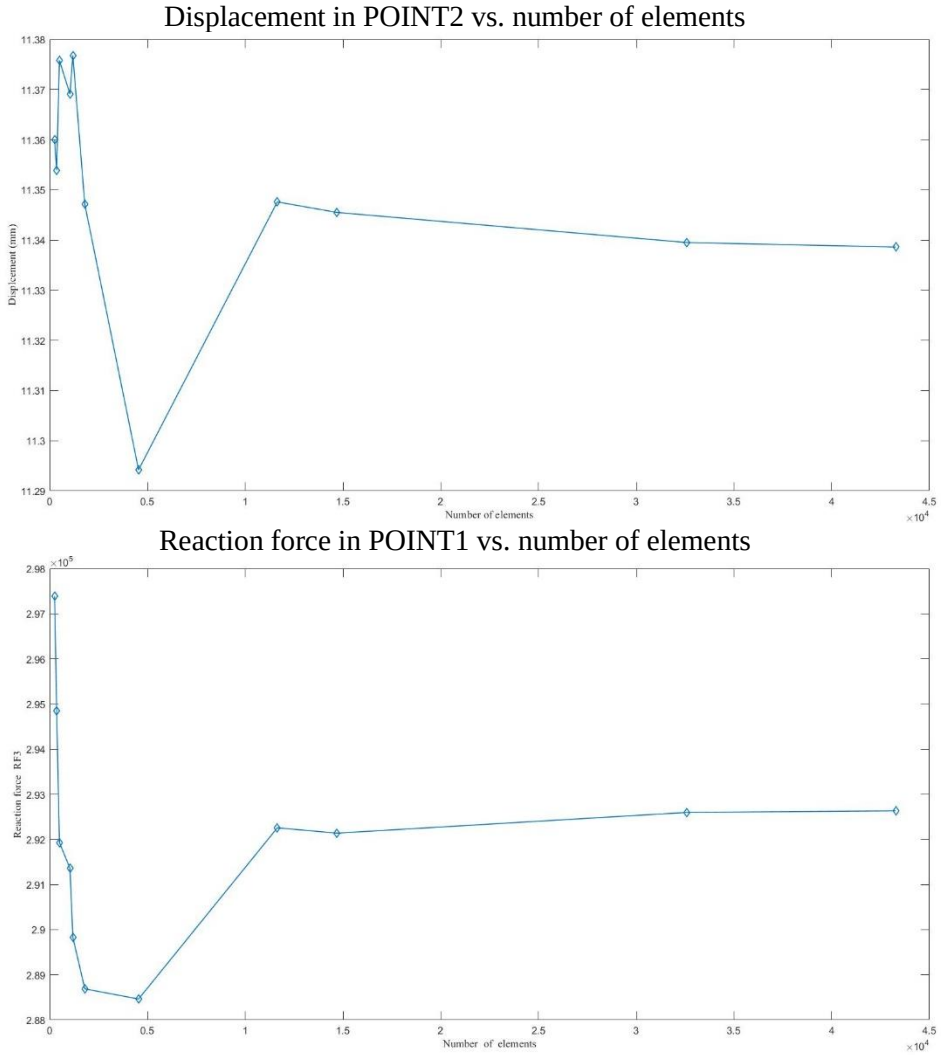

Figure 3-38. convergence curve for displacement and Reaction forces

3.5. The optimization module

In this section, the Abaqus Topology Optimization Module (ATOM) is described. ATOM was launched in Abaqus 6.11 version and it contain two features: Topology optimization and shape optimization. Both types are treated within this TFM. First, some terminology that is needed to understand the optimization process is extracted from the Abaqus user's manual and herein explained:

- *Design area*: The design area is the region of the model that ismodified optimally. This can be the whole model or a subset of selected regions within the model. A topology optimization removes and adds material for elements in the desing area while shape optimization modifies its surface by moving its boundary nodes.

- *Design variables*: The design variables represent the parameter to be changed during an optimization process. In the case of topology optimization, the design variables are the densitiesof the elements, which are changed accroding to prescribed optimization conditions while for shape optimization the design variables are the displacement of the surface nodes.

- *Design cycle:* a design cicle is simply an iteration of the optimization process.

- *Design response:* The inputs of the optimization process are called design responses. They are tjken from the outputs of the analysis through which the optimization is created. Tipacl design reponses are Stiffness, stresses, eigenfrequencies, etc. The design response is associated with a region in the model and it is computed as a single scalar, which can be calculated as the maximum/minimum value or the sum of a design response in a given region.

- *Objective functions:* they are the scalr value extracted from the design response and define the objective of the optimization i.e. the optimization module seeks to maximize or minimize the such scalar value.

- *Constraints:* they are also a single scalar value extracted from a design response which are restricted by the constraint, for example, imposing that the optimization objective must be accomplish achieving a given % of the initial volume of the design area.

The optimization module supports two topology optimization algorithms. The general and the condition-based algorithms. The former, described in [25] offer two density interpolation methods: SIMP and RAMP, it is more flexible and can be applied to most problems. The latter is more efficient, but it is limited to stress, strain and volume design responses. Shape optimization algorithm is similar to the algorithm used in condition-based topology optimization. It is implemented at the end of the design process when the general layout of the model is fixed, and only minor changes are allowed by repositioning the nodes in the surface.

3.5.1. The minimum compliance problem

This TFM bases the optimization procedure in the minimum compliance optimization problem. The compliance, also called the strain energy is stored within an elastic solid when the solid is deformed under load and it can be defined, in absence of other energy losses, as the work done by the solid by external loads.

Consider the work done by an elastic solid by a single point force F. when the elastic solid is subjected to the load F, it deforms with strains ε and γ and the material is subjected to stresses σ and τ. Then the strain energy is defined as U:

$$U = \frac{1}{2}\int \sigma_{xx}\varepsilon_{xx} + \sigma_{yy}\varepsilon_{yy} + \sigma_{zz}\varepsilon_{zz} + \tau_{xy}\gamma_{xy} + \tau_{xz}\gamma_{xz} + \tau_{yz}\gamma_{yz} \tag{3.4}$$

In Abaqus the compliance is defined as the sum of the strain energy all the elements allocated within a same design response a region:

$$U = \sum u^t k u \tag{3.5}$$

Where ‘u’ is the displacement vector and ‘k’ is the global stiffness matrix.

Note that for an imposed load, minimizing compliance implies minimizing the displacement to which the elements are subjected, which means to make the structure stiffer. However, at a given imposed displacement, minimizing the compliance does not increase the stiffness of the structure, but it weakens it. Since the displacements are fixed, the minimization focuses in minimizing the stresses produced by such deformations, providing a structure that does not offer any resistance to deformation and, thus, a weak structure. On the contrary, if any structural optimization problem is dedicated to maximizing the compliance while imposing a displacement, not necessarily will get a stiffer structure but a more energy dissipative structure.

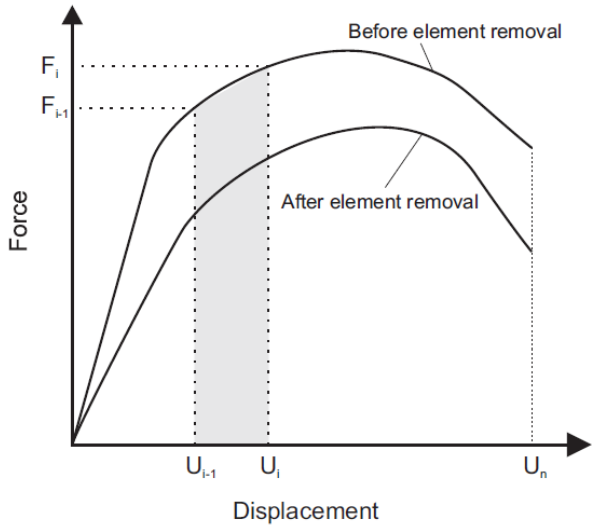

Figure 3-39. Scheme showing the expected result from a compliance problem with imposed displacement

Since the main purpose structural fuses is to absorb energy during large deformations, the topology optimization using maximum compliance problem with displacement-controlled deformations seems to be convenient.

Compliance optimization problems are usually subjected to volume reduction constraints, then, the compliance optimization problem to optimize dissipative elements like EBF links, for a structure discretized in m elements, can be defined as follows:

$$\text{Maximize: } U=\sum u^t k u$$

$$\text{Subject to: } \sum V_e \leq a * V_0 \qquad \text{for e:1}\dots m \tag{3.6}$$

3.5.2. Topology optimization

The compliance problem is a strain-volume optimization which can take advantage of the Condition-based algorithm in Abaqus. Then, a condition-based optimization process of at least 15 design cycles is defined.

The design area must be selected according to the needs of the element. In this case, the optimization results must provide a geometry capable of connecting the link with the adjacent beams avoiding any violation of the boundaries of a HEB beam. Since it still has to support other building elements like floors, a vertical irregularity, even if it could provide a good link behaviour, it is not practical. Therefore, the design area selected is a solid rectangular prism with sizes in height, width and depth which are identical to the corresponding beam for which is trying to provide the optimized topology.

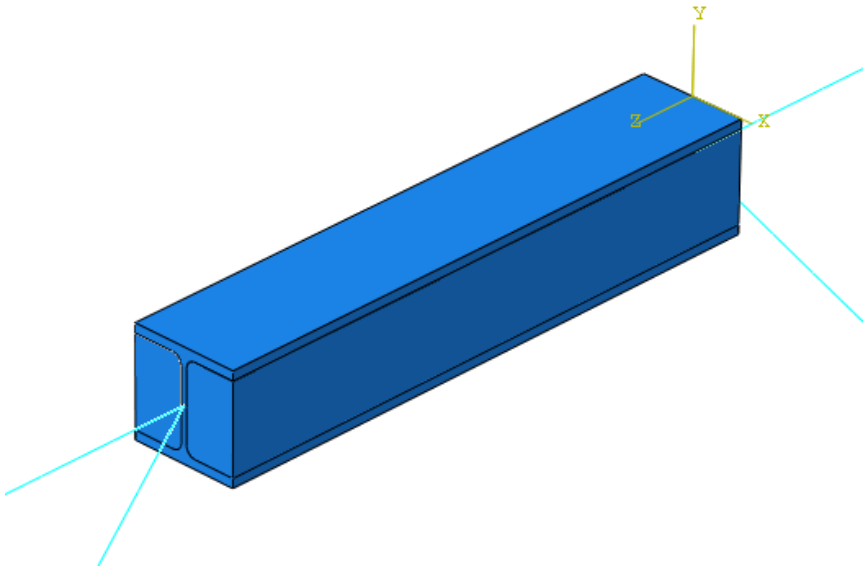

Figure 3-40. Design area of the links

The design responses are the strain energy and the volume of the design area. The objective function is to maximize the strain energy, while the constraints is to reduce the volume. The reduction of volume of the design area is condition by the volume of the corresponding HEB beam: the objective of the optimization is to improve the energy dissipation using at least the same amount of material that is used for actual links. Consequently, the percentage of volume reduction is equal to the volume ratio between the HEB beam and the design area. The calculations for the volume constraints are summarized in *Table 3-7:*

Link section	Link volume (mm^3)	Design area volume (mm^3)	Volume ratio constraint
HEB140_short	3221712.50	14700000.00	21.91%
HEB140_long	6116958.50	27910400.00	21.91%
HEB160_short	4502875.50	21248000.00	21,2%
HEB160_long	8490361.00	40064000.00	21,2%
HEB180_short	6133642.00	30456000.00	20.1%
HEB180_long	11582143.00	57510000.00	20.1%
HEB220_short	10742882.00	57112000.00	18.8%
HEB220_long	20211186.00	107448000.00	18.8%

Table 3-7 sizes of the elements for the EBF frames

3.5.3. Shape optimization

Shape optimization is conducted to the outputs of the previous topology optimization. Like it was previously mentioned, shape optimization is used only when minor changes are needed, then, it is used as a refinement o the results, to improve the behaviour of the link and ensure that all the geometrical constrains area accomplished.

The design area is selected to be the whole surface area of the optimized link. Two design responses are configurated: von mises stresses and the volume of the link. The objective function

for the optimization procedure is set as to minimize the stress localizations within the link element. To compute the stresses, the algorithm uses Von mises stresses:

$$\sigma_{VM} = \sqrt{\sigma_{XX}^2 + \sigma_{YY}^2 + \sigma_{ZZ}^2 - (\sigma_{XX}\sigma_{YY} + \sigma_{YY}\sigma_{ZZ} + \sigma_{ZZ}\sigma_{XX}) + 3(\tau_{XY}^2 + \tau_{YZ}^2 + \tau_{ZX}^2)} \quad (3.7)$$

Or alternatively,

$$\sigma_{VM} = \sqrt{\frac{(\sigma_1 - \sigma_2)^2 + (\sigma_2 - \sigma_3)^2 + (\sigma_3 - \sigma_1)^2}{2}} \quad (3.8)$$

Von mises stresses are calculated in every design node of the link and the surface is modified to minimize them. The constraints are applied using the volume design response, which is set as to maintain the same volume if the topology optimization reached the desired volume fraction, or to reduce volume in case topology optimization procedure did not reach the volume constraints.

All the models herein defined have been structured, among other processes, in a sequence that outputs the optimized geometry of the link. This structure is defined in the following chapter.

4. Numerical study

In this chapter, the design procedure is explained and numerical studies using different optimization configuration and different link sections are presented. The main objectives of the numerical studies are:

- To determine how the obtained results are mesh dependent.

- To determine whether these optimization results vary with the link geometry (short, longs)

4.1. Design Procedure

Any design follows a specific procedure formed by several steps including modelling and post-processing. In the particular case of a EBF, the design is aimed at establishing the final optimized geometry of the link. In this chapter, all the steps are described in detail.

The first step consists of assemblying the frame geometry using the HEB beam sections, applying the corresponding material properties for every section and adding the necessary constraints. This is followed by setting up a push over analyisis on the geometry.

A "Push-Over" is a nonlinear static analysis method where a structure is subjected to gravity loading and a monotonic displacement-controlled lateral load which continuously increases through elastic and inelastic behaviour until an ultimate condition is reached. Generally, it is used for performance-based seismic design, where the lateral load may represent the range of base shear induced by earthquake loading. The push-over analysis outputs generate a static push-over curve, or capacity curve, which plots strength against displacement, The response curve provides insight into the ductile capacity of the structural system, and indicate the mechanism, load level and deflection at which failure occurs (Figure 4.1).

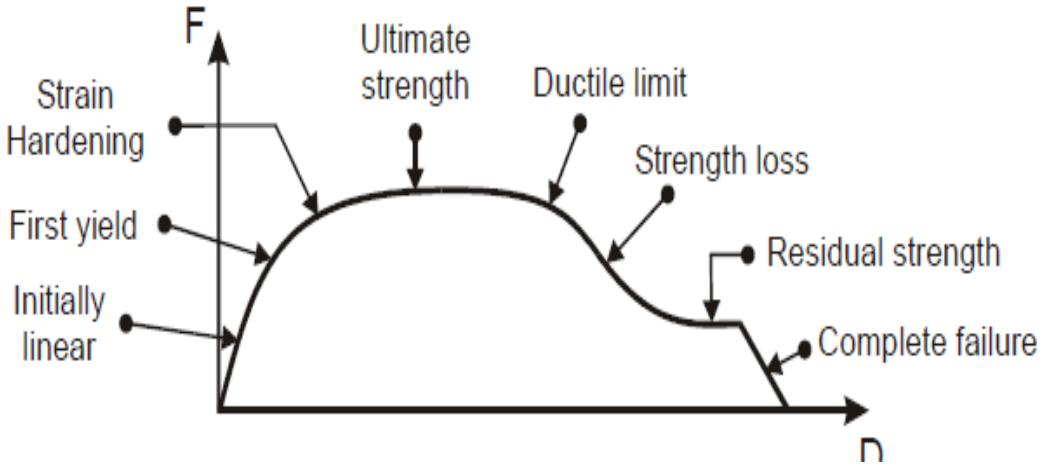

Figure 4-41. Capacity curve indicating typical behaviour stages.

EBF focus most of their lateral resistance on the links. Then, the optimization design is based on the response of the structure when it is submitted to a push-over force, where the behaviour of the frame is considered as a direct cause of the plastic behaviour of the link,

and then, results can be considered equivalent to those which only focus on the behaviour of the link.

The push over analysis set up for the frames using commercial HEB beams have been implemented using a controlled displacement applied linearly on the top corner of the frame. This implemented displacement, from now on denominated δ_{push} , takes a maximum value of $\delta_{push} = 200\,mm$. The capacity curve obtained is expected to show a continuous bilinear shape, accordingly to the bilinear properties of the defined steel to which no failure criteria has been assigned. This initial capacity curve is used as a graphical comparison tool that to check the improved behaviour of the optimized link.

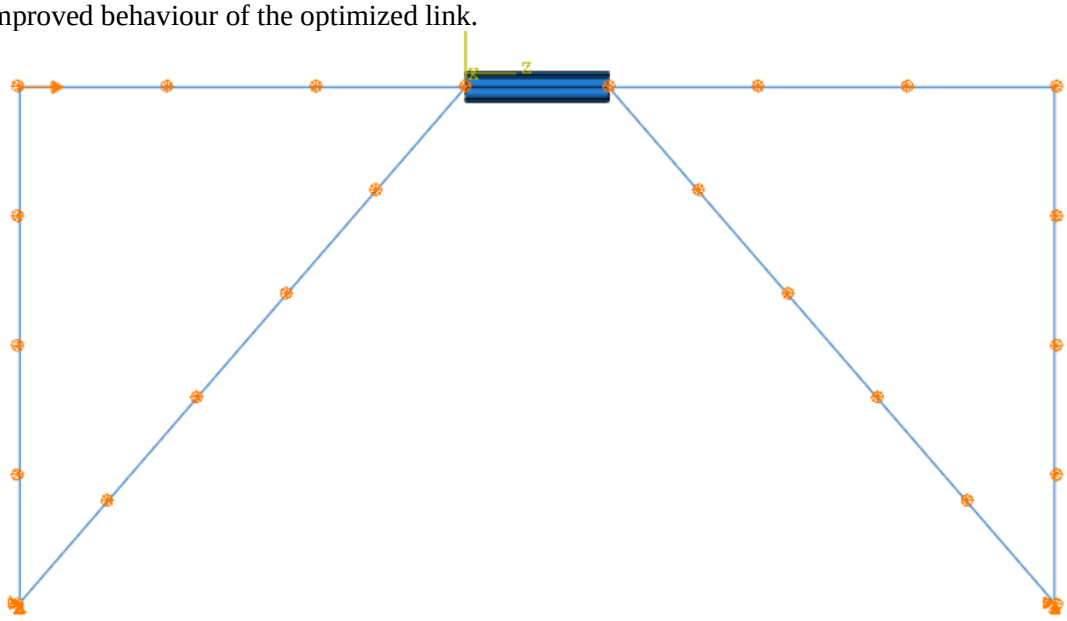

Figure 4-42. Push over configuration for HEB beams.

From the resulting response curve, strategical points located in the capacity curve have been selected to define the displacement δ_{Fmax} applied in the optimization push-over conditions that are defined subsequently. These points are selected according to the following statements.

- As the objective is to increase the capacity of the frame, the displacements where the structure provides the largest reaction force Vmax are desired to be used as optimization condition.

- Then, the point at which the maximum force is registered, for every push-over analysis, is defined.

- Additionally, for every push-over analysis, the point at which the frame yields is defined.

- The displacement selected for the optimization analysis is determined by the capability of the software to converge to a solution. Knowing that if the displacement applied is below the yield point of the frame no convergence problems appear; the final displacement is determined with the displacement of the yielding point as a lower boundary and the displacement at the point of maximum reaction force as an upper boundary.

Therefore, the (δ_{Fmax}, F_{max}) data points from the capacity curve are selected in arrange between the first yield point and the ultimate strength point, depending on the computational limitations.

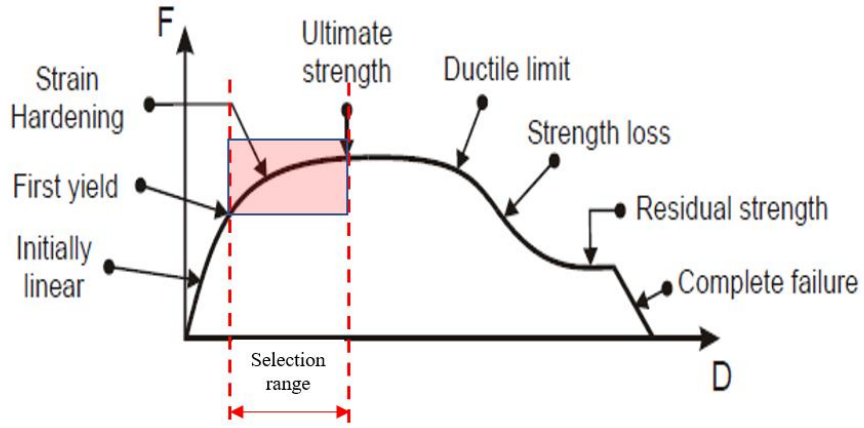

Figure 4-43. Capacity curve indicating typical behaviour stages.

Once the displacement for the push-over analysis that is used for the topology optimization procedure is selected, the design area is created and included in the frame. A topology optimization task is created to maximize the strain energy constrained to the volume percentages given in Table 2-7. The optimization process is initialized and after it is finished, convergence is checked in the objective function and constraints. If the convergence curves are unstable, the optimization constraint is modified to reach the desired stability. If it cannot be reached, δ_{Fmax} is updated and the procedure starts again.

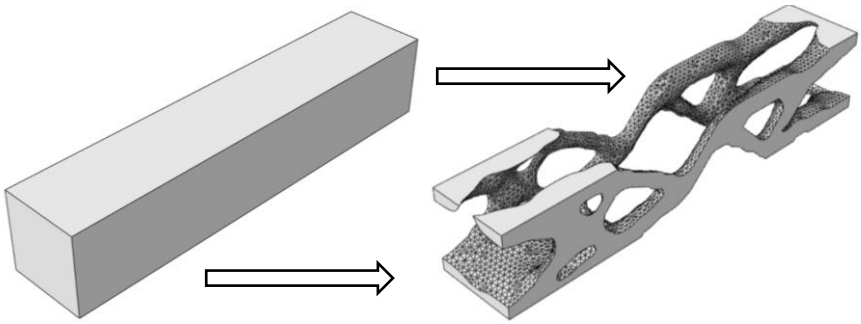

Figure 4-44. Topology optimization output.

The links with optimized topology are extracted in .igs format as a surface mesh. Post processing using Rhinoceros [26] is done to transform the surface mesh into a solid object.

Rhinoceros is a commercial 3D computer graphics and computer-aided design (CAD) application software that is used to create a NURBS surface from the mesh elements and therefore create a volume, which is imported as a new geometry in the Abaqus model.

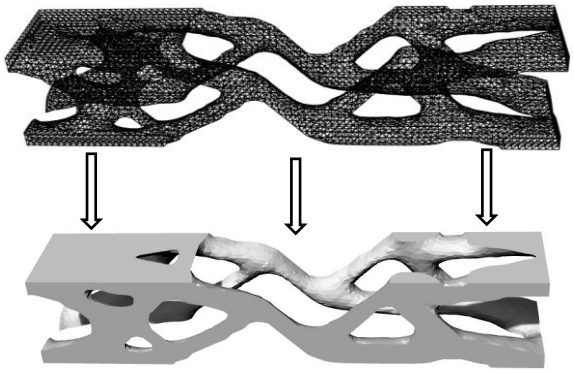

Figure 4-45. Geometry transformation from surface mesh to 3D solid using rhino.

The new geometry is sharp and contains a lot of faces and edges, which makes difficult to do the coupling with the rest of the frame, then the geometry is simplified using virtual topology tool in ABAQUS. The Virtual Topology toolset allows to remove small details by combining a small face with the adjacent face or by combining a small edge with an adjacent edge, which makes the meshing and the assignment of boundary conditions easier.

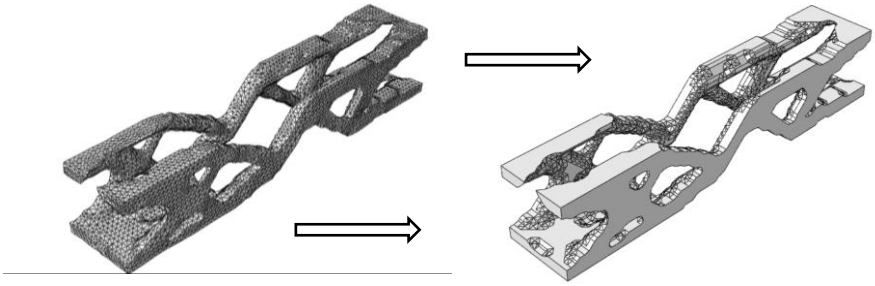

Figure 4-6. Creation of a virtual topology.

Addtionaly, it is checked wether the volume constraints are reached. Generally, the solutions converge to a geometry that outputs a volume slightly above of what is required in the optimization set up, ranging form a 5% to 20% of exceeding material. This volume gap is caluculated and is used as a constraint in the shape optimization process.

Once the model is again defined with the optimized link, the shape optimization is set up to reduce the concentration of stresses. After the shape optimization is finished, a similar post - processing is undertaken and the final link is introduced in the model again. A final push over analysis is done for the δ_{push} stablished at the beginning of the design procedure in order to obtain an improved capacity curve.

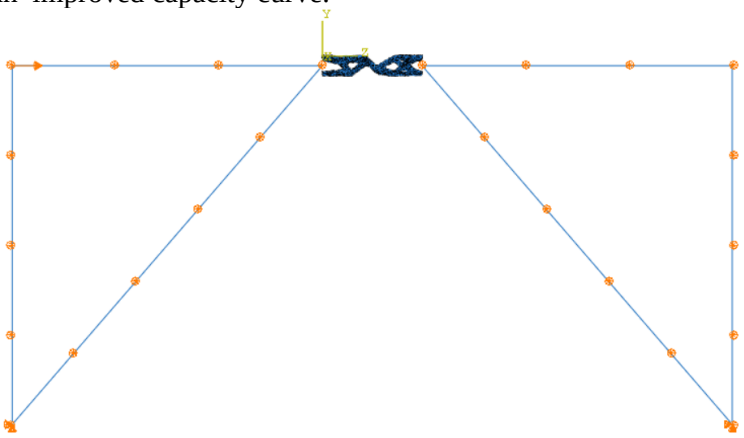

Figure 4-7. Final push over configuration for the optimized link.

The optimized capacity curve provides the needed mechanical information to compare the results in termes of rigidity, maximum strength, yielding, energy dissipated, strength loss, etc. The whole design procedure is summarize in the next squeme and is followed for all configurations that are studied:

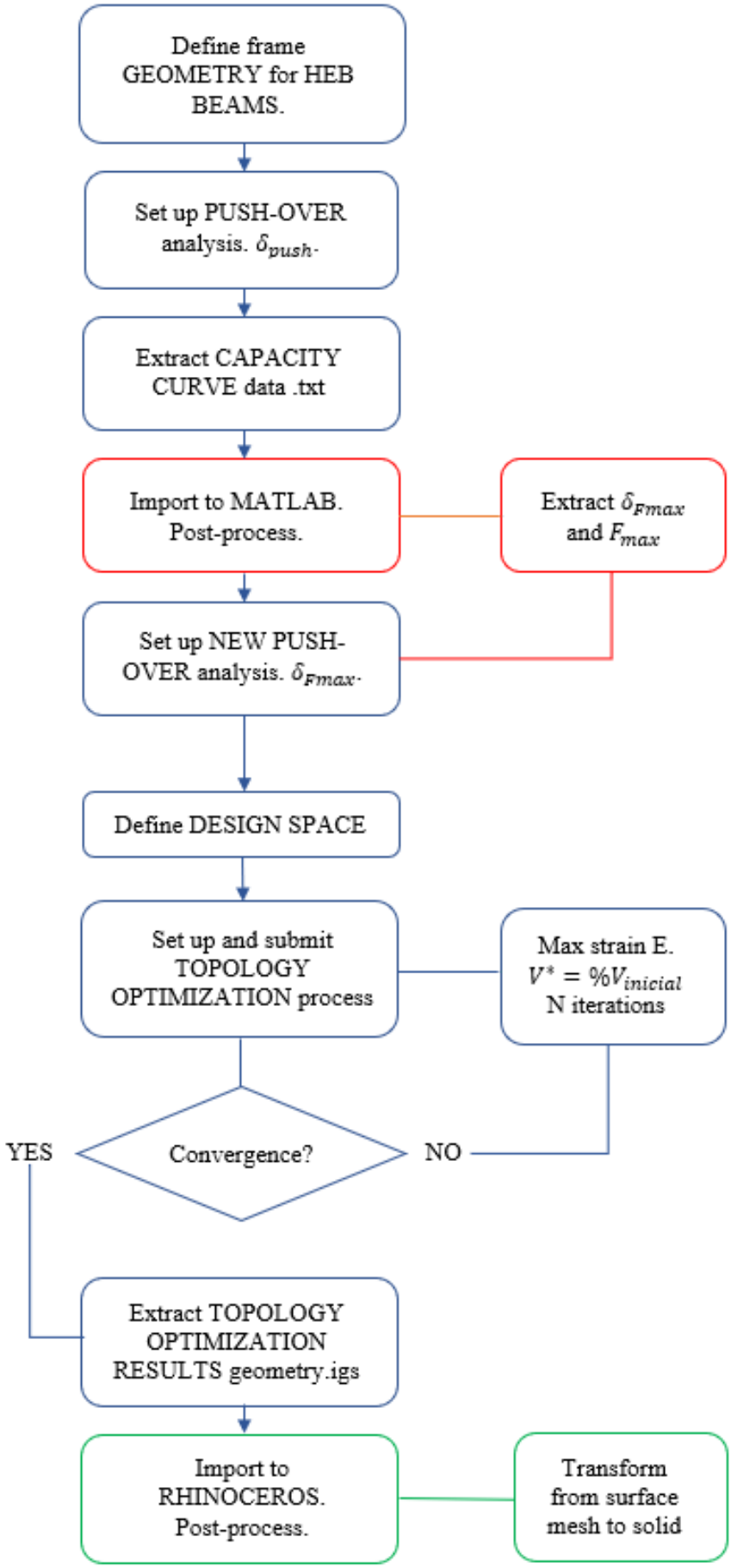
Define frame GEOMETRY for HEB BEAMS.
Set up PUSH-OVER analysis. δ_{push}.
Extract CAPACITY CURVE data .txt
Import to MATLAB. Post-process.
Extract δ_{Fmax} and F_{max}
Set up NEW PUSH-OVER analysis. δ_{Fmax}.
Define DESIGN SPACE
Set up and submit TOPOLOGY OPTIMIZATION process
Max strain E.
$V^* = \%V_{inicial}$
N iterations
YES
Convergence?
NO
Extract TOPOLOGY OPTIMIZATION RESULTS geometry.igs
Import to RHINOCEROS. Post-process.
Transform from surface mesh to solid

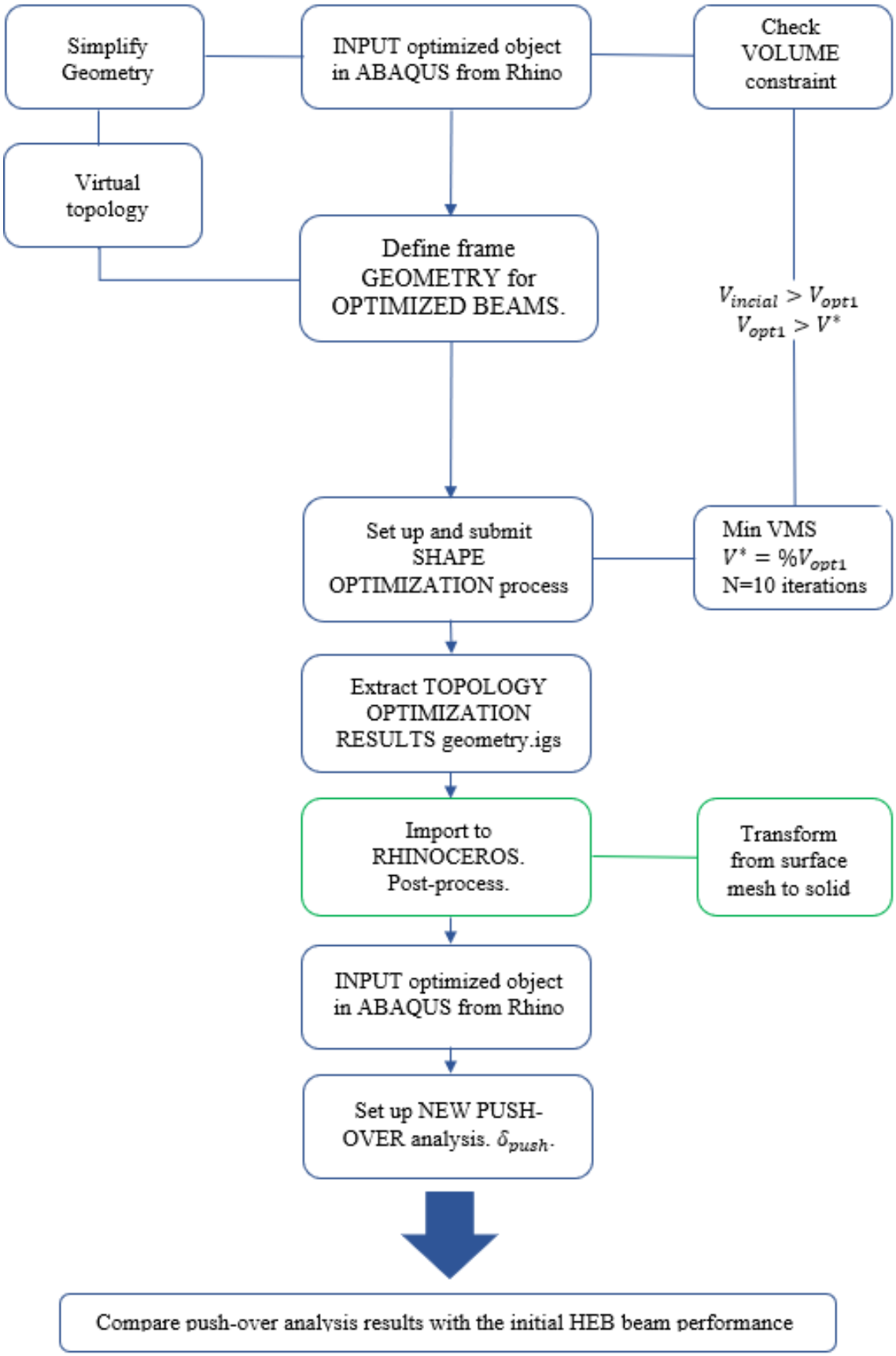
Simplify Geometry
INPUT optimized object in ABAQUS from Rhino
Check VOLUME constraint
Virtual topology
Define frame GEOMETRY for OPTIMIZED BEAMS.
$V_{incial} > V_{opt1}$
$V_{opt1} > V^*$
Set up and submit SHAPE OPTIMIZATION process
Min VMS
$V^* = \%V_{opt1}$
N=10 iterations
Extract TOPOLOGY OPTIMIZATION RESULTS geometry.igs
Import to RHINOCEROS. Post-process.
Transform from surface mesh to solid
INPUT optimized object in ABAQUS from Rhino
Set up NEW PUSH-OVER analysis. δ_{push}.
Compare push-over analysis results with the initial HEB beam performance

4.2. Numerical studies

In this chapter, numerical studies using different optimization configuration and different link sections are presented. The main objectives of the numerical studies are:

- To determine how the obtained results are mesh-dependent.
- To determine whether these optimization results vary with the link geometry (short, intermediate, longs)

4.2.1. Mesh dependency

Mesh- dependent results like checkerboards and non unique solutions [7] are situations that must be avoided when optimizing the topology of a structure. Generally, this is achieved by changing the optimization conditions that, these probblems can beare solved. This numerical study conducts topology optimization using the design space that optimizes the HEB140 in order to check wether the solutions obtained for the specific problem definition in this thesis.

For that purpose, several mesh sizes are assigned to the design space up to the maximum size that was obtained for the convergence study in Chapter 3.4, which was a mesh with an element density of approximately 0.01 elements per cubic millimetre. The following table summarizes the study:

Design space for HEB140

Mesh size shear link	**Nodes**	**Elements**	**Density** $\left(\frac{Elements}{mm^3}\right)$
10	17100	14700	0.001
7	47628	42800	0.003
6	72576	66125	0.0045
5	126991	117600	0.008

Table 4-8. Mesh sizes, number of nodes, elements, and mesh density of shear link for the mesh dependency study

Mesh size flexure link	**Nodes**	**Elements**	**Density** $\left(\frac{Elements}{mm^3}\right)$
10	32175	27832	0.001
7	89964	81200	0.003
6	137088	125373	0.0045
5	240526	223440	0.008

Table 4-2. Mesh sizes, number of nodes, elements, and mesh density of flexure link for the mesh dependency study

4.3. Assesment

This study is carried out using for different sizes of HEB links made of S275 steel. The links are HEB140, HEB160, HEB180 and HEB220 where flexure and shear links are considered as explained in Chapter 3. The geometry of the flexure and shear links is calculatedin section 3.1, the material assigned to them is described in section 3.2 and the topology uptimization set up is described in section 3.5.

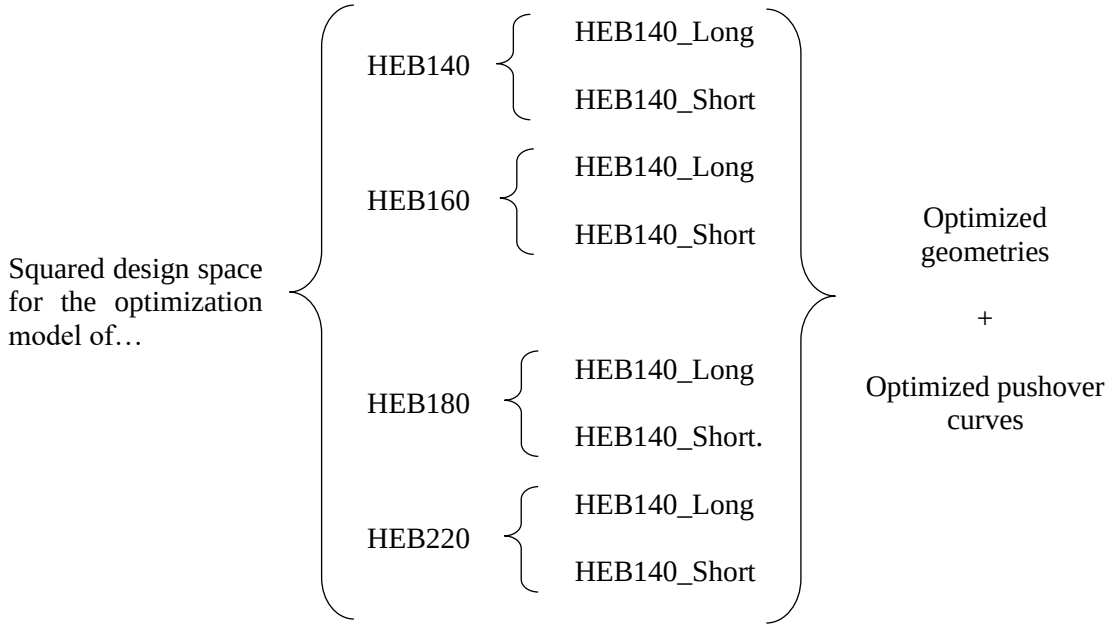

Figure 4-8. Scheme representing the numerical study

The optimized links are compared to determine how does the shape that the optimization outputs changes when the design space is modified and how related are all the results obtained. Furthermore, the optimized push-over curves provide the mechanical information that allow to compare the links in terms of energy dissipation, initial stiffness, yield limit and maximum plastic strength.

To ease the comparison of the displacement-force curves from the pushover analysis, the curves shall be replaced with an idealized linear relationship. The linearization is done according to FEMA 356 [?] for nonlinear static procedure for seismic analysis of buildings. The linearized curve allows to calculate the effective lateral stiffness K_e and the effective yield strength V_y of the frame.

The effective lateral stiffness K_e shall be taken as the secant stiffness calculated a lateral force equal to the 60% of the effective yield strength of the structure. The post-yield factor α shall be determined by a line segment that passes through the actual curve at the calculated target displacement δt. As no target displacement has been defined for these analyses, it is considered to be the displacement at which the maximum lateral force Vm is found. The effective yield Vy shall never be greater than the maximum lateral force along the curve.

In the case that the curve is smooth during the decay of the strength, a trilinear curve is defined using a factor α_{decay} which multiplies Ke, resulting in a line passing through the maximum strength point Vm and the final displacement considered for the analysis.

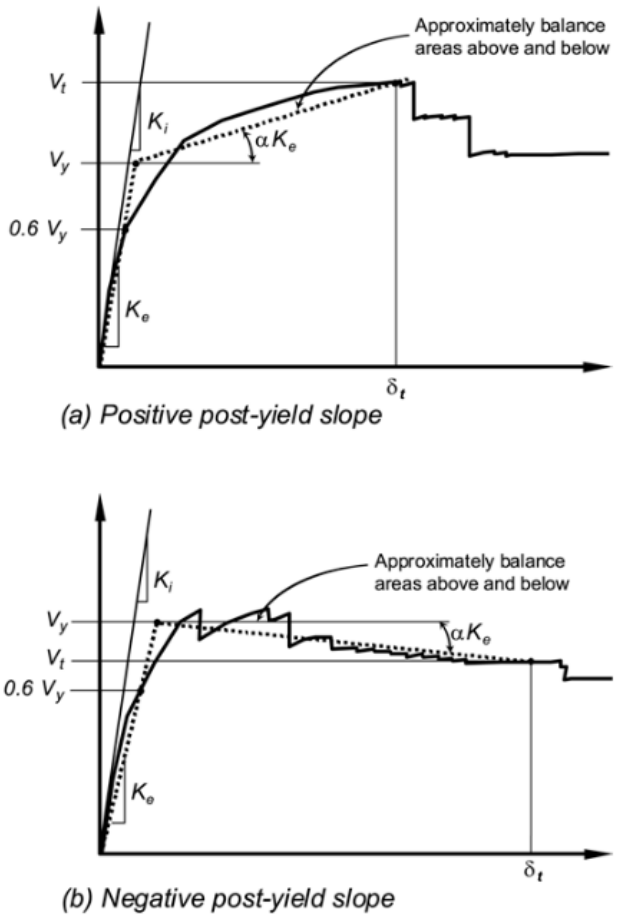

Figure 4-9. scheme of the linearization of typical pushover curves.

Then, the initial stiffness Ke, the yield lateral force Vy, the displacement when the maximum lateral force is applied δt, the maximum lateral force Vm are the parameters used to qualify and compare the plastic behaviour of the optimized geometries. Also, Abaqus records the plastic energy dissipated (E) in every step of the push-over analysis. Then, a comparison of 'E' is also stablished.

5. Results

In this chapter, the results obtained are presented. First, results from the analysis of original EBF links are shown, followed by the mesh dependence analysis of the topology optimization. Finally, results from the optimization procedure and the push-over analysis of optimized links are presented and compared with those corresponding to the original HEB profiles.

5.1. Results: original HEB beams

Results obtained from a total of eight push-over analysis are presented. The analysis is implemented over 4 types of steel profiles: HEB220, HEB180 HEB160 and HEB140. For each profile, shear and flexure links are generated according to the rules exposed in Chapter 3. The push-over response curve is extracted from a static nonlinear analysis with an incremental procedure of displacement control implemented until an arbitrary maximum horizontal displacement of 50 mm is reached.

Results in stress distribution for short links show how these elements are able to yield using most of the material within their volume, finding the higher stress concentration in their web. The contours displayed in Figure *5-1* are set in away grey colour shows a von Mises stress higher than f_y. Despite buckling instabilities have not been taken into account for these analyses, they can be produced in the web due to the stress concentration causing a sudden loss of the strength of the link.

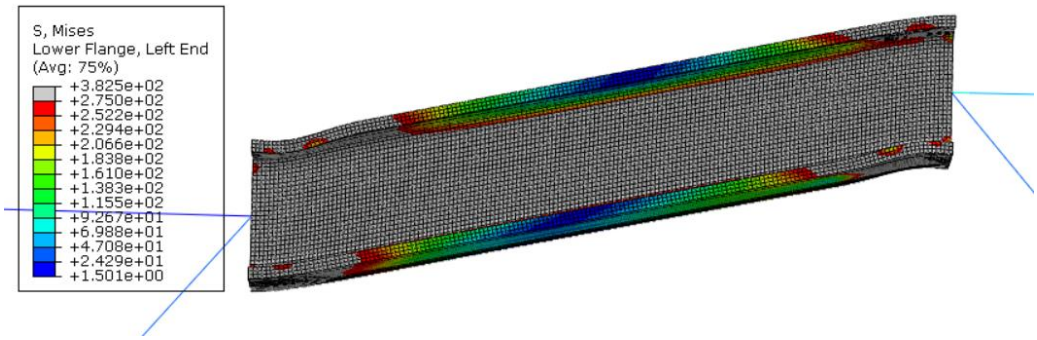

Figure 5-46 Stress concentration contour plot in shear links (HEB160).

On the other hand, stress distribution in flexure links shows how yielding is concentrated in their both ends, where there can be found large deformations in the web and the flanges (See *Figure 5-2*).

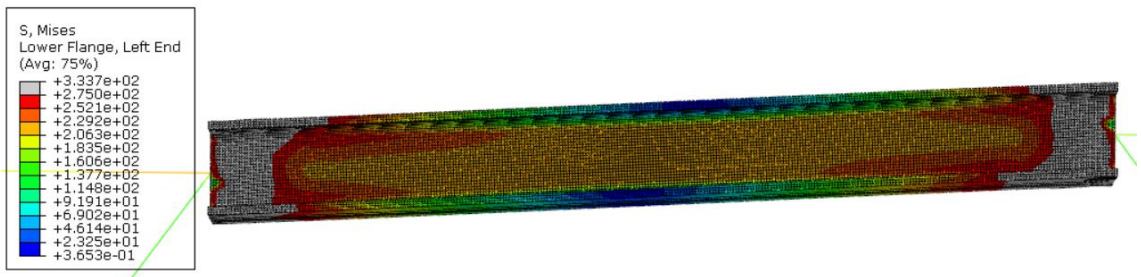

Figure 5-47 Stress concentration contour plot in flexure links (HEB160).

For every type of profile, capacity and plastic energy dissipation are compared. The parameters that describe the behaviour of the links, as defined in Chapter 4, are tabulated. Finally,

a brief discussion on the results obtained is carried out, regarding the general behaviour of shear and flexure links.

5.1.1. HEB140

Capacity curves corresponding to the push-over analysis and plastic dissipation are plotted in *Figure 5-3.*

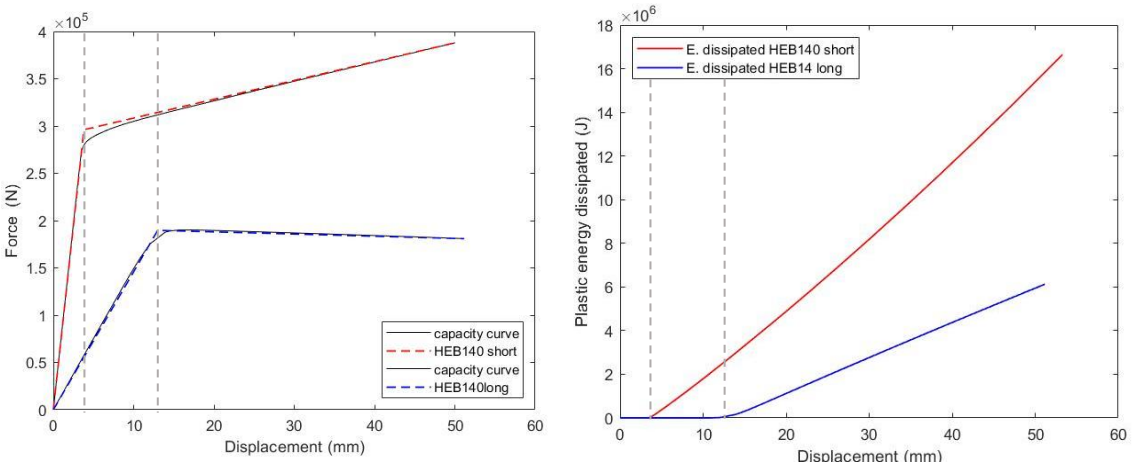

Figure 5-48 Capacity curves for HEB140 links.

The capacity curves show that shear links (short) provide considerably higher strength and initial stiffness than bending links (long). For the shear link, the structure yields when a displacement of 3.8 mm is applied, at which the structure presents a lateral reaction force of 296 kN. Flexure link provides the structure with a yield displacement of 13 mm while presenting a force against lateral movement of 189 kN. Post-yielding curves show a hardening effect for shear links, while a softening effect is produced in flexure links. The behaviour parameters for the bilinear approximations of the capacity curves are summarized in *Table 5-1*:

HEB140	Dy (mm)	Vy (N)	Ke (N/mm)	α	Vm	Dm
Shear	3,80	296074	77914	0,026	388000	50,00
Flexure	13,00	189683	14591	-0,016	190100	15,69

Table 5-9 linear approximation curve parameters for HEB140 link.

According to the capacity curves, the plastic dissipation starts when the yield displacement is overpassed. Higher dissipative rates are found in shear links, presenting an energy dissipation at the final displacement of 50 mm of 15398360 Joules, 2.6 times higher than the energy dissipated in flexure links, reaching a value of 5945796 Joules when the same displacement is applied.

5.1.2. HEB160

Capacity curves corresponding to the push-over analysis and plastic dissipation for the HEB160 links are plotted in *Figure 6-4.*

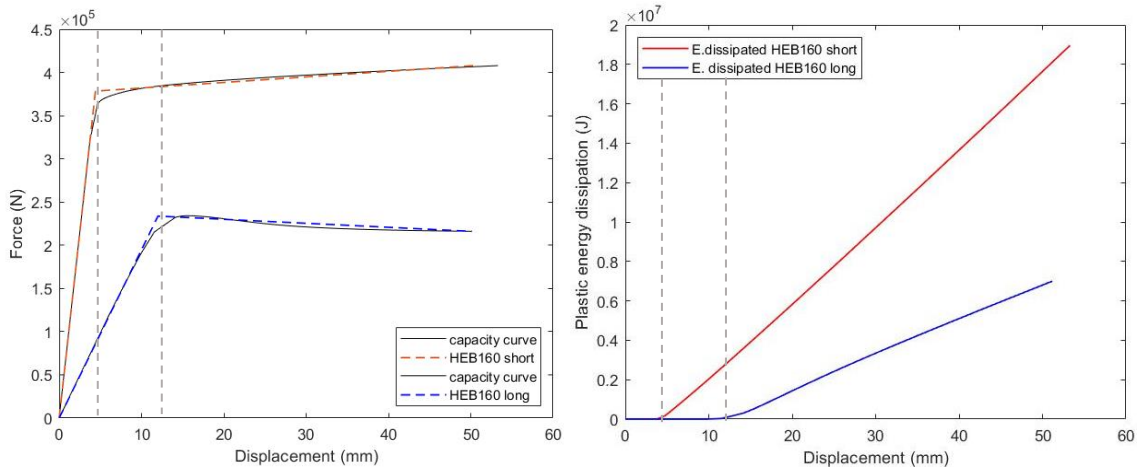

Figure 5-49 Capacity and plastic energy dissipation curves for HEB160 links.

The frame using the shear link yields at a displacement of 4,4 mm at which shows a reaction force of 378 kN. The frame using the flexure link yields when a displacement of 12 mm is applied, showing a reaction force of 234 kN. The structure shows similar post-yielding behaviour than for the HEB140, presenting hardening for the shear link and softening for the flexure link. The behaviour parameters for the bilinear approximations of the capacity curves are summarized in *Table 5-2*:

HEB160	Dy (mm)	Vy (N)	Ke (N/mm)	α	Vm	Dm
Shear	4,40	378400	86000	0,007	407900	53,30
Flexure	12,00	233723	19477	-0,024	15,4	234200

Table 5-10 linear approximation curve parameters for HEB160 link..

The plastic energy dissipation behaviour is similar to the previous link. For the shear link, the plastic energy dissipated at a displacement of 50 mm is 17637802 Joules, while flexure links dissipate 6801650 Joules, 2,6 times less that shear links.

5.1.3. HEB180

Capacity curves corresponding to the push-over analysis and plastic dissipation for the HEB180 links are plotted in *Figure 5-5.*

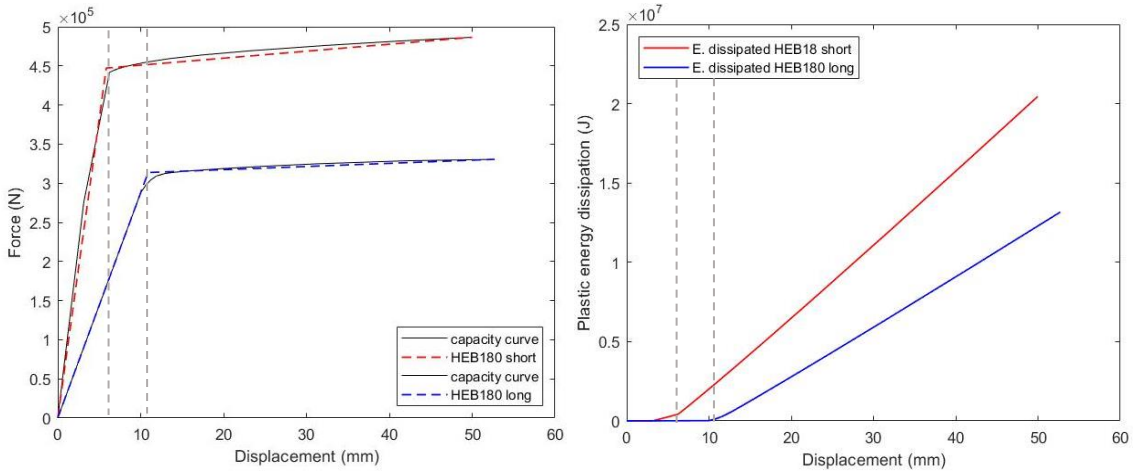

Figure 5-50 Capacity and plastic energy dissipation curves for HEB180 links.

The frame using the shear link present a yield displacement of 5,9 mm showing a lateral reaction force of 447 kN, while flexure link provides a yield displacement of 11 mm with a lateral reaction force of 314 kN. In this case, the flexure link, as well as the shear link, presents a hardened post-yielded curve, differently form HEB140 and HEB160. The behaviour parameters for the bilinear approximations of the capacity curves are summarized in *Table 5-3*:

HEB160	Dy (mm)	Vy (N)	Ke (N/mm)	α	Vm	Dm
Shear	5,85	447221	76448	0,012	486600	50
Flexure	10,90	313702	28780	0,014	330600	52,7

Table 5-11 linear approximation curve parameters for HEB180 link.

The energy dissipated by the shear link at a displacement of 50 mm is 20450000 Joules while the flexural link dissipates 12297314 Joules. The shear link presents a lower difference in terms of energy dissipation, since it only dissipates 1,6 times the energy dissipated by the flexural link.

5.1.4. HEB220

Capacity curves corresponding to the push-over analysis and plastic energy dissipation for the HEB220 links are plotted in *Figure 5-6.*

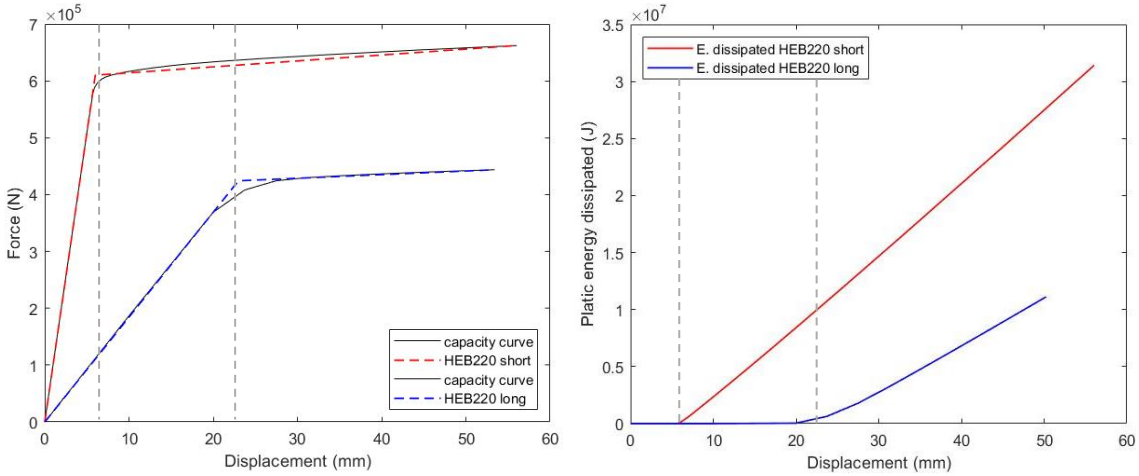

Figure 5-51 Capacity and plastic energy dissipation curves for HEB220 links.

The frame using the shear link yields at an imposed displacement of 6 mm with a lateral reaction force of 610 kN while the frame using the flexure link yields at a displacement of 23 mm, providing a lateral force of 424 kN. As in the case of HEB180, bot post-yielding curves present hardening. The behaviour parameters for the bilinear approximations of the capacity curves are summarized in *Table 5-4*:

HEB160	Dy (mm)	Vy (N)	Ke (N/mm)	α	Vm	Dm
Shear	6,00	609960	101660	0,010	662100	56,00
Flexure	23,00	424235	18445	0,035	443600	53,40

Table 5-12 linear approximation curve parameters for HEB220 link.

The energy dissipated by the frame using the shear link at a displacement of 50 mm is 27495789 Joules while the frame using the flexure link dissipates 11120000 Joules, which is 2.5 times less that the energy dissipated by the shear link.

5.1.5. Discussion

Results obtained from these initial push-over analyses verify that shear links provide a better structural behaviour than flexure links in terms of initial stiffness, strength and energy dissipation. The properties of both types of links are increased as the links section increases.

As seen in *Figures 5-1* and *5-2*, the ability of shear links of using its whole web material volume to yield allows them to bear the imposed deformations more efficiently. At the same time a larger quantity of energy is dissipated, since most of the link is yielding. On the contrary, long links, despite having a larger volume offered to be deformed, the load bearing is concentrated in their ends, and thus, the quantity of material that dissipates energy is not optimal. Table 5-5 summarizes the parameters evaluated for the original EBF links:

Link	Dy (mm)	Vy (N)	Ke (N/mm)	α	Vm (N)	Dm (mm)	E (kJ)
HEB140 Shear	6,00	609960	101660	0,010	662100	56,00	15398
HEB140 Flexure	23,00	424235	18445	0,035	443600	53,40	5946
HEB160 Shear	6,00	609960	101660	0,010	662100	56,00	17638
HEB160 Flexure	23,00	424235	18445	0,035	443600	53,40	6802
HEB180 Shear	6,00	609960	101660	0,010	662100	56,00	20450
HEB180 Flexure	23,00	424235	18445	0,035	443600	53,40	12297
HEB220 Shear	6,00	609960	101660	0,010	662100	56,00	27496
HEB220 Flexure	23,00	424235	18445	0,035	443600	53,40	11120

Table 5-513 summary of evaluated parameters for original EBF links.

Topology optimization carried out in these types of links can provide new geometries that improve their main properties at the same time that provide new yielding mechanisms and failure modes.

5.2. Results on optimized HEB beams

The results for the topology optimization procedures implemented in the EBF links are herein presented. First, a preliminary study regarding the mesh dependence of the optimization results is carried out. Finally, Topology optimization results on beams with different cross-sections are presented and compared with the original HEB links performance. To conclude, a discussion on the results obtained is carried out.

5.2.1. Mesh dependence

To perform the study, the design space for the optimization of the HEB140 link is taken as reference. Topology optimization has been conducted using different mesh sizes to discretize the design space, in order to detect variations in the output geometries that could affect the evaluation of the optimized link. Mesh sizes are exposed in Table 5-1 in Chapter 5.

The topology optimizations are constrained to volume reductions. The volume of the discretized prismatic design spaces are constrained to a reduction to, at least, the volume of the corresponding original link.

The use of coarse poor meshes, which have a low number of elements, provide a low computational cost to the optimization procedure. However, the accuracy of the results is limited by the element size, and the capacity of the optimization algorithm to accomplish the imposed volumetric constraints is reduced by the use of a poor meshes.

Then, the aim of this study is to find a mesh density to discretize the design space that shows convergence in geometry when increasing the accuracy of the mesh, while requires as low computational cost as possible. The geometric results are presented providing the front views, cross sections and elevation views of the optimized link.

The results for shear links geometry, number of elements used, and computation time are described in tables from *Table 5-6* to *Table 5-9*:

Mesh size: 10	
Front view	
Elevation view	
Cross-section	
Number of elements: 14700	
Computation time: 1 hour 18 min	

Table 5-6 Topology optimization results of HEB140 shear link for a maximum mesh element size of 10 mm

The geometry resulting of applying an optimization procedure using a mesh size with a maximum element size of 10 mm shows a structure composed by two lateral V-like structures at the ends of the link and a diagonal element in the centre, joining them. Observing the elevation view can be seen that the optimized structure presents a void space in the centre of the geometry, optimizing the geometry at the boundaries of the design space. Due to the nonsymmetric lateral loading, the resulting element is also nonsymmetric and it is expected to optimize the behaviour of the element only in the direction of the lateral load.

Mesh size: 7	
Front view	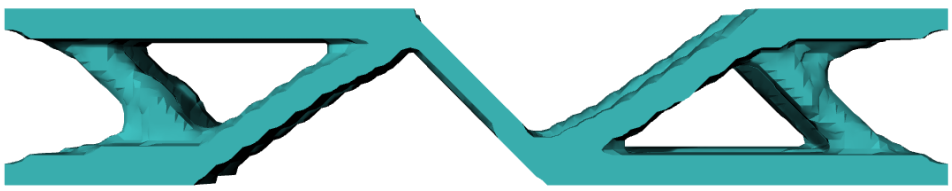

Elevation view	*Cross-section*
	
Number of elements: 42800	
Computation time: 7 hours 56 min	

Table 5-7 Topology optimization results of HEB140 shear link for a maximum mesh element size of 7 mm

The mesh maximum element size is reduced to 7 mm. The results present visible geometrical changes, where the ends of the link adopt a shape similar to a truss-like structure, which are joined by a diagonal element in the centre of the geometry.

Mesh size: 6

Front view

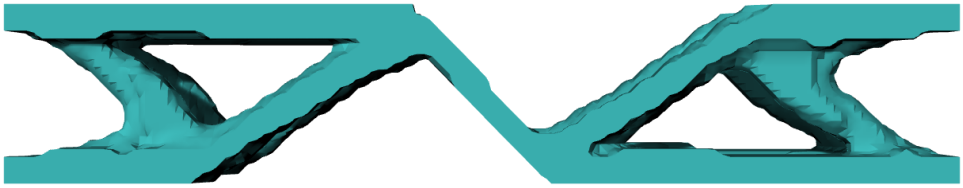

Elevation view	*Cross-section*
	
Number of elements: 66125	
Computation time: 8 hours 50 min	

Table 5-8 Topology optimization results of HEB140 shear link for a maximum mesh element size of 6 mm

The maximum element size is reduced to 6 mm and no changes are observed. The result shows the same geometries than in the previous topology optimization.

Mesh size: 5

Front view

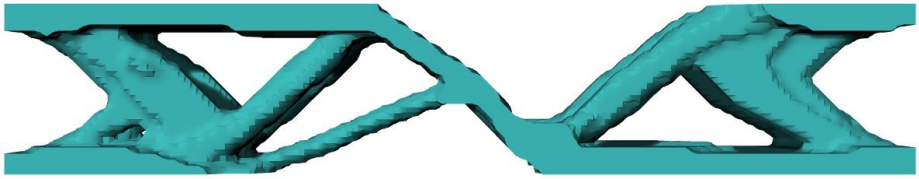

Elevation view *Cross-section*

Number of elements: 117600

Computation time: 23 hours 20 min

Table 5-9 Topology optimization results of HEB140 shear link for a maximum mesh element size of 5 mm

The geometry resulting from a maximum element size of 5 mm show geometrical changes at one of the ends of the link, were a more complex truss-like structure is presented. The computational time has increased considerably from the mesh size of 10 mm to the mesh size of 5 mm. Then, for the sake of having a reasonable computing time for the posterior study, the mesh density implemented in this topology optimization will be maintained in subsequent topology optimization procedures on shear link.

The results for flexure links geometry, number of elements used, and computation time are described in tables from *Table 5-10* to *Table 5-13*:

Mesh size: 10

Front view

Cross-section

Elevation view

Number of elements: 27832

Computation time: 6 hours 56 min

Table 5-10 Topology optimization results of HEB140 flexure link for a maximum mesh element size of 10 mm

The geometry obtained from the topology optimization carried out using the design space for the HEB140 flexure link show similar results than for shear links, where various parts can be differentiated: at the ends of the links the lateral V-like joints are generated and two truss-like structures are shown joined by a diagonal element. Observing the elevation view can bee seen that an elliptical material void is formed.

Mesh size: 7

Front view

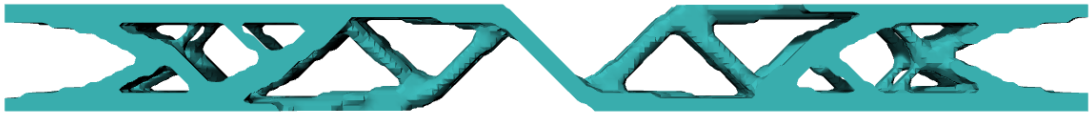

Cross-section

Elevation view

Number of elements: 81200

Computation time: 9 h 15 min

Table 5-141 Topology optimization results of HEB140 flexure link for a maximum mesh element size of 7 mm

The maximum element size is reduced to 7 mm and it can bee seen that the complexity of the truss is increased, where thinner members are formed, and the number of connections is increased. From these connections it can be glimpsed a geometrical pattern that is repeated at both sides of the link.

Mesh size: 6

Front view

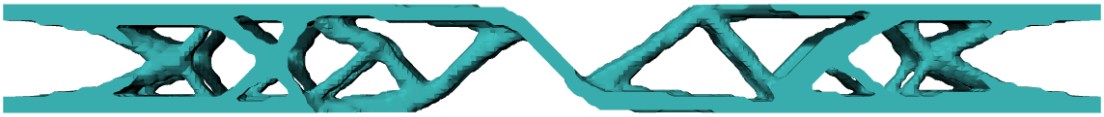

Cross-section

Elevation view

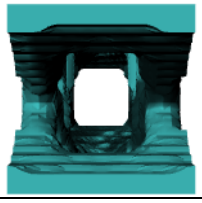

Number of elements: 137088

Computation time: 16 hours 08 min

Table 5-152 Topology optimization results of HEB140 flexure link for a maximum mesh element size of 6 mm

Mesh size: 5

Front view

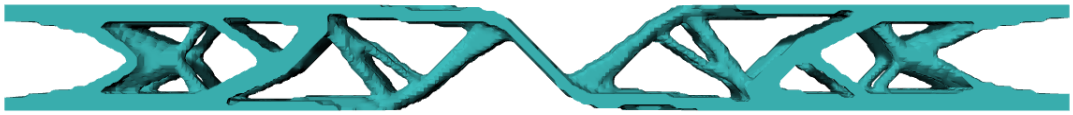

Cross-section

Elevation view

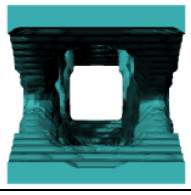

Number of elements: 223440
Computation time: 40 hours 52 min

Table 5-163 Topology optimization results of HEB140 flexure link for a maximum mesh element size of 5 mm

Similar patterns are obtained when the mesh size is reduced to 6 mm and 5 mm. Then, the mesh density obtained with the maximum mesh element size of 6 mm is used for subsequent optimization procedures, since it shows converged geometry with a reasonable computation time.

Table 5-14 summarizes the mesh characteristics, the computation time and whether there are significant geometric changes from previous discretization for the shear and flexure links previously exposed.

Type of link	Mesh size	elements	Computation time	Geometric changes
Shear	10	14700	1 h 18 min	-
Shear	7	42800	7 h 56 min	Yes
Shear	6	66125	8 h 50 min	Yes
Shear	5	117600	23 h 20 min	No
Flexure	10	27832	6 h 56 min	-
Flexure	7	81200	9 h 15 min	Yes
Flexure	6	137088	16 h 08 min	No
Flexure	5	424235	40 h 52 min	No

Table 5-174 Topology optimization results of HEB140 flexure link for a maximum mesh element size of 5 mm

Now, all computational conditions for the topology optimization of different links sections have been obtained and then, the assessment on the optimized links can be carried out.

5.2.2. Assessment of optimized links

The optimization procedure described in Chapter 5 has been implemented to the design spaces corresponding to shear and flexural links of the sections described in Chapter 3: HEB140, HEB160, HEB180, and HEB220.

First, the topology optimization procedures are described through the optimization graphs, which show the evolution of the design responses for every iteration. The final output of the constraint design response is evaluated at the end of the procedure to determine the posterior set up for the shape optimization.

Then, the results from the shape optimization are obtained and the constraint fulfilment is verified. The new geometries are submitted to a push-over analysis with a maximum lateral displacement of 50 mm. The yield mechanism and the stress concentrations are evaluated. Finally, the capacity curves are obtained, and linear approximations are done to extract the behaviour parameters (Dy, Vy, Ke, α1 and)and the maximum lateral for and its corresponding displacement (Vm, Dm) for a posterior comparison with the corresponding original HEB link. The plastic energy dissipation (E) of the optimized links is also presented and compared.

5.2.2.1. Optimized HEB140

The optimization results for the HEB140 for shear and flexural links are herein presented. The optimization procedure follows the scheme presented in *Figure 5-7*, where the objective is to get an optimized geometry with the same material volume than the original links.

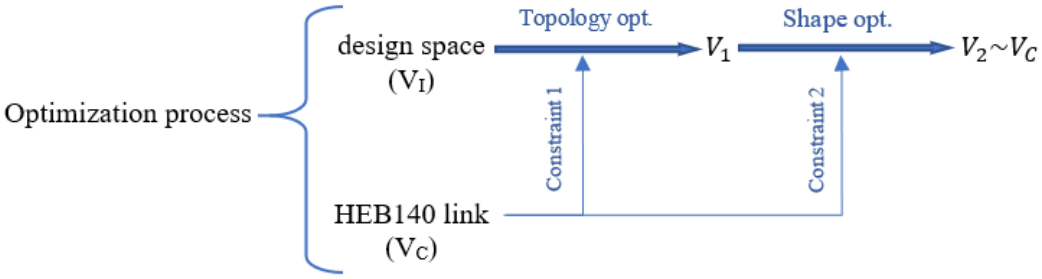

Figure 5-7 optimization for HEB140 links

Shear link

The topology optimization procedure on the shear link is carried out over its design space which has been defined with an initial volume of 14700000 mm^3. The optimization of the objective response is constrained to a reduction of volume of 21.91% up to 3221712.5 mm^2. The evolution of the procedure is described in *Figure 5-8*:

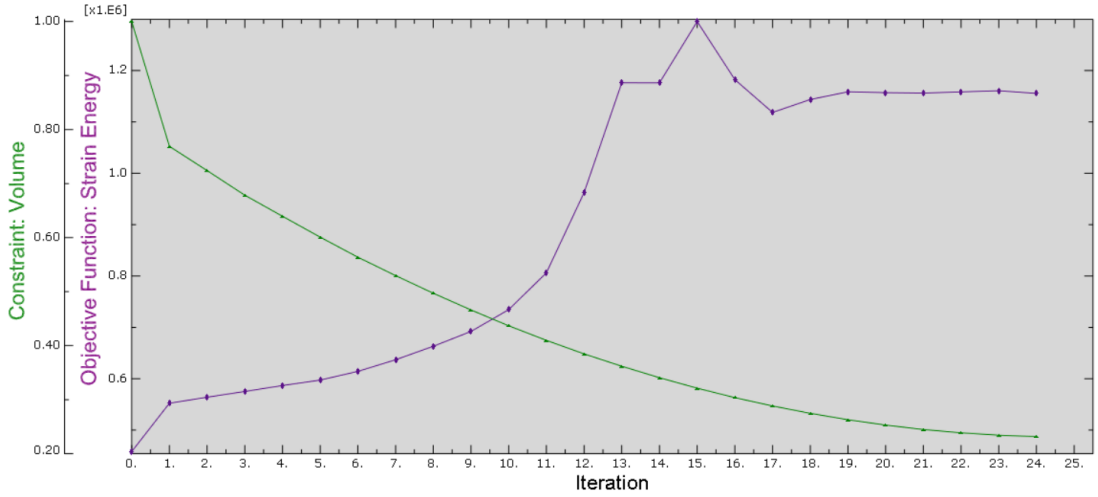

Figure 5-8 Optimization process of HEB140 shear link.

The topology optimization procedure shows a stable convergence after 24 iterations, where the strain energy is increased at the same time that the constrained volume design response is approximated. The final volume obtained is 3720003 mm^3. Then, it is necessary to constrain the shape optimization to volume reduction of an 86.6% of the actual volume, to achieve the objective of 3221712 mm^3. The new geometry is submitted to a shape optimization process that outputs an optimized geometry that uses the same volume of material than the original HEB140 shear link.

The optimized geometry is subjected to the final push-over analysis showing a final stress distribution as illustrated in *Figure 5-9*:

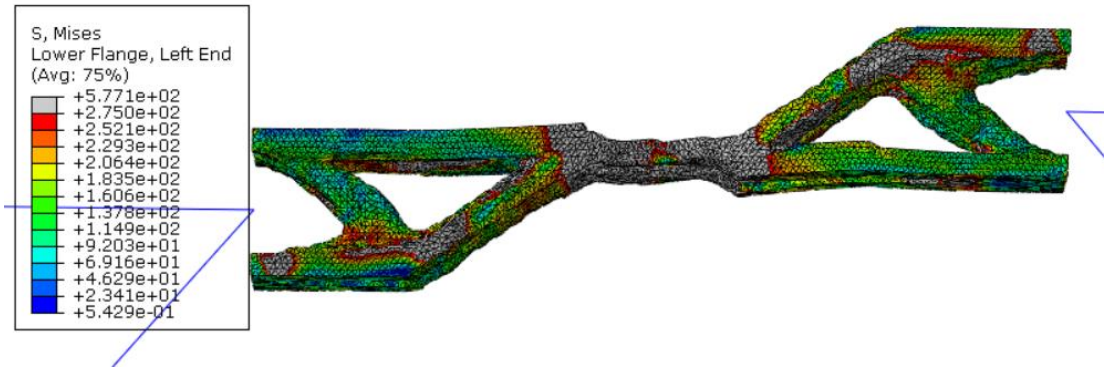

Figure 5-9 stress concentration contour plot of optimized HEB140 shear link.

The final stresses concentrate mainly in the joint diagonal element in the centre. The link uses the plastic behaviour in the diagonal element to pivot around it and then, deform.

Flexural link

The topology optimization procedure on the flexural link is carried out over its design space which has been defined with an initial volume of 27910400 mm^3. The optimization of the objective response is constrained to a reduction of volume of 21.91% up to 6116958.5 mm^3. The evolution of the procedure is described in *Figure 5-10*:

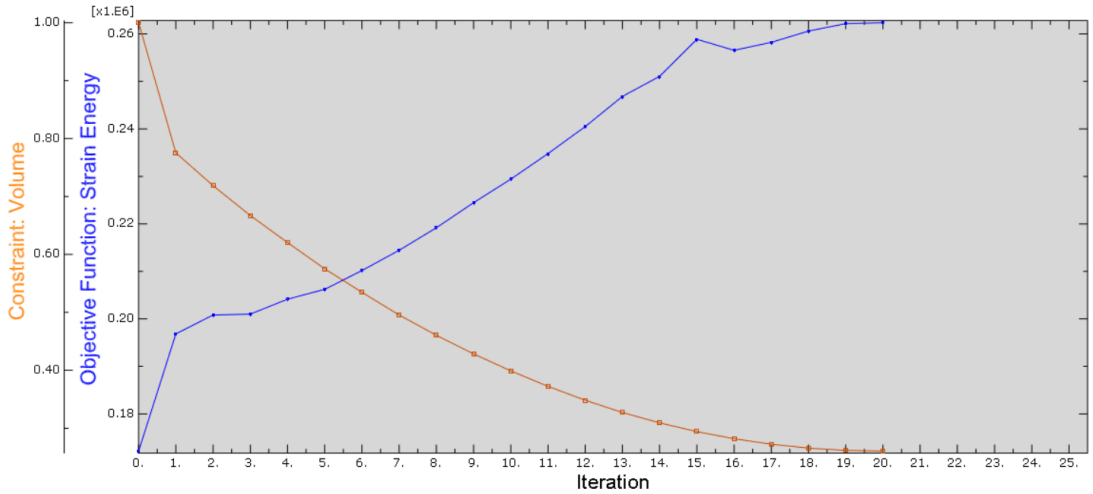

Figure 5-10 Optimization process of HEB140 flexure link.

The process finishes after 15 iterations with minor oscillations in the strain energy values. The outputs from the topology optimization show a final volume design response of 7639817 mm^3. Then it will be necessary to set up the shape optimization procedure using a reduction volume constraint of an 80% to accomplish the initial goal.

Shape optimization is implemented on the optimized topology of the link; however, the process is not able to accomplish the volume constraints, ending with a final optimized link that is slightly oversized with respect the original link.

The new geometry is subjected to the push-over analysis where it is seen that the plastic behaviour of the frame is concentrated in the new link generating a stress distribution illustrated in *Figure 5-11*:

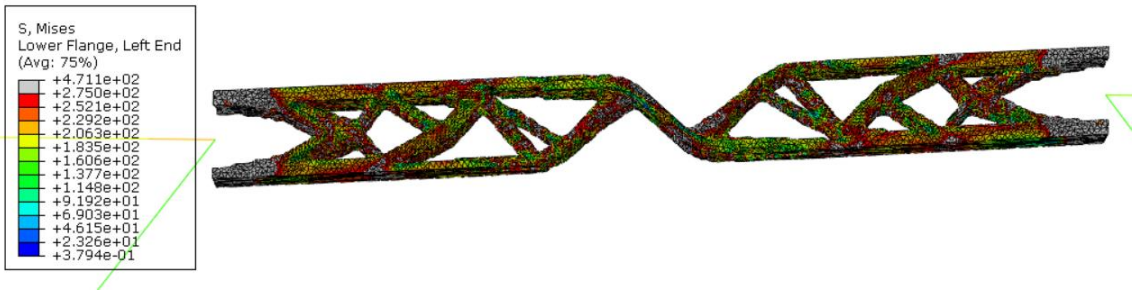

Figure 5-11 stress concentration contour plot of optimized HEB140 flexure link.

The optimized geometry presents a stress distribution with yielding concentrated mainly at the ends of the link and, in a minor scale, in the centre of the link.

Push-over curves

Capacity curves for the original and optimized HEB140 shear and flexure link have been plotted in *Figure 5-12*:

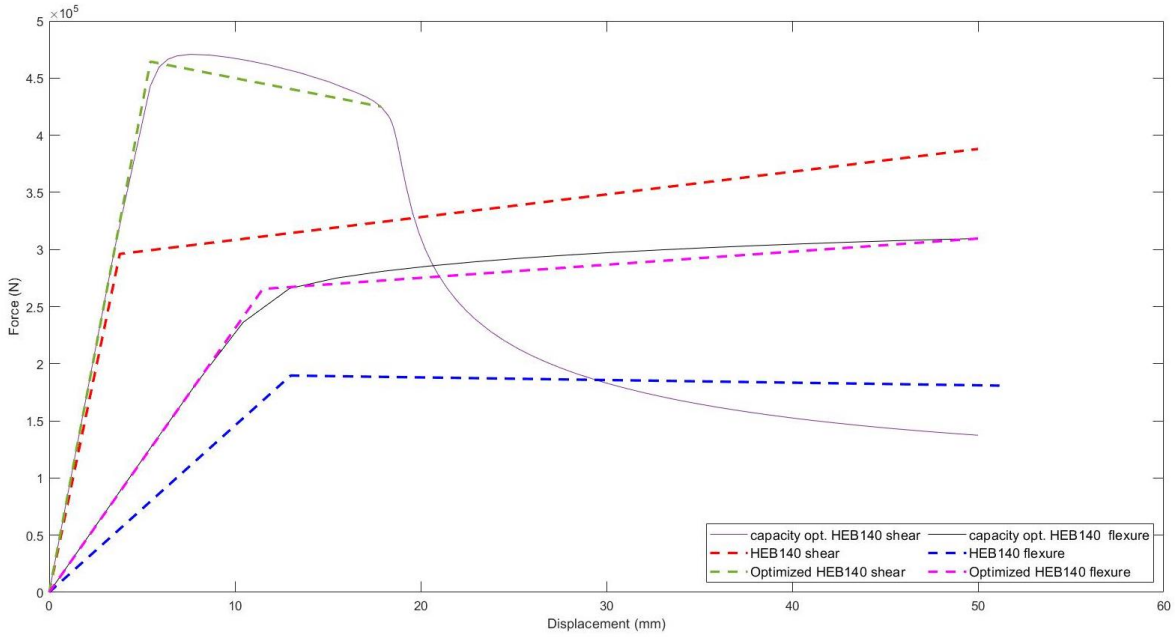

Figure 5-522 Optimized capacity curves against original capacity curves for HEB140 link

The frame using the optimized shear link yields at an imposed displacement of 5.45 mm with a lateral reaction force of 464401 N. It presents a big increase of the strength of the yield point while its ductility is decreased, showing a strength drop when the structure is moved further than 20 mm. The frame using the optimized flexure link yields at a displacement of 11.50 mm, providing a lateral force of 265463 N. The link maintains its ductile properties showing a post-yielded curve similar to the corresponding post-yield curve of the original link.

The parameters that describe the behaviour of the links and that define the linear approximations of the capacity curves are summarized in *Table 6-13:*

Optimized HEB160	Dy (mm)	Vy (N)	Ke (N/mm)	α_1	α_2	Vm	Dm
Shear	5,45	464401	85211	-0,037	-	469400	6,87
Flexure	11,50	265463	23084	0,050	-	309600	50

Table 5-18 linear approximation parameters for HEB140 link.

The plastic energy dissipation curves for original and optimized HEB140 shear and flexure links obtained from the push-over analysis are plotted in *Figure 5-13*:

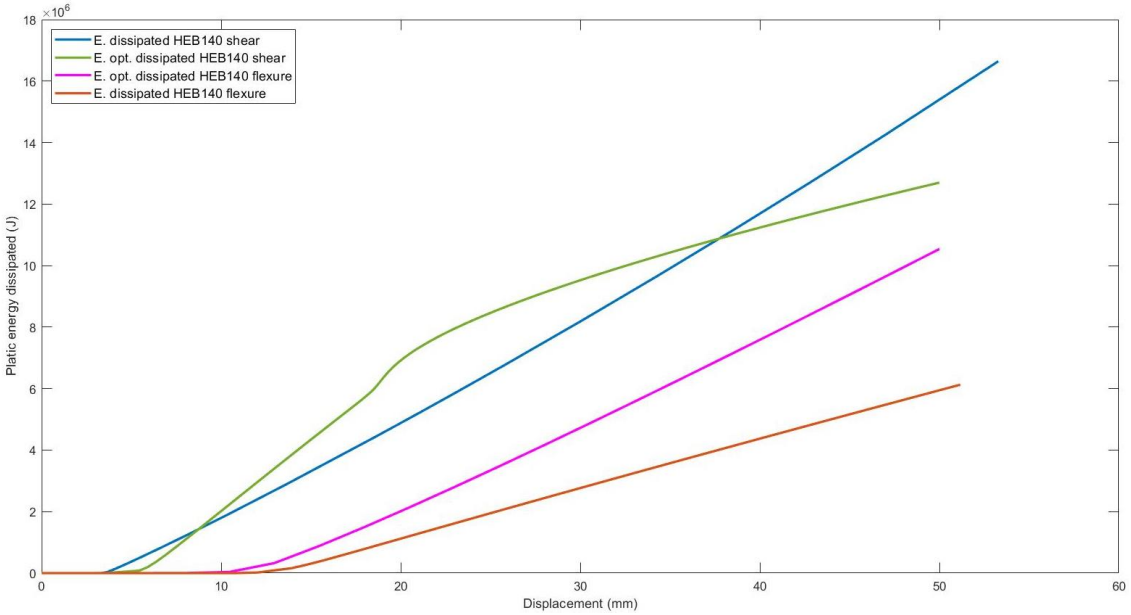

Figure 5-533 Optimized plastic dissipation curves against original plastic dissipation curves for HEB140 link

According to the capacity curves, the plastic dissipation starts when the yield displacement is overpassed. Higher dissipative rates are found in the optimized shear link, presenting an energy dissipation at the final displacement of 50 mm of 12700000 Joules, while the flexure link reach a value of 10540000 Joules when the same displacement is applied. For the optimized flexural links, the energy dissipation curve is linear and shows a higher dissipation rate than its corresponding original link. The optimized shear link present a non-linear dissipation curve which improves the energy dissipated when the displacement applied ranges from 10 to 37 mm. If the structure is moved further, the original link shows a higher energy dissipation.

5.2.2.2. Optimized HEB160

The optimization results for the HEB160 for shear and flexural links are herein presented. The optimization procedure follows the scheme presented in *Figure 5-14*, where the objective is to get an optimized geometry with the same material volume than the original links.

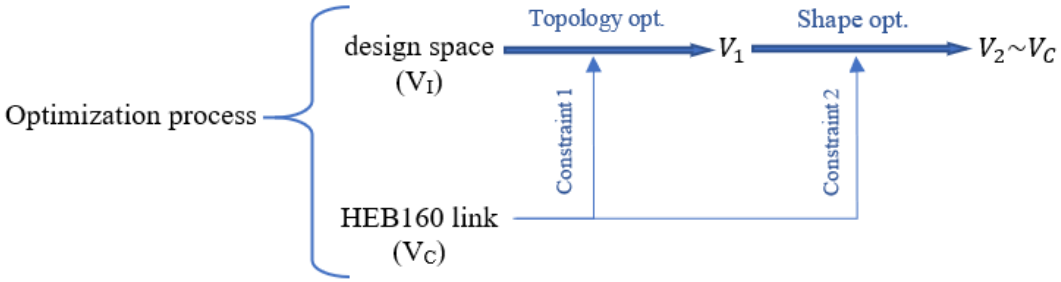

Figure 5-14 optimization for HEB160 links

Shear link

The topology optimization procedure on the shear link is carried out over its design space which has been defined with an initial volume of 212480000 mm^3. The optimization of the objective response is constrained to a reduction of volume of 21.2% up to 4502875.5 mm^3. The evolution of the procedure is described in *Figure 5-15*:

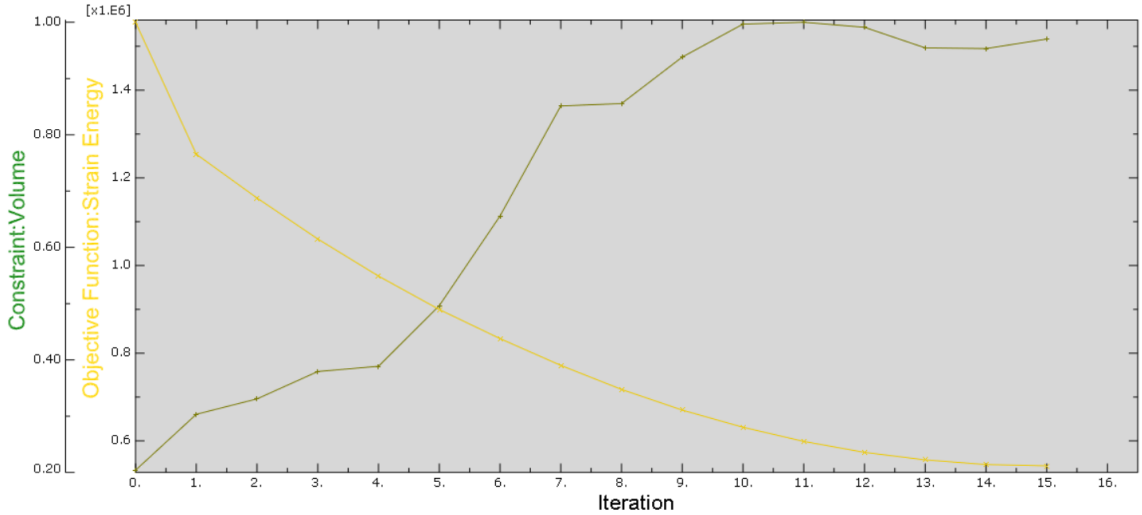

Figure 5-545 Optimization process of HEB160 shear link.

The optimization process shows a stable convergence increasing the strain energy while approximating the constraints imposed. The outputs from the topology optimization show a final volume design response of 5146943 mm^3. Then, it will be necessary to set up the shape optimization procedure using a reduction volume constraint to an 87.4% of the actual volume to accomplish the initial goal. Shape optimization is implemented in the new geometry successfully, reaching the constraint values imposed. Then it is obtained an optimized geometry with the same material usage than the original HEB160 link.

The optimized geometry is subjected to the push-over analysis. The distribution of stresses for a lateral displacement of 50 mm as described in *Figure 5-16*:

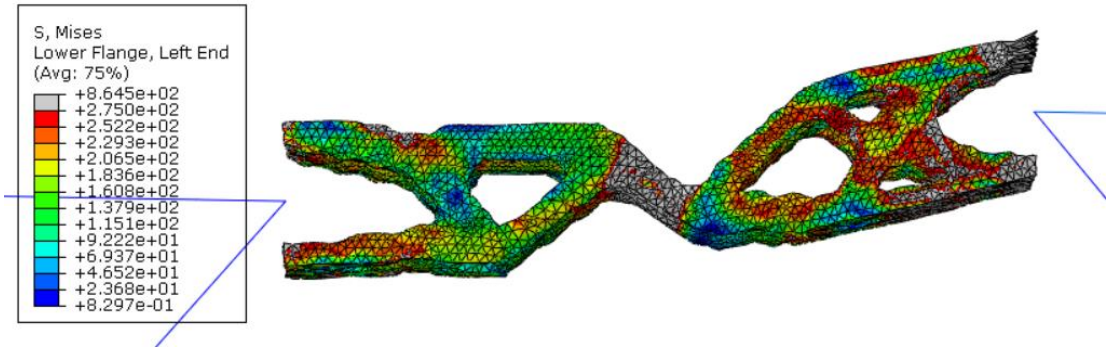

Figure 5-556 stress concentration contour plot of optimized HEB160 shear link..

The new geometry maintains that characteristic shape obtained for HEB140 shear link optimization. The stresses concentrate in the diagonal joint in the centre and in the unions with the frame, where the mesh elements acting as the joint between the link and the frame are overstrained. This overstrain leads to the observed relative rotation between the right and left parts of the dissipator and it is caused by an excess of rigidity of the truss-like parts of the link.

Flexure link

The topology optimization procedure on the flexural link is carried out over its design space which has been defined with an initial volume of 40064000 mm^3. The optimization of the objective response is constrained to a reduction of volume of 21.2% up to 8490361 mm^3. The evolution of the procedure is described in *Figure 5-17*:

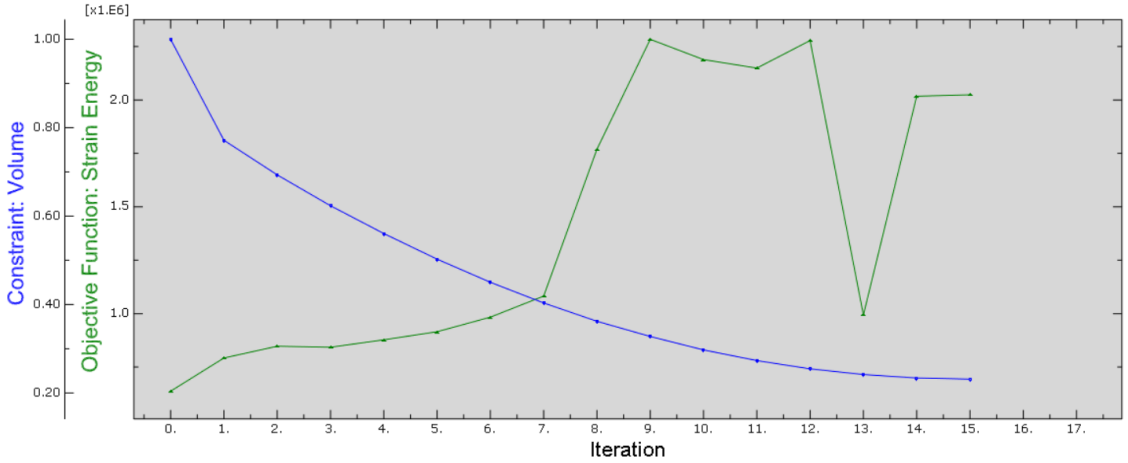

Figure 5-567 Optimization process of HEB160 flexure link.

The optimization process ends after 15 iterations showing some peaks in the convergence of the objective design response. The outputs from the topology optimization show a final volume of 9852825 mm^3. Then it will be necessary to set up the shape optimization procedure using a reduction volume constraint to an 86.2% of the actual volume to accomplish the initial goal. Shape optimization is implemented, and it is successfully obtained an optimized geometry using the same material volume than the original HEB160 flexure link.

The new geometry is subjected to the push-over analysis showing a stress distribution after a lateral displacement of the frame of 50 mm as it is illustrated in *Figure 5-18*:

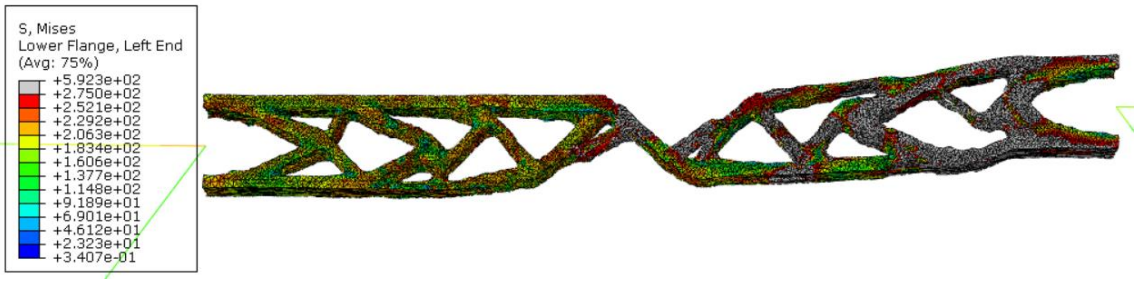

Figure 5-578 stress concentration contour plot of optimized HEB160 flexure link..

The resulting geometry shows a similar pattern for the truss-like structures and the diagonal element has been shortened, and thus reinforced. It is observed that the plastic behaviour is concentrated in the centre element and all over the truss located in the side of the EBF which is not being loaded. The yielding occurs distributed evenly along the link, showing no strain concentration locations in the structure.

Push-over curves

Capacity curves for the original and optimized HEB160 shear and flexure link have been plotted in *Figure 5-19*:

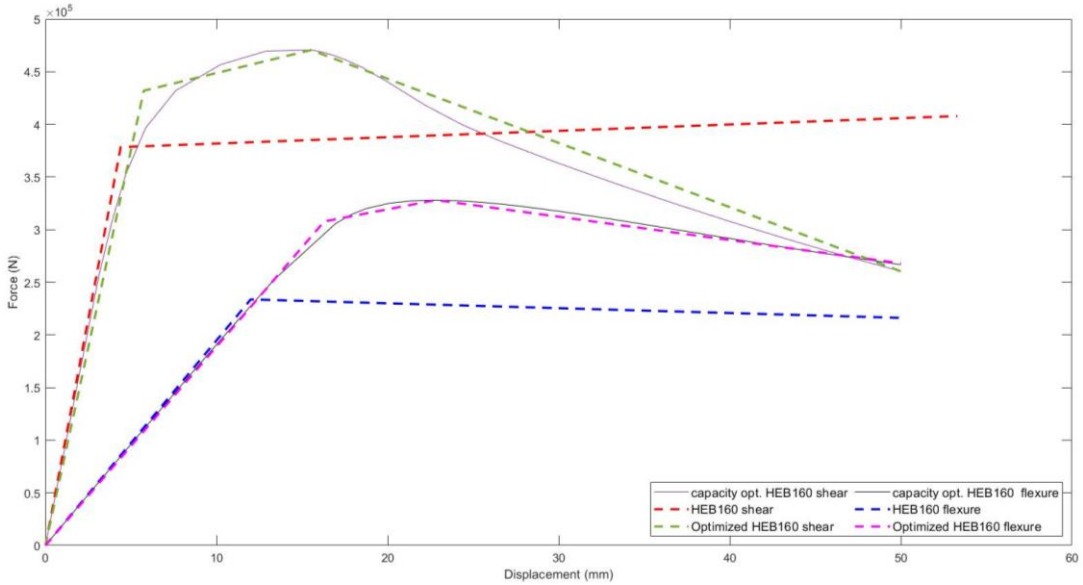

Figure 5-589 Optimized capacity curves against original capacity curves for HEB160 link

The frame using the shear link yields at an imposed displacement of 5.75 mm with a lateral reaction force of 432 kN while the frame using the flexure link yields at a displacement of 16.30 mm, providing a lateral force of 308 kN. Both links present a softened post-yield curve which show a high strength decrease rate in the shear link than in the flexure link.

The parameters that describe the behaviour of the links and that define the linear approximations of the capacity curves are summarized in *Table 6-14:*

Optimized HEB160	Dy (mm)	Vy (N)	Ke (N/mm)	α_1	α_2	Vm	Dm
Shear	5,75	431986	75128	0,053	-0,081	470600	15,53
Flexure	16,30	307834	18885	0,164	-0,117	328100	22,83

Table 5-19 linear approximation parameters for HEB160 link.

The plastic energy dissipation curves for original and optimized HEB140 shear and flexure links obtained from the push-over analysis are plotted in *Figure 5-20*:

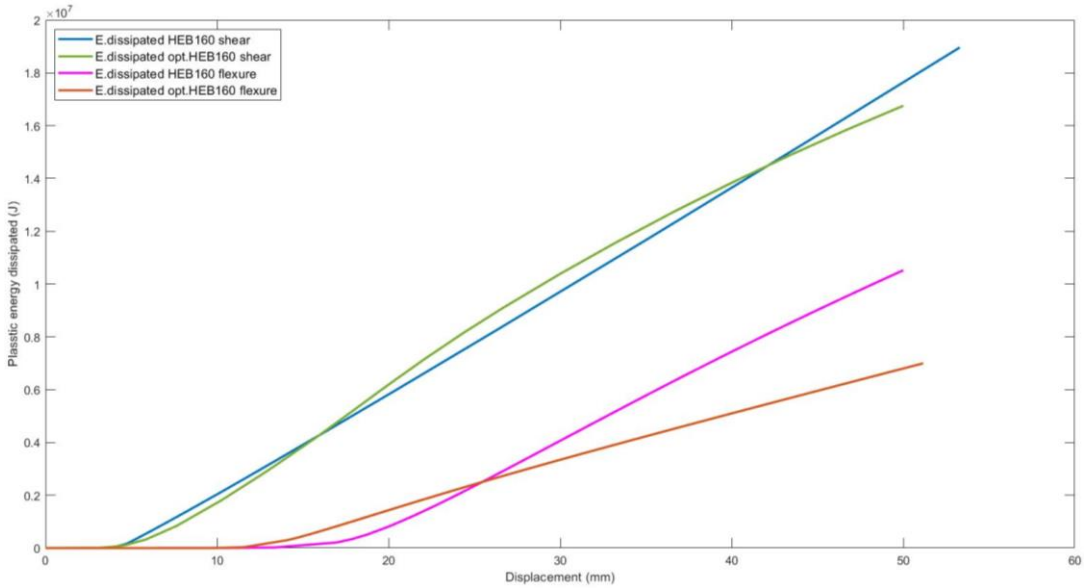

Figure 5-20 Optimized plastic dissipation curves against original plastic dissipation curves for HEB160 link

The plastic energy dissipation behaviour is similar to the previous link. For the shear link, the plastic energy dissipated at a displacement of 50 mm is 16760000 Joules, while flexure links dissipate 10520000 Joules. The curves maintain the same characteristics than for the previous link: Shear link provides a nonlinear curve which improves the energy dissipation in a range of movement between 15 and 40 mm while the flexure link provides a linear curve with a higher dissipation rate than its corresponding original link.

5.2.2.3. Optimized HEB180

The optimization results for the HEB180 for shear and flexural links are herein presented. The optimization procedure follows the scheme presented in *Figure 5-21*, where the objective is to get an optimized geometry with the same material volume than the original links.

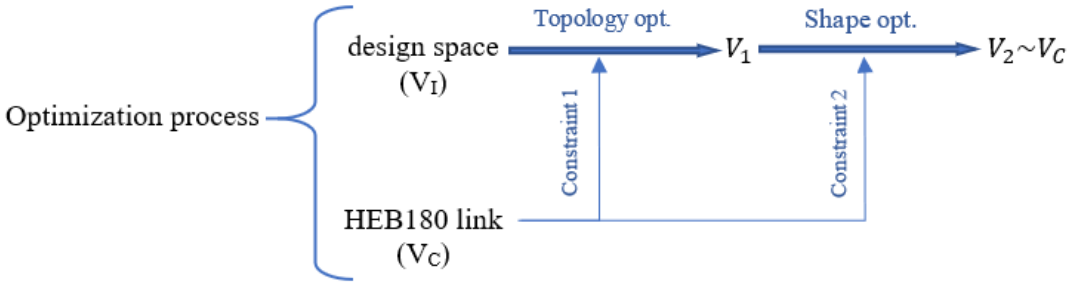

Figure 5-21 optimization for HEB180 links

Shear link

The topology optimization procedure on the shear link is carried out over its design space which has been defined with an initial volume of 30456000 mm^3. The optimization of the objective response is constrained to a reduction of volume of 20.1% up to 6133642 mm^3. The evolution of the procedure is described in *Figure 5-22*:

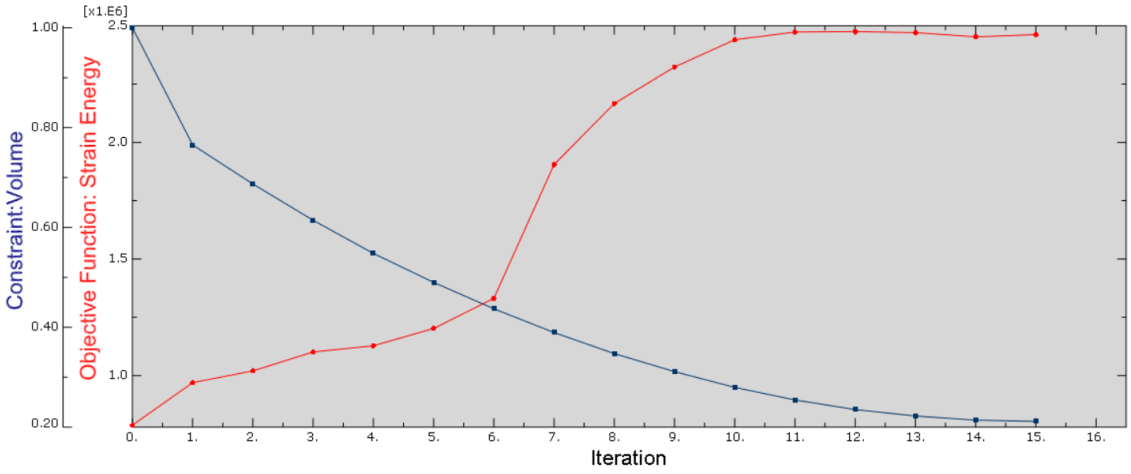

Figure 5-22 Optimization process of HEB180 shear link.

The procedure ends after 15 iterations showing a stable convergence of the strain energy optimization. The final volume output is 7260270.5 mm^3. Then, it is necessary to constrain the shape optimization procedure to a volume reduction of an 84.5%. After shape optimization is implemented, a new optimized geometry with the same volume of material than the original HEB180 shear link is achieved.

The push-over analysis is implemented on the new geometry, obtaining a stress distribution as it is illustrated in *Figure 5-23*:

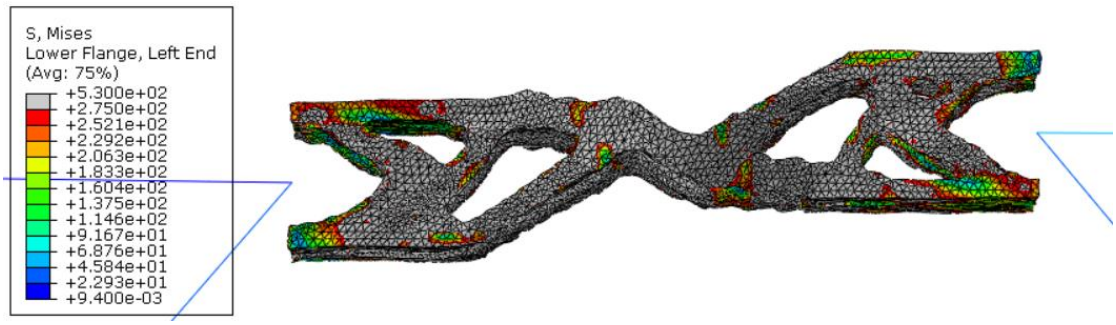

Figure 5-593 stress concentration contour plot of optimized HEB180 shear link..

The optimized geometry maintains the structure obtained in previous link. It is observed that the plastic behaviour is produced evenly in the whole link without showing strain concentrations at any location.

Flexure link

The topology optimization procedure on the flexural link is carried out over its design space which has been defined with an initial volume of 57510000 mm^3. The optimization of the objective response is constrained to a reduction of volume of 20.1% up to 11582143 mm^3. The evolution of the procedure is described in *Figure 5-24*:

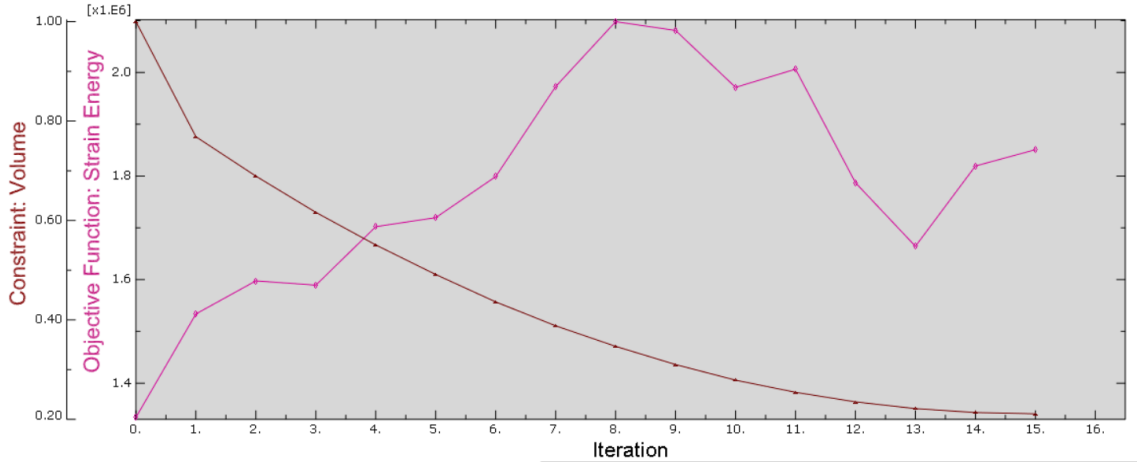

Figure 5-604 Optimization process of HEB180 flexure link.

The process ends after 15 iterations showing unstable convergence in the strain energy design response. The final volume is 15163218mm^3. Then, it is necessary to constrain the shape optimization procedure to a volume reduction to a 76.38% of the actual volume. After shape optimization is implemented, it is achieved a new optimized geometry with the same volume of material than the original HEB180 link.

The push-over analysis is implemented on the new geometry, obtaining a stress distribution as it is illustrated in *Figure 5-25*:

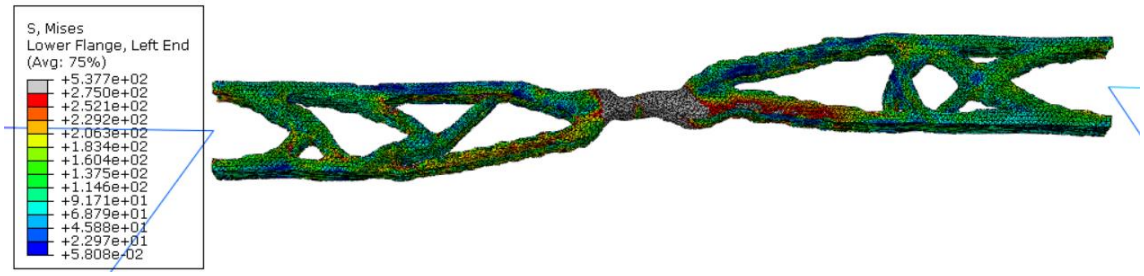

Figure 5-615 stress concentration contour plot of optimized HEB180 flexure link..

The optimized geometry shows larger voids than the structures previously obtained when optimizing flexure links. Stresses are mainly concentrated in the diagonal element in the centre while the rest of the structure of the link present relatively relaxed stresses. Then, the link rotates pivoting around the centre joint.

Push-over curves

Capacity curves for the original and optimized HEB180 shear and flexure link have been plotted in *Figure 5-26*:

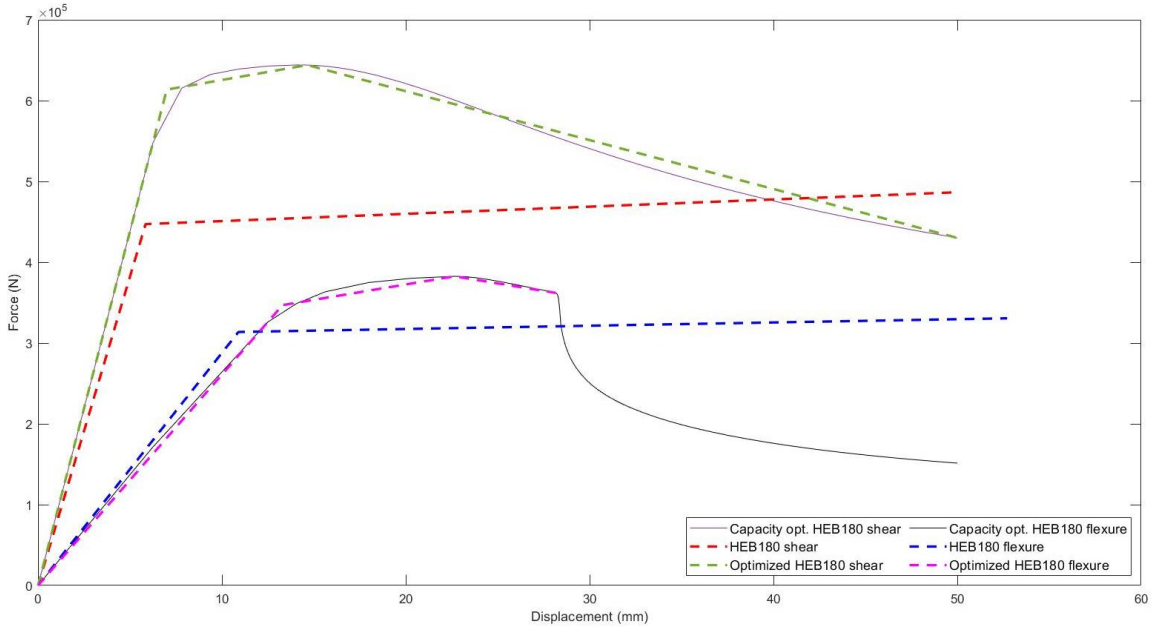

Figure 5-626 Optimized capacity curves against original capacity curves for HEB180 link

The frame using the optimized shear link yields at an imposed displacement of 7 mm with a lateral reaction force of 614 kN while the frame using the flexure link yields at a displacement of 13.3 mm, providing a lateral force of 347 kN. The shear link present a more ductile post-yielding curve caused by the even yielding in the whole link volume. In the other hand, the flexural link present a sudden drop in its strength when the structure is moved further than 30 mm.

The parameters that describe the behaviour of the links and that define the linear approximations of the capacity curves are summarized in *Table 5-15:*

Optimized HEB180	Dy (mm)	Vy (N)	Ke (N/mm)	α_1	α_2	Vm	Dm
Shear	7,00	613648	87664	0,045	-0,069	644000	14,65
Flexure	13,30	346970	26088	0,146	-0,144	382600	22,66

Table 5-20 linear approximation parameters for HEB180 link.

The plastic energy dissipation curves for original and optimized HEB180 shear and flexure links obtained from the push-over analysis are plotted in *Figure 5-27*:

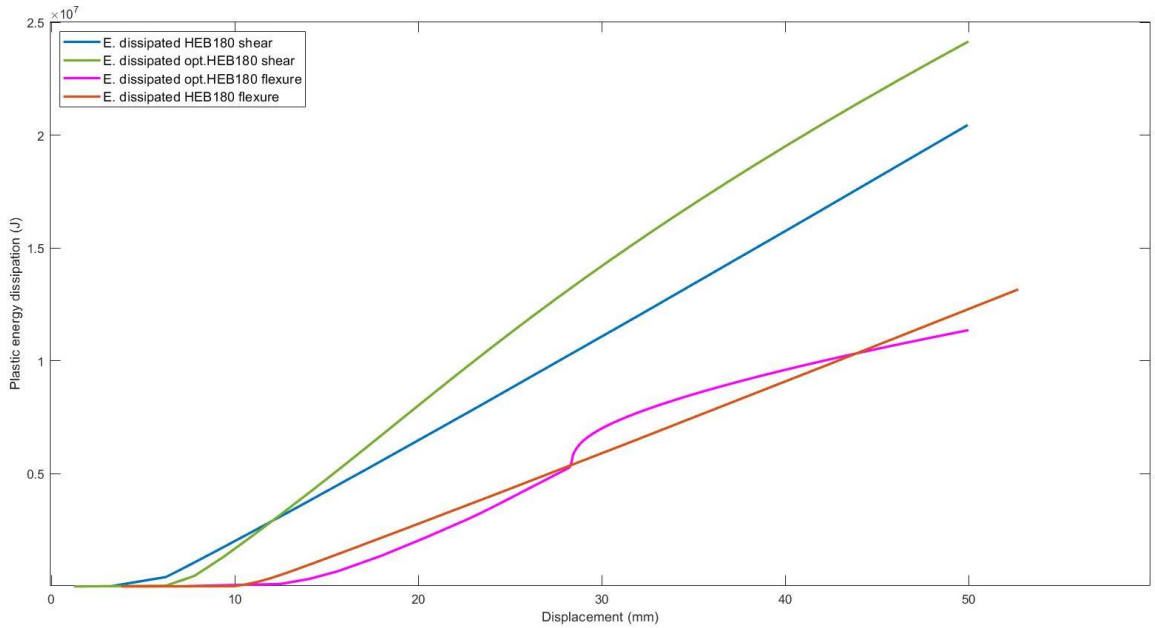

Figure 5-637 Optimized plastic dissipation curves against original plastic dissipation curves for HEB180 link

The plastic energy dissipation behaviour is similar to the previous link. For the shear link, the plastic energy dissipated at a displacement of 50 mm is 24150000 Joules, while flexure links dissipate 11300000 Joules. The curve corresponding to the shear link shows similar behaviour than the previous optimized shea links. The curve of the flexure link shows sudden increase in the plastic energy dissipated when the drop in the resistance strength is produced in the corresponding capacity curves.

5.2.2.4. Optimized HEB220

The optimization results for the HEB220 for shear and flexural links are herein presented. The optimization procedure follows the scheme presented in *Figure 5-28*, where the objective is to get an optimized geometry with the same material volume than the original links.

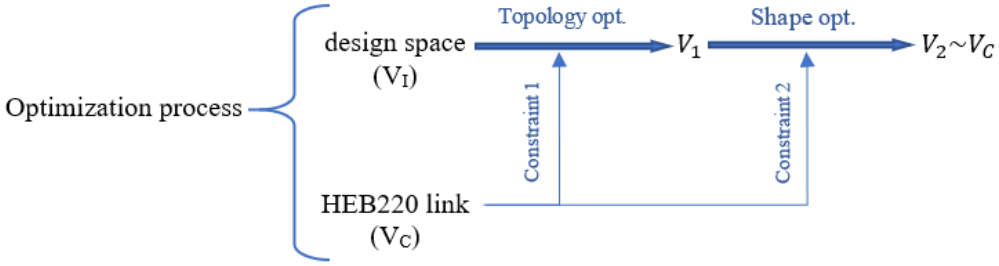

Figure 5-28 optimization for HEB220 links

Shear link

The topology optimization procedure on the shear link is carried out over its design space which has been defined with an initial volume of 57112000 mm^3. The optimization of the objective response is constrained to a reduction of volume of 18.8% up to 10742882 mm^3. The evolution of the procedure is described in *Figure 5-29*:

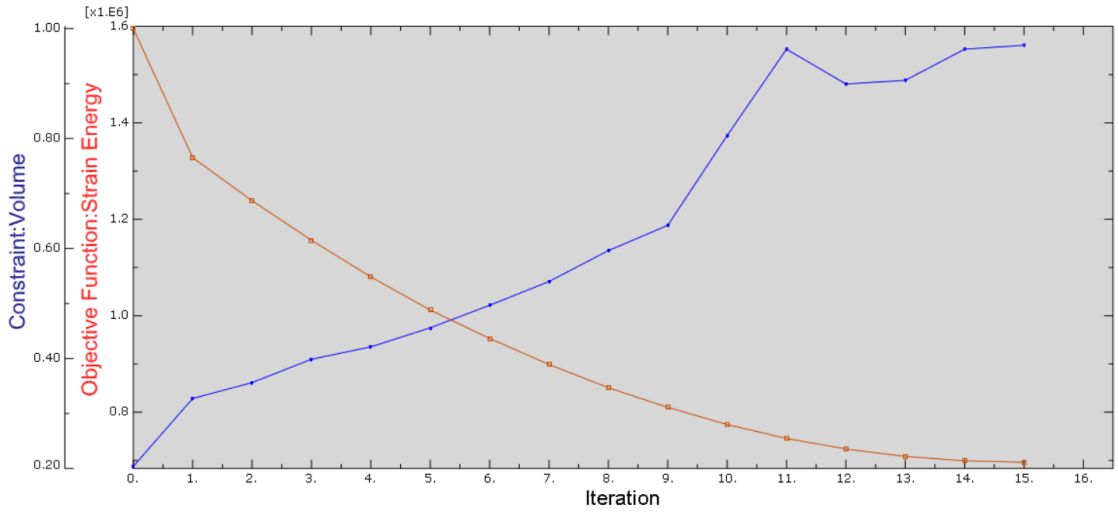

Figure 5-29 Optimization process of HEB220 shear link.

The process finishes after 15 iterations with minor oscillations in the strain energy values. The outputs from the topology optimization show a final volume design response of 13379267 mm^3. Then it will be necessary to set up the shape optimization procedure using a reduction volume constraint of an 80.3% to accomplish the initial goal. Shape optimization is implemented, and it is successfully obtained an optimized geometry using the same material volume than the original HEB220 shear link.

The push-over analysis is implemented on the new geometry, obtaining a stress distribution as it is illustrated in *Figure 5-30*:

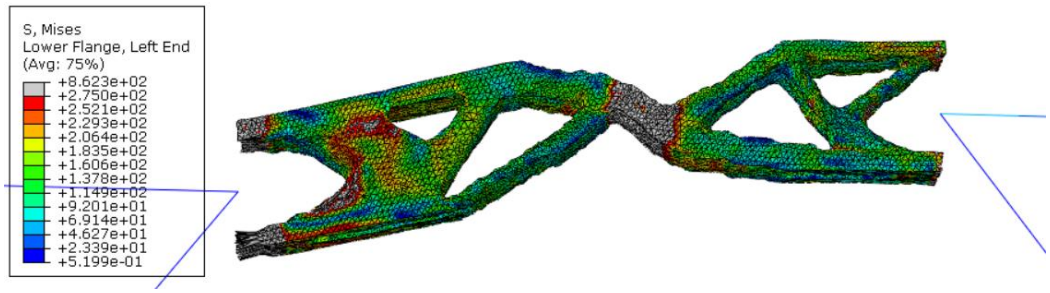

Figure 5-30 stress concentration contour plot of optimized HEB220 shear link.

The new geometry suffers from the stress concentrations described for the optimization of the HEB160 shear link. The excess of rigidity of the ends of the links cause strain concentrations in one of the ends joints with the frame i.e. make it rotate unsymmetrically.

Flexure link

The topology optimization procedure on the flexural link is carried out over its design space which has been defined with an initial volume of 107448000 mm^3. The optimization of the objective response is constrained to a reduction of volume of 18.8% up to 20211186 mm^3. The evolution of the procedure is described in *Figure 5-31*:

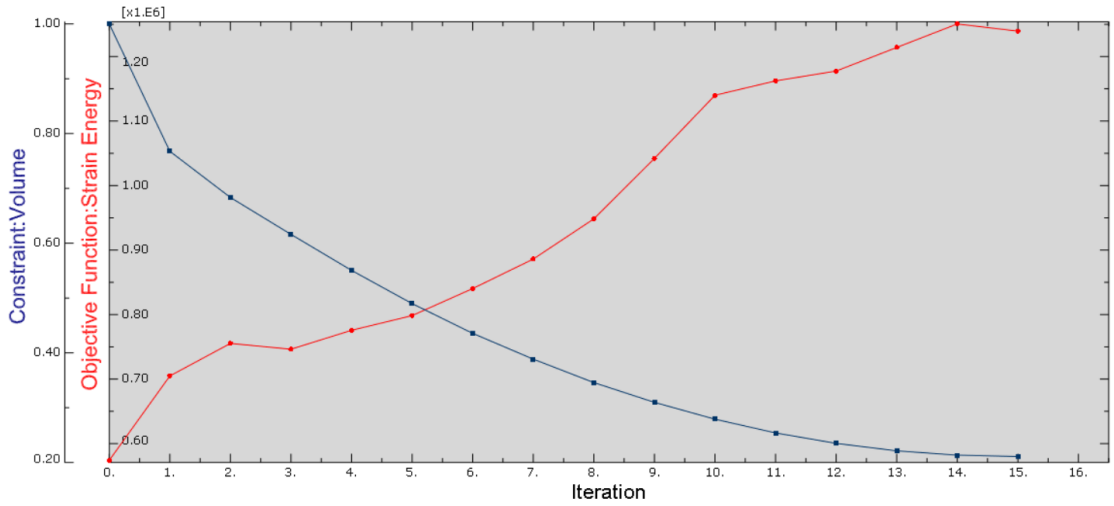

Figure 5-31 Optimization process of HEB220 flexure link.

The procedure ends after 15 iterations showing a stable convergence of the strain energy optimization. The final volume output is 25259776 mm^3. Then, it is necessary to constrain the shape optimization procedure to a volume reduction of an 80%. After shape optimization is implemented, a new optimized geometry with the same volume of material than the original HEB220 flexure link is achieved.

The push-over analysis is implemented on the new geometry, obtaining a stress distribution as it is illustrated in *Figure 5-32*:

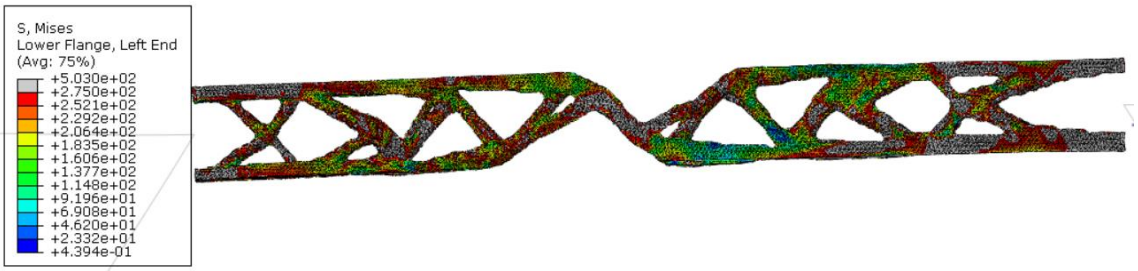

Figure 5-64 stress concentration contour plot of optimized HEB220 flexure link.

The new geometry shows even distribution of stresses at both ends of the links and in the center joint. The optimized link shows a high similarity with the optimized HEB160 link.

Push-over curves

Capacity curves for the original and optimized HEB220 shear and flexure link have been plotted in *Figure 5-33*:

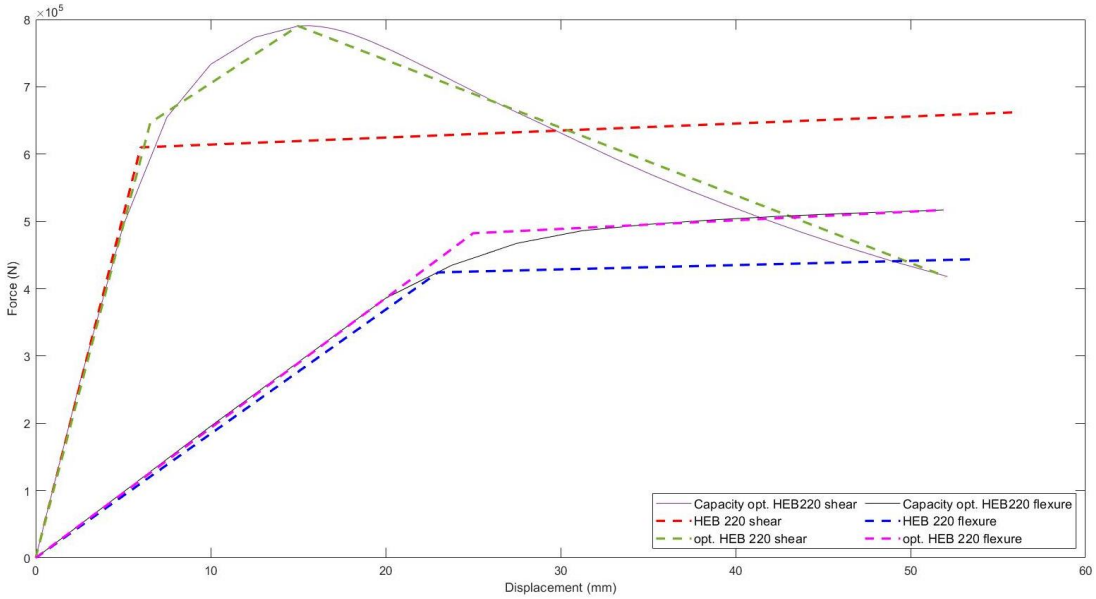

Figure 5-65 Optimized capacity curves against original capacity curves for HEB220 link

The frame using the shear link yields at an imposed displacement of 6.55 mm with a lateral reaction force of 647 kN while the frame using the flexure link yields at a displacement of 25 mm, providing a lateral force of 482 kN. The behaviour of the optimized link is consistent with the results previously obtained.

The parameters that describe the behaviour of the links and that define the linear approximations of the capacity curves are summarized in *Table 6-16:*

Optimized HEB220	Dy (mm)	Vy (N)	Ke (N/mm)	α_1	α_2	Vm (N)	Dm (mm)
Shear	6,55	646616	98720	0,172	-0,102	790200	15,00
Flexure	25,00	482375	19295	0,067	-	790200	15,00

Table 5-21 linear approximation parameters for HEB220 link.

The plastic energy dissipation curves for original and optimized HEB220 shear and flexure links obtained from the push-over analysis are plotted in *Figure 5-34*:

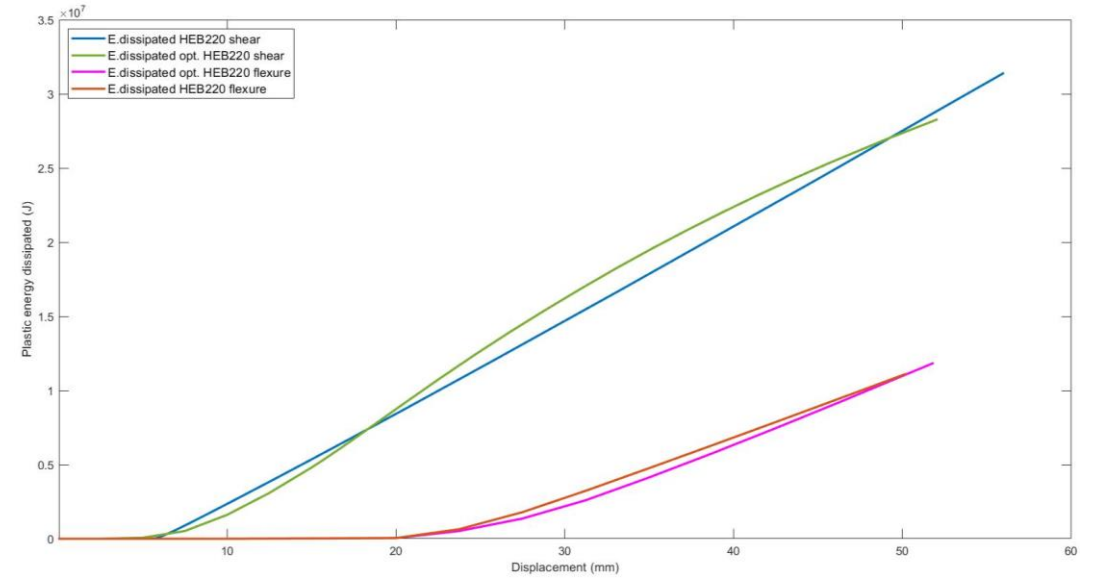

Figure 5-664 Optimized plastic dissipation curves against original plastic dissipation curves for HEB220 link

The plastic energy dissipation behaviour is similar to the previous link. For the shear link, the plastic energy dissipated at a displacement of 50 mm is 28290000 Joules, while flexure links dissipate 11120000 Joules. The characteristics of the curves are consistent with what is observed in previous the previous optimized link. The improvement in energy dissipation is not very pronounced in both, flexural and shear link cases.

5.3. Comparison

From the results of the optimization studies carried out in the previous sections can be summarized in the following statements:

- The optimization results for shear and flexure links show notable geometric differences form their corresponding original links. The optimization algorithm tends to transform the links into rigid structures, showing truss-like elements developing from the ends of the link to its centre, where they are connected using a diagonal element. The diagonal element is oriented in a direction such as it is capable to resist the rotation produced in the frame when the lateral force is applied at one of the top corners, which makes the new geometry resistant in the direction of the applied load but weak when the load is applied in counter-direction.

- In HEB140, HEB160 and HEB220 optimized shear links, the yielding mechanism is identified by the localization of plastic behaviour in two weak points: the diagonal element located at the centre of the link and in the connections of the ends of the links with the frame. In these localized plastic points can be found large deformations that create pivots through which the link rotate to allow the movement of the whole frame. Only in the case of HEB180 optimized shear link it is found an even yielding of the link, which leads to improved properties for the pot-yielding behaviour of the frame using it.

- In the optimized flexure links, yielding is generally producing evenly throughout the whole link, caused by a good stress distribution along the truss elements. Then, problem related to the concentration of stresses at the ends of the flexure links that suffered the original geometries is solved, generating improved elastic and plastic behaviour of the frames. Only the case HEB180 optimized link is found to have stress concentrations in the centre of the link, which causes the sudden drop in strength observed previously.

- The parameters used to create the linear approximations of the capacity curves for the optimized links effectively represent the behaviour of the links along the curves. Thus, they are used as a comparison tool between the behaviour of original links and the optimized links. The comparison is represented in Table 6-X, showing the curve parameters of the optimized links as a percentage of the parameters of the original links:

link	$\frac{Dy\ opt.}{Dy}$	$\frac{Vy\ opt.}{Vy}$	$\frac{Ke\ opt.}{Ke}$	$\frac{Dy\ opt.}{Dy}$	$\frac{Dm\ opt.}{Dm}$
Shear HEB140	143%	157%	109%	121%	14%
Flexure HEB140	88%	140%	158%	163%	319%
Shear HEB 160	131%	114%	87%	115%	29%
Flexure HEB160	136%	132%	97%	140%	148%
Shear HEB180	120%	137%	115%	132%	29%
Flexure HEB180	122%	111%	91%	116%	43%
Shear HEB220	109%	106%	97%	119%	27%

Flexure HEB220	109%	114%	105%	178%	28%

Table 5-22 Comparison of the parameters defining the linear approximation curves.

- The plastic energy dissipation curves show a higher dissipation for optimized shear and flexure links. Shear links present a smooth nonlinear curve that higher dissipation for for a given range of large nonlinear displacement. Flexure links present a linear curve with a higher dissipation rate.

To conclude, the optimized geometries obtained indicate that it is possible to optimize the performance of actual EBF links. From the results using topology optimization, are observed geometries and mechanisms that were unknown for these types of elements and could, with further development, generate links resistant in both directions maintaining their improved properties.

6. Conclusions

Structural topology optimization has been implemented in EBF horizontal links using Abaqus Optimization Module (ATOM). Then, the behaviour of the optimized links has been compared with the behaviour of original links.

Horizontal links are replaceable elements intended to cope with the plastic behaviour of the structure when it is subjected to high lateral forces, acting as an energy dissipator. The geometry of the links has not been specifically designed to resist optimally their particular load cases and imposed deformations. However, the complexity the boundary conditions of the links makes difficult to intuitively come up with a novel geometric design that perform better than the original geometries.

Nowadays, the development of advanced computational tools for solving engineering problems and the modernization of computational hardware allow the scientific community to deal with large volumes of calculations in a reduced amount of time. Additionally, the development of additive manufacturing is increasing in recent years, allowing to manufacture complex shapes for industrial engineered products. These facts and the nature of the EBF links open new design paths for this type of elements.

Structural optimization methods have been introduced i.e. topology optimization, shape optimization and sizing optimization. While sizing optimization algorithms allow to vary a set of predefined geometric variables to find the optimum of a given objective function, topology and shape optimization algorithms are directly involved in determining the material distribution and the shape of the boundaries of a design space, given a set of boundary conditions. Since it is not needed to define a preselected set of variables to modify the geometry, shape and topology optimization have been of special interest for this TFM.

Abaqus models have been created to analyse and optimize links using four different I-shaped section sizes: HEB140, HEB160, HEB180 and HEB220. For every section, shear and flexure links have been considered, which geometries have been obtained using the formulation exposed in EC8. A total of 16 models have been created: 8 models to analyse the behaviour of original links and 8 models to optimize the links and analyse their behaviour.

To evaluate the behaviour of original and optimized links, push-over analyses have been conducted. Results on original links show that shear links are able to withstand larger lateral forces, and the plastic behaviour is distributed homogeneously in the link ends and through the whole link web, presenting a hardened post-yielded curve. On the other hand, flexure links present weaker curves due to the localization of the plastic behaviour at the ends of the link, causing in the smaller sections a softened post-yielded curve.

The approach of evaluating the links by using a single storey frame with columns pinned at the bases have shown to provide a good method to characterize the behaviour of the links, since they provide the only lateral resistance to the structure and, thus, the frames push-over capacity curves are generated tracking directly the capacity of the links.

Results of push-over analyses for optimized links are presented, showing a general improvement of the capacity of the frame in both shear and flexural links. The optimization of the compliance of the links rigidize their structure by turning the design spaces into truss-like structures. The truss-like structures are developed from the ends towards the centre of the links where a diagonal joint element is produced.

Optimized shear links present capacity curves in which a more brittle behaviour is encountered, with a large increase in the yielding strength of the elements. The yielding mechanism show concentrations of plastic behaviour at the ends and in the centre diagonal element, which actuates as a pivot for the link to rotate and allow the movement of the frame. The plastic energy dissipated shows nonlinearity and generally improves the amount of energy dissipated by original links. On the contrary, flexure optimized links show a more ductile behaviour, where it can be seen that the plastic behaviour is spread throughout the truss. The energy dissipation is linear and presents a large improvement comparing the energy dissipated by the original links.

It can be concluded that the design approach using topology and shape optimization algorithms lead to interesting and complex geometrical results that could not be reached by using classical design methods. Furthermore, the general objective of the TFM i.e. improving the behaviour of the links has been accomplished, especially for flexure links. However, the results obtained can just be served as a beacon for future projects using these type of computer-aided design methods, since the links have only been optimized when the load is applied in one direction.

Furthermore, it is of interest to highlight that the results provided by the compliance optimization algorithm present a stiffening of the links. Although the final geometries show an improvement in the capacity curves, more interesting and efficient geometries would be obtained if the optimization algorithms were specifically designed for the purpose of energy dissipation that structural fuses like the horizontal EBF links have.

To conclude, future works might focus on the development of efficient algorithms dedicated to the optimization of structural fuses, and the optimization task should be carried out in both loading directions, in order to provide new EBF links that can be implemented in real-life design cases, in a time where computers and modern additive-manufacturing methods can allow engineers to produce optimized and economical structures.

7. References

[1] P. W. Christensen and A. Klarbring, An introduction to structural optimization. Dordrecht: Springer, 2009.

[2] W. Zhang, J. Zhu, and T. Gao, Topology optimization in engineering structure design. London, UK: ISTE Press Ltd, 2016.

[3] M. P. Bendsøe and O. Sigmund, Topology optimization: theory, methods, and applications. Berlin: Springer, 2004.

[4] Dassault Systèmes. Topology optimization with abaqus. Presentation 2011.

[5] C. F. Hvejsel and E. Lund, "Material interpolation schemes for unified topology and multi-material optimization," Structural and Multidisciplinary Optimization, vol. 43, no. 6, pp. 811–825, 2011.

[6] O. Sigmund and J. Petersson, "Numerical instabilities in topology optimization: A survey on procedures dealing with checkerboards, mesh-dependencies and local minima," Structural Optimization, vol. 16, no. 1, pp. 68–75, 1998.

[7] M. Stolpe, and K. Svanberg, "An alternative interpolation scheme for minimum compliance topology optimization," Structural and Multidisciplinary Optimization, vol. 22, no. 2, pp. 116–124, 2001.

[8] R. Meske, J.Sauter, E. Schnack, "Nonparametric gradient-less shape optimization for real-world applications". Structural and Multidisciplinary Optimization Struct Multidisc Optim vol. 30, pp. 201–218, 2005

[9] A. Hassanzadeh and S. Gholizadeh, "Collapse-performance-aided design optimization of steel concentrically braced frames," Engineering Structures, vol. 197, p. 109411, 2019.

[10] S. Lee and A. Tovar, "Outrigger placement in tall buildings using topology optimization," Engineering Structures, vol. 74, pp. 122–129, 2014.

[11] J. L. Jewett and J. V. Carstensen, "Topology-optimized design, construction and experimental evaluation of concrete beams," Automation in Construction, vol. 102, pp. 59–67, 2019.

[12] K. D. Tsavdaridis, E. Efthymiou, A. Adugu, J. A. Hughes, and L. Grekavicius, "Application of structural topology optimisation in aluminium cross-sectional design," Thin-Walled Structures, vol. 139, pp. 372–388, 2019.

[13] K. D. Tsavdaridis, J. J. Kingman, and V. V. Toropov, "Application of structural topology optimisation to perforated steel beams," Computers & Structures, vol. 158, pp. 108–123, 2015.

[14] Z. Xiao, Y. Yang, R. Xiao, Y. Bai, C. Song, and D. Wang, "Evaluation of topology-optimized lattice structures manufactured via selective laser melting," Materials & Design, vol. 143, pp. 27–37, 2018.

[15] S. D. Hague, 2013.

[16] S. K. Azad and C. Topkaya, "A review of research on steel eccentrically braced frames," Journal of Constructional Steel Research, vol. 128, pp. 53–73, 2017.

[17] G. D. Corte, M. Daniello, and R. Landolfo, "Analytical and numerical study of plastic overstrength of shear links," Journal of Constructional Steel Research, vol. 82, pp. 19–32, 2013.

[18] P. W. Richards and C.-M. Uang, "Effect of Flange Width-Thickness Ratio on Eccentrically Braced Frames Link Cyclic Rotation Capacity," Journal of Structural Engineering, vol. 131, no. 10, pp. 1546–1552, 2005.

[19] A. Mohebkhah and B. Chegeni, "Overstrength and rotation capacity for EBF links made of European IPE sections," Thin-Walled Structures, vol. 74, pp. 255–260, 2014.

[20] L. Mastrandrea and V. Piluso, "Plastic design of eccentrically braced frames, I: Moment–shear interaction," Journal of Constructional Steel Research, vol. 65, no. 5, pp. 1007–1014, 2009.

[21] L. Mastrandrea, E. Nastri, and V. Piluso, "Validation of a Design Procedure for Failure Mode Control of EB-Frames: Push-Over and IDA Analyses," The Open Construction and Building Technology Journal, vol. 7, no. 1, pp. 193–207, 2013.

[22] K. Kasai and E. P. Popov, "Cyclic Web Buckling Control for Shear Link Beams," Journal of Structural Engineering, vol. 112, no. 3, pp. 505–523, 1986.

[23] EN 1998-1, 2004. Eurocode 8: Design of Structures for Earthquake Resistance. 1st ed. Brussels: BSi.

[24] M. Ohsaki and T. Nakajima, "Optimization of link member of eccentrically braced frames for maximum energy dissipation," Journal of Constructional Steel Research, vol. 75, pp. 38–44, 2012.

[25] M. Smith. ABAQUS/Standard User's Manual, Version 6.9. Providence, RI: Dassault Systèmes Simulia Corp, 2009.

[26] R. McNeel. Rhinoceros (version 6.0). Windows. Robert McNeel & Associates 2018.

[28] C. Buchanan, L. Gardner. "Metal 3D printing in construction: A review of methods, research, applications, opportunities and challenges" Journal of Engineering Structures, vol. 180, pp. 332-348, 2019.

[29] P. Kyvelou, H. Slack, D.D. Mountanou, M.A. Wadee, T.B. Britton, C. Buchanan, L. Gardner. "Mechanical and microstructural testing on wire and arc additively manufactured sheet material," Journal of Materials and Design, vol. 192, 2020

[30] MX3D. 2020. MX3D Bridge | MX3D. [online] Available at: <https://mx3d.com/projects/mx3d-bridge/> [Accessed 21 June 2020].